BEHAVIOR OF CONCRETE AND SLENDER REINFORCED CONCRETE COLUMNS UNDER CYCLIC AXIAL COMPRESSION WITH BIDIRECTIONAL ECCENTRICITIES

by
Byong Youl Bahn

A Dissertation
Submitted to the Faculty of
New Jersey Institute of Technology
in Partial Fulfillment of the Requirements for the Degree of
Doctor of Philosophy

Department of Civil and Environmental Engineering

January 1994

APPROVAL PAGE

Behavior of Concrete and Slender Reinforced Concrete Columns under Cyclic Axial Compression with Bidirectional Eccentricities

Byong Youl Bahn

12/20/93

Dr. C. T. Thomas Hsu, Dissertation Advisor — Date
Professor of Civil and Environmental Engineering, NJIT

12/20/93

Dr. Farhad Ansari, Committee Member — Date
Professor of Civil and Environmental Engineering, NJIT

12/20/93

Dr. Methi Wecharatana, Committee Member — Date
Professor of Civil and Environmental Engineering, NJIT

12/21/93

Dr. John Schuring, Committee Member — Date
Associate Professor of Civil and Environmental Engineering, NJIT

12/20/93

Dr. Benedict Sun, Committee Member — Date
Associate Professor of Engineering Technology, NJIT

BIOGRAPHICAL SKETCH

Author: Byong Youl Bahn

Degree: Doctor of Philosophy in Civil Engineering

Date: January 1994

Undergraduate and Graduate Education:

- Doctor of Philosophy in Civil Engineering,
  New Jersey Institute of Technology, Newark, NJ, 1994
- Master of Science in Civil Engineering,
  New Jersey Institute of Technology, Newark, NJ, 1989
- Master of Science in Architectural Engineering,
  Hanyang University, Seoul, Korea, 1981
- Bachelor of Science in Architectural Engineering,
  Hanyang University, Seoul, Korea, 1979

Major: Civil Engineering

Presentation and Publication:

Hsu, C. T., B. Y. Bahn and Z. C. Yang, 1990 "A Knowledge-Based Expert System for Design of Square and Rectangular R/C Columns," Technical Report ST. No. 90-3, Department of Civil and Environmental Engineering, NJIT, September, pp.1-79.

Bahn, B. Y., S. K. Ham, B. H. Lee and L. H. Lee, 1981 "Theoretical and Experimental Study of the Stub-Girder System," Journal of Korea Architectural Institute, Seoul, Korea, April 36-104, pp. 47-53.

iv

BIOGRAPHICAL SKETCH
(Continued)

Ham, S. K., S. Y. Lee and B. Y. Bahn, 1980 "A Study on Rebar Detection in R.C. Members," Journal of Korea Architectural Institute, Seoul, Korea, March 24-93, pp. 51-57.

ACKNOWLEDGMENT

The author wishes to express his deepest gratitude to his advisor, Professor C. T. Thomas Hsu, for his invaluable encouragement and guidance during the preparation of the thesis. The author is also grateful to the members of the dissertation committee, Professor Farhad Ansari, Professor Methi Wecharatana, Professor John Schuring and Professor Benedict Sun for their helpful suggestions.

The author wishes to thank Mr. Allyn Luke, a staff of the Structural Concrete Laboratory at NJIT, for his assistance in the experiment. Appreciation is expressed to Y. M. Omar and W. Wang for their help during the experimental stage, and Mr. B. J. Yu, Dr. C. Jaturapitakkul and Dr. S. Mehta for their sharing of helpful opinions.

The experiments were performed using the MTS testing system which was purchased under the NSF grant, No. CEE8308339. Unlimited computing time on SPARC workstation provided by Computer Aided Engineering Laboratory is appreciated. Financial support to purchase the research materials from several New Jersey Corporations and Companies, graduate assistantship from NJIT which enabled the author to complete this study, are also greatly acknowledged.

TABLE OF CONTENTS

TABLE OF CONTENTS
(Continued)

LIST OF TABLES

LIST OF FIGURES

LIST OF FIGURES
(Continued)

LIST OF FIGURES
(Continued)

LIST OF FIGURES
(Continued)

Figure **Page**

LIST OF FIGURES
(Continued)

LIST OF SYMBOLS

a_k: Area of element k.

A_i: Area of fictitious load at segment i .

c_p: Coefficient of plastic strain ratio.

c_r: Coefficient of reloading curve.

c_u: Parameter of unloading curve.

d_i: Strain depth of mechanical strain gage number i .

e_x, e_y: Eccentricities in X, Y directions, respectively.

E_{sk}: Secant modulus of elasticity for element k.

E_{unlo}: Modulus of elasticity for the unloading and reloading paths.

f_c': Ultimate strength of concrete.

f_k: Stress of discrete element k at the corresponding strain ε_k.

$I'_{x_o k}, I'_{y_o k}$: Moments of inertia of element k about elemental centroidal x_o and y_o axes, respectively.

$[K_{sc}]$: Incremental stiffness matrix of cross-section.

L_i: Length of column segment i .

l_{ij}: Deformed length of mechanical strain gage number i at the loading stage j.

l_{oi}: Initial length of mechanical strain gage number i .

M_{xc}, M_{yc}: The calculated moments with respect to X and Y axes, respectively.

$(M_{xk})_{\lambda=1}$, $(M_{yk})_{\lambda=1}$: The calculated moments due to the unit load factor at element k.

P_c: The calculated axial force under axial load λP with bidirectional eccentricities.

$(P_k)_{\lambda=1}$: The calculated force due to unit load factor at the element k.

S_{eu}: Unloading strain ratio on the envelope curve.

S_{er}: Reloading strain ratio on the envelope curve.

S_{erpu}: Envelope reloading strain ratio due to the history of partial unloading.

S_{ieupr}: Imaginary envelope unloading strain due to the history of partial reloading.

LIST OF SYMBOLS
(Continued)

S_{pu}: Unloading plastic strain ratio.

U_{env}: Envelope curve in the normalized coordinate system.

U_{eu}: Unloading stress ratio on the envelope curve.

U_{relo}: Reloading curve in the normalized coordinate system.

U_{rpr}: Reloading stress ratio due to the history of partial reloading.

U_{unlo}: Unloading curve in the normalized coordinate system.

V_{ic}, V_{ip}: The calculated and proposed deflections at the segment point i, respectively.

$(V_{ic})_{\lambda=1}$: The calculated deflection due to unit load factor at the segment point i.

x_k, y_k: Centroidal coordinates of element k in the cross section.

ε_{ij}: Experimental strain of mechanical strain gage number i at the loading stage j.

ε_k: Strain of a discrete element k under combined biaxial bending and axial load.

ε_{kh}: Strain history corresponding to the solution at which a updated strain ε_k at the element k.

ε_o: Strain at the coordinate origin.

$(\varepsilon_{ok})_{\lambda=1}$: The calculated strain at coordinate origin due to unit load factor.

ϕ_i: The calculated curvature at the segment i.

ϕ_x, ϕ_y: Curvatures with respect to M_x, M_y, respectively.

ϕ_{xh}, ϕ_{yh}: Curvatures corresponding to the solution at which a updated strain history ε_{kh} at the element k.

$(\phi_{xk})_{\lambda=1}$, $(\phi_{yk})_{\lambda=1}$: The calculated curvatures due to unit load factor at the element k.

ζ: Incompatibility in control deflection.

$\delta\zeta$: A finite change in incompatibility.

λ_p: Load factor for the applied axial load.

$\delta\lambda_p$: A finite change in load factor.

ABSTRACT

Behavior of Concrete and Slender Reinforced Concrete Columns under Cyclic Axial Compression with Bidirectional Eccentricities

by
Byong Youl Bahn

A rational analysis of reinforced concrete (R/C) structures requires satisfactory modeling of the behavior of concrete under general loading patterns. The behavioral characteristics of concrete dominantly depends upon its load history. For the study of concrete behavior, parametric study and experimental investigation into the behavior of concrete under load history of random cycles are performed. Through parametric study, the applicability of the previous concrete models is examined and a physically motivated modeling for the cyclic stress-strain relationships is proposed. The present modeling of concrete under general cyclic loading is initiated to provide substantial applicability, flexibility of mathematical expressions and furthermore to describe the behavior of random cycles. For the experimental study of concrete subjected to cyclic axial compressions, tests of 3 in. by 6 in. concrete cylinders are conducted under four different loading regimes to determine the major experimental parameters for the proposed analytical expressions. The model developed is based on the results of parametric study and experimental data obtained for the present study. The validity of the proposed general cyclic model is confirmed through a comparison of the experimental results and simulated behavior of the model. Furthermore, the analytical model proposed has been idealized and incorporated into the procedures in analyzing R/C columns.

The behavior of R/C columns having various properties and subjected to a variety of loading conditions have been the topics of considerable investigation. Of particular

significance in the area of unexplored problems is the behavior of R/C columns under cyclic compressive load. It should be noted that cyclic loads with bidirectional eccentricities considered are in the longitudinal direction, and not in the transverse direction, with respect to the column axis. For the experimental investigation, tests of four foot long columns are conducted under stroke control to achieve both ascending and descending branches of the load-deformation curves.

Analysis of R/C columns subjected to cyclic axial compressions with bidirectional eccentricities should be approached from the standpoint of a three dimensional problem. A numerical procedure based on extended finite segment method is proposed here to predict the ultimate load, deflections and moment-curvature of experimental results. It is found that the proposed numerical analysis can reasonably simulate the loading and unloading behavior of R/C columns under combined biaxial bending moments and axial compressions.

CHAPTER 1

INTRODUCTION

1.1 General

The inelastic behavior of reinforced concrete members, especially the biaxially loaded reinforced concrete (R/C) column has been the subject of research for many years. Due to the locations of the structural members, the shape of structures and the nature of the applied loads, many members are subjected to combined biaxial bending and axial compression. Structural R/C members are subjected to two main types of load, dead load and live load. For any member, the dead load is present throughout the life of the structure and can be considered to be constant. However, this is not the case for live load which has a cyclic form during the life of the structure. The behavior of reinforced concrete column depends on many parameters including the material properties, the section geometry, and the history of moment and/or axial load to which the column is subjected.

The behavior of concrete is dependent upon its load history. In most cases, quantitatively accurate predictions on the load-deformation history up to and beyond the ultimate load remain difficult to obtain. The highly nonlinear nature of the concrete stress-strain relationship under a cyclic loading can not be easily described by any mathematical formulas. Although a considerable amount of effort has been directed at the development of the concrete model under cyclic compressive loading, most original concrete models can not be incorporated into the analysis of reinforced concrete structures. A reliable and substantial cyclic stress-strain relationship is thus needed for the analysis of structures subjected to repetitive loadings.

Despite the progress made in recent years on the study of in-plane behavior of reinforced concrete columns, their extension to three dimensional cases is restricted,

although some studies have been reported. Furthermore, most previous research is limited to studies of behavior of R/C columns subjected to combined biaxial bending and monotonically increasing axial load.

For members where stability and secondary effects influence the strength, for example, eccentrically loaded R/C columns, the changes in live load may have either a beneficial or detrimental effect on the strength of a member. The influence of repeated cycles of live load on column behavior is of interest in this study. The cyclic compressive loading with bidirectional eccentricities considered in this study is in the longitudinal direction, and not in the transverse direction, with respect to the column axis. Such a loading and member might be present in a bridge substructure or a column of building structures which is subjected to repetitive loadings. In both cases changes in live load can occur frequently.

1.2 Literature Review

1.2.1 Stress-Strain Relationships for Cyclic Loading

An accurate and rational analysis of reinforced concrete structures requires satisfactory analytical modeling of the material behavior of the concrete and the steel. The reinforcing steel is almost invariably in form of small diameter bars. As a result, the uniaxial stress-strain relationship of steel is all that is often required to model the response of reinforcing elements.

In contrast to steel, concrete is almost invariably subjected to a multiaxial state of stress. However, depending on the structural type, the nature of loading and the reasonable accuracy, it may be possible to make simplified assumptions. Columns and beams can be analyzed with sufficient accuracy using the uniaxial models of concrete. Shear walls and shell structures require biaxial modeling whereas massive structures like dams and nuclear pressure vessels can be better analyzed by a generalized triaxial

constitutive model [Fafitis 1984].

A large variety of models has been proposed in recent years, which are based on the more sophisticated theory of plasticity in mathematics. The complexity and incompleteness of many of these models, and the rather complex behavior of concrete under pattern of random cyclic loading, have led to simplified material models in the empirical way. These simplified models are essentially mathematical formulations and generalizations of the test results of various loading histories. Although the capability of prediction of such models is restricted to certain load patterns in which the experimental data are selected originally, their simplicity is very attractive. Due to the mathematical complexity, the models based on plasticity seems generally far from being substantial in implementation into the procedure of R/C structural analysis. Furthermore, it should be mentioned that the major parameters of these models are determined from the test results.

There is an uncommon computer aided approach in the development of concrete model. This alternative is to use a computation and knowledge representation paradigm, called neural networks, developed by researchers in a subfield of artificial intelligence (AI) to model the concrete behavior under compressive uniaxial cyclic loading. The main benefits in using a neural network approach are that all behavior can be represented within a unified environment of a neural network which is built directly from test data using the self-organizing capabilities of the neural network. The network is presented with the experimental data and "learns" the relationships between stresses and strains [Ghaboussi, et. al. 1991]. The self-learning of neural network, however, can only be obtained through the training of reliable experimental data until the network is able to recognize the certain deviated data. The preliminary research of using neural networks to model the concrete behavior seems promising.

Thus, the stress-strain relationships for concrete under cyclic compressive uniaxial loading are surveyed herein. The envelope curve, unloading and reloading curves and load history are reviewed for the behavior of concrete under cyclic loading.

The available empirical and analytical models are presented through the numerous simulations.

1.2.1.1 Envelope Curve. Although the behavior of nonlinear and strain softening material like concrete is quite complex, some simplifications can be made for the purpose of analysis. For example, it has been postulated that when concrete is subjected to repeated uniaxial compressive loading, an envelope curve exists and that this envelope curve is approximately the same as the stress-strain curve obtained under the monotonically increasing strain [Sinha 1964, Karsan 1969 and Shah 1983].

An envelope curve is the line in which no stress-strain curve exceeds regardless of the loading paths. The validity of the concept of the envelope curve is rested primarily on the data of unconfined concrete in early researches. Fafitis, et. al. [1984] found that under some limitations the concept is valid for confined, normal weight concrete as well as unconfined and confined lightweight concrete. These similar observations for the envelope curve were also reported by Desayi, et. al. [1979].

The envelope curve, or monotonic stress-strain curve is affected by concrete strength, strain rate, and confinement as well as other parameters. A proper constitutive model for analysis of concrete structures, however, requires a complete description of the behavior of concrete, not only in its hardening range, but also including its softening behavior. Physically, stiffness degradation in the post peak range is generally considered to be related to some kind of material damage (perhaps, microcracks or microvoids), which is rather complex. Recently many mathematical models have been proposed to simulate observed monotonic stress-strain curves.

The stress-strain relationships for concrete under monotonic uniaxial loading are summarized extensively as shown in Table 1.1. Influence of confinement and effect of strain rate are reviewed for concrete behavior under monotonic uniaxial loading.

Influence of Confinement: Use of lateral reinforcement in R/C columns is based

Table 1.1 Stress-Strain Relations of Concrete under Monotonic Loading

Author	Equation	Remark
Smith and Young [1956]	$\sigma = \sigma_o x e^{(1-x)}$	$x = \frac{\varepsilon}{\varepsilon_o}$
Kabaila [1964]	$\sigma = \sigma_o(2x - 1.189x^2 + 0.1763x^3 + 0.0027x^4)$	$\sigma_o = Peak\ Stress = f_c'$ $\varepsilon_o = Strain\ at\ Peak$
Saenz [1964]	$\sigma = \sigma_o \frac{E_c}{E_o}[\frac{x}{1+(\frac{E_c}{E_o}-2)x+x^2}]$	$E_o = \sigma_o / \varepsilon_o$, $E_c = \frac{10^5\sqrt{\sigma_o}}{1+0.006\sqrt{\sigma_o}}$
Desayi, et. al. [1978]	$\sigma = E_c[\varepsilon / (1+x^2)]$	$E_c = 2\sigma_o / \varepsilon_o$
Tulin, et. al. [1964]	$\sigma = E\varepsilon / (A+x^3)$	$A = 2$, $E = E_o(A+1)$
Sargin [1971]	$\sigma = k_3\sigma_o \frac{Ax+(D-1)x^2}{1+(A-2)x+Dx^2}$	$k_3 = 1.0$, $D = Exp.\ Constant$ $A = 5975\sqrt{\sigma_o}\varepsilon_o / (k_3\sigma_o)$
Popovics [1970]	$\sigma = \sigma_o x[n / (n-1+x^n)]$	$n = 0.4 \times 10^{-3} + 1.0$
Kent and Park [1971]	$\sigma = \sigma_o(2x - x^2)$, $0 \le \varepsilon \le \varepsilon_o$ $\sigma = \sigma_o[1 - Z(\varepsilon - \varepsilon_o)]$, $\varepsilon_o \le \varepsilon \le \varepsilon_{20}$	$Z = 0.5 / (\varepsilon_{50} - \varepsilon_o)$ $\varepsilon_{50} = (3 + \varepsilon_o\sigma_o) / (\sigma_o - 1000)$
Liu, et. al. [1972]	$\sigma = \sigma_o \frac{E_c}{E_o} \frac{x}{[1+(\frac{E_c}{E_o}-2)x+x^2]}$	$E_c = Initial\ Modulus$ $E_o = Secant\ Modulus\ at\ Peak$
Shah, et. al. [1983]	$\sigma = \sigma_o[1-(1-x^A)]$, $\varepsilon \le \varepsilon_o$ $\sigma = \sigma_o e^{-k(x-1)^\lambda}$, $\varepsilon > \varepsilon_o$	$A = E_c / E_o$ $\lambda = 1.15$

on two concepts, the first, confinement increases compressive strength so that it is possible to offset the strength loss from spalling of concrete cover, and the second, confinement increases the capacity of concrete to sustain large deformations without a substantial strength loss [Ahmad 1982]. The effectiveness of confinement depends on geometry of confining reinforcement, compressive strength of plain concrete as well as other parameters.

Desayi, et. al. [1978] found that the confinement becomes effective only when the pitch of confining reinforcement is less than the least lateral dimension of the confined specimen. Of the three types of lateral reinforcement studied, circular spirals, square spirals and stirrups, the first was the most and the last the least effective. Ahmad[1982] also reported a similar observation that when the spacing of lateral reinforcements exceeds the value of about 1.25 times of the least dimension of the confined concrete core, the influence of confinement is negligible.

It is well known that the shape of stress-strain curve is significantly affected by the lateral reinforcement especially in the post peak range. Dilger, et. al. [1984] showed that the strain at maximum stress is considerably more affected by the presence of transverse steel than by the strain rate. The predominant effects of confinement are to increase the strain at maximum stress and to reduce slope of the descending branch of the stress-strain curve. The shape of stress-strain curve for confined concrete with 1 inch stirrup spacing was not affected by the strain rate in the range of 33 to 200000 microstrain per second.

A laterally reinforced concrete member may be treated as a composite member consisting of a confined core and unconfined cover. The ductility, the rotational capacity of the so-called hinging regions in reinforced concrete members can be improved to a large extent through the use of lateral confinement.

Effect of Strain Rate: Most of the experimental studies on concrete materials and structural systems have been conducted quasi-statically. The strain rate sensitivity

has generally been measured in terms of the strength, modulus of elasticity, or the strain at the peak stress in compression.

In most studies, the compressive strength of concrete has been observed to increase approximately linearly with each order of magnitude (factor of 10) increase in strain rate, up to strain rate about 1000 microstrain per second. Generally, the increase has been 7 to 15 percent with each order of magnitude increase in strain rate or stress rate. There is little agreement among researchers on the strain rate effect on the strain at the maximum stress [Harsh 1990].

Scott, et. al. [1982] reported that the peak stress and the slope of the descending branch in stress-strain curve are increased by about 25 percent by comparing the high strain rate (0.0167/sec) with the low strain rate (0.0000033/sec).

Comparing two test parameters between the influence of lateral confinement and effect of strain rate on the behavior of concrete, it is noted that the confinement of concrete plays a dominant role than the applied strain rate in the experimental study of concrete.

1.2.1.2 Unloading and Reloading Curves. Karsan and Jirsa [1969] proposed the stress-strain relationships of concrete subjected to cyclic compressive loading. The stress-strain curves possess a locus of common points which are defined as the point where the reloading curve of any cycle intersects the unloading curve. Stresses above the common points produce additional strains, while stresses at or below these points will result in the stress-strain path going into a loop. The values of common points depend on the minimum stress in the cycle, i.e., the stress amplitude.

When the material is unloaded, additional permanent or plastic strain is accumulated. For cycling at large strains, deformation consists mainly of sliding along the macroscopic cracks. The resistance to deformation is provided primarily by friction [Maher 1982]. The incremental strains under cyclic loading are a result of creep

deformations and incremental damage. These phenomena are likely to depend on the number of cycles, the rate of loading and the range of loading.

When reloading is performed from zero stress to meet the envelope curve, it is found that the reloading curve changes curvatures. The shape of the reloading curve is more complex. It is characterized by a double curvature with mild concavity in the low stress region, and a sharp reversal in curvature near the envelope. Many of the existing models simply use a straight line to simulate the reloading response [Sinha 1964]. A few models adopt bilinear [Park 1972, Darwin 1976 and Yankelevsky 1987] or parabolic expression [Karsan 1969]. In spite of its simplicity, the linear equation provides a reasonable approximation to the observed behavior of concrete.

It is well known that the behavior of concrete between plain and confined concrete shows significant difference in descending branch of stress-strain envelope curve. However, Desayi [1979] reported that there was no noticeable difference between the confined and plain concrete in the behavior of unloading and reloading. Thus, it is possible to characterize an unified plastic strain between the confined and unconfined concretes for the unloading behavior. The analytical model of unloading curve showed a good agreement with his experimental data in both confined and plain concretes. But, the mathematical expression of reloading curve is not analytical at reloading strain on the envelope curve.

1.2.1.3 Load History. Figure 1.1 shows patterns of loading history in the previous studies involving cyclic loading test. Most patterns of loading can be classified in two categories based on available experimental results and analytical models. The first one is a full loading of cycles in which the loading is up to the envelope curve and then unloading down nearly to zero stress level. The second one is a partial loading and unloading at specified stress levels within the envelope curve.

However, behavior of various elements in structural system may not fall into

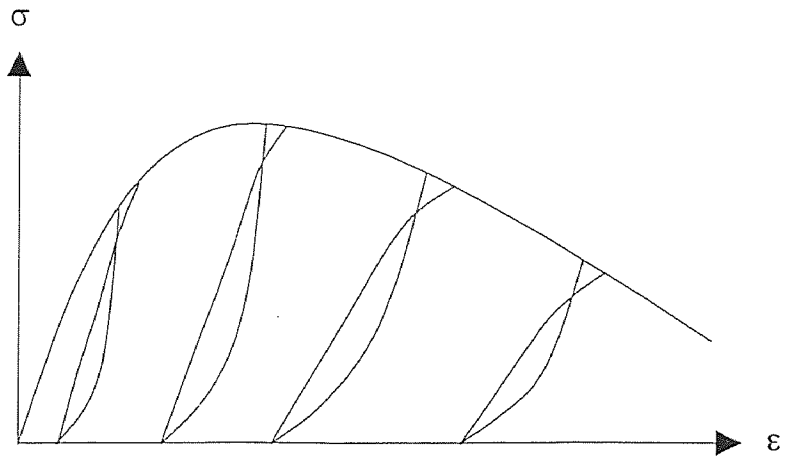

(a) Cycles to Envelope

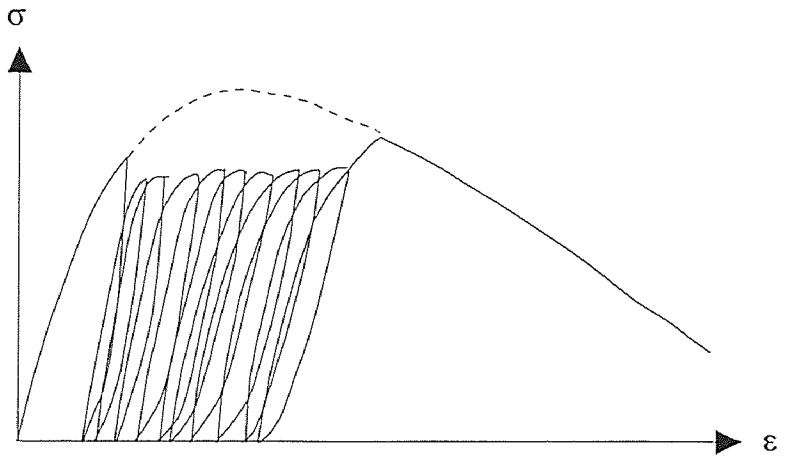

(b) Cycles between Fixed Stress

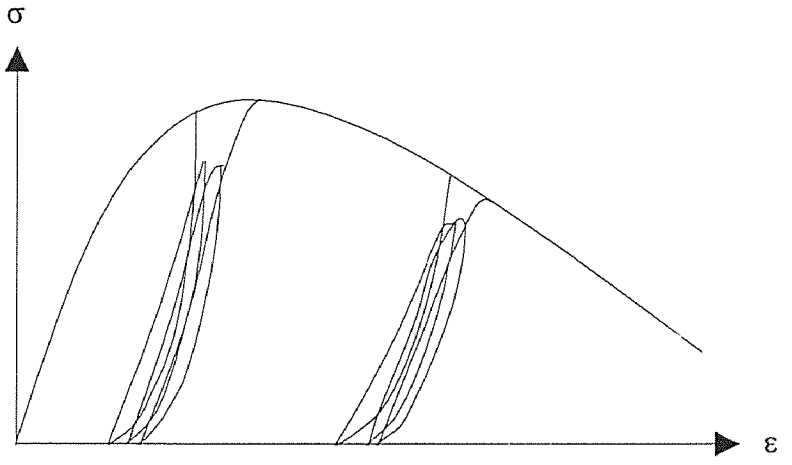

(c) Cycles to Common Points

Figure 1.1 Patterns of Load History in Previous Study

either of the above mentioned categories. There is a possibility that the loading may hit the envelope curve in a cycle and may not reach the envelope curve in the subsequent cycles. Such a behavior can only be presented by an empirical and/or mathematical model having a capacity to simulate the random cyclic loading. The stress-strain relationship under conditions of general loading is needed to reflect the observed behavior of structural components. The test results of concrete under random cyclic loading are not available upto date. In addition, the test results of this type of loading should also be employed to calibrate the analytical model for a random cycle.

1.2.2 Behavior of R/C Columns under Combined Biaxial Bending and Axial Load

1.2.2.1 R/C Columns under Monotonic Loading. Determining the strength of a reinforced concrete (R/C) column has been the subject of lengthy research by many investigators. The case of a column subjected to uniaxial bending and axial load is satisfactorily developed while a column under combined biaxial bending and axial load is solved using empirical procedures. The load-deformation relations for any reinforced concrete sections and the behavior of slender R/C columns under monotonic loading were thoroughly reviewed in Tsao's [1991] study.

R/C Sections under Biaxial Bending and Axial Load: Bresler [1960] proposed two analytical expressions, reciprocal load method and load-contour method, respectively. The criteria suggested in these methods are based on the approximations of failure surfaces which are defined as a function of its eccentricities e_x and e_y or of the components of bending moments M_X and M_y. These two approaches were extended to give better prediction of a plane approximation to a curved surface by Pannell [1961].

The finite difference approach was used for the computation of internal force and moments in the section. The concrete and reinforcements in the cross section were divided into many small elements. The summation of the elemental forces acting on the discrete areas allows the axial force to be determined, while summation of moments of

the elemental forces is used to calculate the biaxial moments [Warner 1969].

A modification of the extended Newton-Raphson method was suggested for the study of the moment-curvature characteristics of structural concrete sections subjected to biaxial bending moments and axial load. The summation of elemental force and moments were expressed by Taylor's expansion. A numerical analysis was also developed for the determination of strain and curvature in a R/C section [Hsu 1973].

A general analysis and design expression of R/C short and tied columns was recently proposed by Hsu [1988]. This equation represents both strength interaction diagrams and failure surface of R/C sections under combined biaxial bending and axial load. The equation of failure surface has been found to be a simpler and more logical approach for the analysis and design of R/C columns. Analysis of R/C columns under biaxial bending and axial tension was also considered in this expression [Hsu 1988].

Biaxially Loaded Slender R/C Columns: Farah and Huggins [1969] proposed the integration method to analyze the R/C columns subjected to biaxial bending. The integration method used in the analysis leads to three simultaneous nonlinear partial differential equations which are solved by a procedure based on Newton-Raphson method. The partial derivatives are the rates of change of force and moments with corresponding the corner strain in the strain distribution of a section.

Finite segment method, developed previously for wide flange steel columns under biaxial bending, was extended to analyze biaxially loaded R/C columns by Al-Noury and Chen [1982]. The column was treated as a space structure after segmentation. The sections were divided into finite elements of reinforcements and concrete in order to calculate its tangent stiffness properties at different levels of strain. The segment stiffness relationship was computed by solving the governing differential equations about the principal axes of the cross section. Nonlinearities due to material plasticity and geometrical change were handled by an iterative procedure based on the modified tangent stiffness approach. The force-deformation equilibrium equations of R/C columns

were also proposed. The moment-curvature-thrust relationships were obtained by step-by-step application of the force-deformation equilibrium equations.

Recently, Wang and Hsu [1990] and Tsao [1991] developed a numerical analysis to evaluate the complete load-deflection and moment-curvature relationships for square and L-shaped slender R/C columns subjected to biaxial bending and axial load. The analysis was based on an incremental deflection theory. A secant stiffness approach was used to model the material nonlinearity and a finite difference method was applied to calculate the curvatures. Idealized piece wise linear stress-strain curve was used for steel and concrete elements, respectively. Furthermore, both ascending and descending behavior of R/C columns under monotonically increasing load was successfully attained in his study.

1.2.2.2 Slender R/C Columns under Cyclic Axial Loading. Behavior of reinforced concrete columns subjected to a variety of loading conditions have been a subject of considerable investigation. In spite of a number of column studies which have been undertaken, there are still several important research topics which have been relatively unexplored. Also, some problems which have been extensively investigated are not satisfactorily resolved at all.

Of particular significance in the areas of unexplored problems are the factors that affect the column behavior under cyclic loading. Most studies on biaxially loaded column behavior are related to the monotonically increasing load. No published experimental or theoretical studies are yet available on the behavior of slender R/C columns subjected to cyclic axial compression with bidirectional eccentricities.

1.3 Statement of Originality

An accurate and rational analysis of reinforced concrete (R/C) structures requires satisfactory modeling of the behavior of concrete. The behavior of concrete is dependent

upon its load history. Although a considerable amount of effort has been directed at developing the concrete model under cyclic compressive loading, most original models can not be incorporated into the analysis of R/C structures. A reliable and substantial cyclic stress-strain relationship is needed for the analysis of structures subjected to repetitive loadings.

An experimental investigation and parametric study into the behavior of concrete under cyclic loading are performed in this study. The direction of physically motivated modeling of cyclic stress-strain relations will be suggested through the parametric study. Cyclic loading test will be conducted on cylindrical specimens under four different loading regimes. Stress-strain curves obtained for 3 in. by 6 in. concrete cylinders under cyclic loading will be presented and analyzed to calibrate the analytical expressions. Analytical concrete model will be proposed here to predict the behavior of concrete under random cyclic loading.

The behavior of R/C columns having various properties and subjected to a variety of loading conditions has been the subject of considerable investigation. There are still several important research topics which have been relatively unexplored. Of particular significance in the areas of unexplored problems are the factors affecting the column behavior under cyclic loading. There are not any published experimental and theoretical studies of the cyclic axial loading on the slender R/C columns subjected to biaxial bending. It should be noted that the cyclic compressive load with bidirectional eccentricities considered in this study is in the longitudinal direction, and not in the transverse direction, with respect to the column axis.

For the present experimental study, four foot long R/C columns are tested under cyclic axial compression with bidirectional eccentricities. The main parameter of column test are the bidirectional eccentricities and its angle to the reference axis. Ultimate strength, load-deflection and moment-curvature characteristics of R/C columns under cyclic axial load with double eccentricities are examined. Furthermore, a computer

model is developed here to simulate the behavior of R/C columns under combined biaxial bending and cyclic axial compression.

1.4 Objectives of Research

An experimental investigation and parametric study into the behavior of concrete under cyclic loading are performed as a part of this research work. The strategy of physically motivated modeling of cyclic stress-strain relationships is proposed through the parametric study. Stress-strain curves obtained for concrete cylinders under cyclic loading are presented and analyzed to calibrate the analytical expressions under the established strategies of reliable modeling. Analytical concrete model for cyclic loading is proposed to predict the behavior of concrete under random cyclic loading. Analytical expressions are made to describe the behavior of concrete that are practical and can be incorporated into a computer model for analyzing the reinforced concrete columns under cyclic loading. The possible flexibility of the proposed model should be able to minimize the gap between the material model and a real implementation. Cyclic loading tests will be conducted on 3 inches diameter by 6 inches high cylindrical specimens under the following four different loading regimes: 1) Monotonic, 2) Cycles to envelope, 3) Cycles to common points, 4) Cycles with random loading.

The objective of this column study, therefore, is to examine the behavior of various cyclic compressive load levels on the ultimate strength, deflection and moment-curvature characteristics of reinforced concrete slender columns with bidirectional eccentricities. Furthermore, a part of this research is to develop a numerical analysis that can simulate the behavior of reinforced concrete columns under combined biaxial bending and cyclic axial compression.

For the experimental study of column, four foot long reinforced concrete columns are tested under cyclic axial compression with bidirectional eccentricities. The main parameter of column test are the bidirectional eccentricities and its angle to the reference

axis. The load pattern considered in this experimental study is cycle to envelope which is a most typical load regime. The applied load is a full loading of cycles which is loading up to the envelope curve and then unloading down to nearly zero stress level. It should be noted that the cyclic axial compressive load with bidirectional eccentricities considered is in the longitudinal direction, but not in the transverse direction, with respect to the column axis. The experimental ultimate load, load-deflection and moment-curvature curves are compared with the prediction of computer model developed in this study.

CHAPTER 2

STRESS-STRAIN BEHAVIOR OF CONCRETE UNDER CYCLIC LOADING

To predict the stress-strain behavior of concrete under cyclic compressive loading, a cyclic model is developed in this chapter based on in-depth parametric study of available concrete models and the experimental results of the present study. Any analytical model developed must be able to represent the general behavior of concrete under different loading paths in the subsequent cycles. Furthermore, the developed model should be able to apply to various different envelope (monotonic) curves. However, most of the cyclic models available are restricted to the domain of their own experimental data.

2.1 Parametric Study of Stress-Strain Relationships

The material behavior can be simulated more satisfactorily by a physically motivated modeling. In other words, a modeling must keep the physical interpretation of analytical terms in mind. They can be expressed by empirical mathematical equations with a number of constants which are calibrated from the experimental data. This gives the empirical models a flexibility by an appropriate choice of the coefficients to achieve a best fit to the test results. However, the predicting power of these models is limited only to the vicinity of the experimental data from which they are derived initially. Therefore, the behavior of concrete may be simulated by the unified characteristics which are somehow distributed through the reliable previous models that simulate the basic features of concrete behavior.

Through the review of previous researches in chapter one, the neural network approach to model the concrete behavior provides a good suggestion that one or more model parameters may be predicted from the theoretical simulation. In addition, the major parameters, which is able to affect dominantly on the overall shape of cyclic

stress-strain curve, can be obtained from the semi-empirical way by combining the theoretical simulation and reliable range of experimental coefficients. Thus, extensive numerical and geometrical simulations are performed here to study the reliable modeling. Furthermore, simultaneous numerical and graphical simulations may be useful to calibrate the experimental parameters of present test results.

An in-depth parametric study is carried out to investigate into the behavior of concrete under uniaxial cyclic compressive loading. Available stress-strain relationships for concrete under both monotonic and cyclic compressive uniaxial loadings are implemented in a computer model to perform such a parametric study. The general cyclic behavior of concrete is examined, and several common characteristics are identified. The change of stiffness in a different stress-strain path, unloading strains on the envelope curve, unloading plastic (residual) strains, common points and reloading strains at the end of reloading curves are the major parameters that control general behavior of concrete under cyclic compressive loading. Available empirical stress-strain relationships for concrete under cyclic loading are analyzed in view of physical characteristics.

A symbolic manipulation procedure leading to the analytical operation of a related mathematical expressions is presented. New computer language MATHEMATICA [Wolfram et.al. 1988] is used to simulate the characteristics of stress-strain relationships.

Envelope Curve: An envelope curve defines a line in which no stress-strain curve exceeds regardless of its loading paths. Various curves for stress and strain of previous models are shown in Figure 2.1. They are nondimensionalized with respect to the maximum stress and peak strain corresponding to the maximum stress. The resulting normalized coordinates are: $U = f_c / f_c'$ and $S = \varepsilon_c / \varepsilon_o$. In Figure 2.1, the ascending branch of monotonic stress-strain curves fairly agrees with each other, but the descending branch shows considerable differences between certain models. Thus it can be concluded

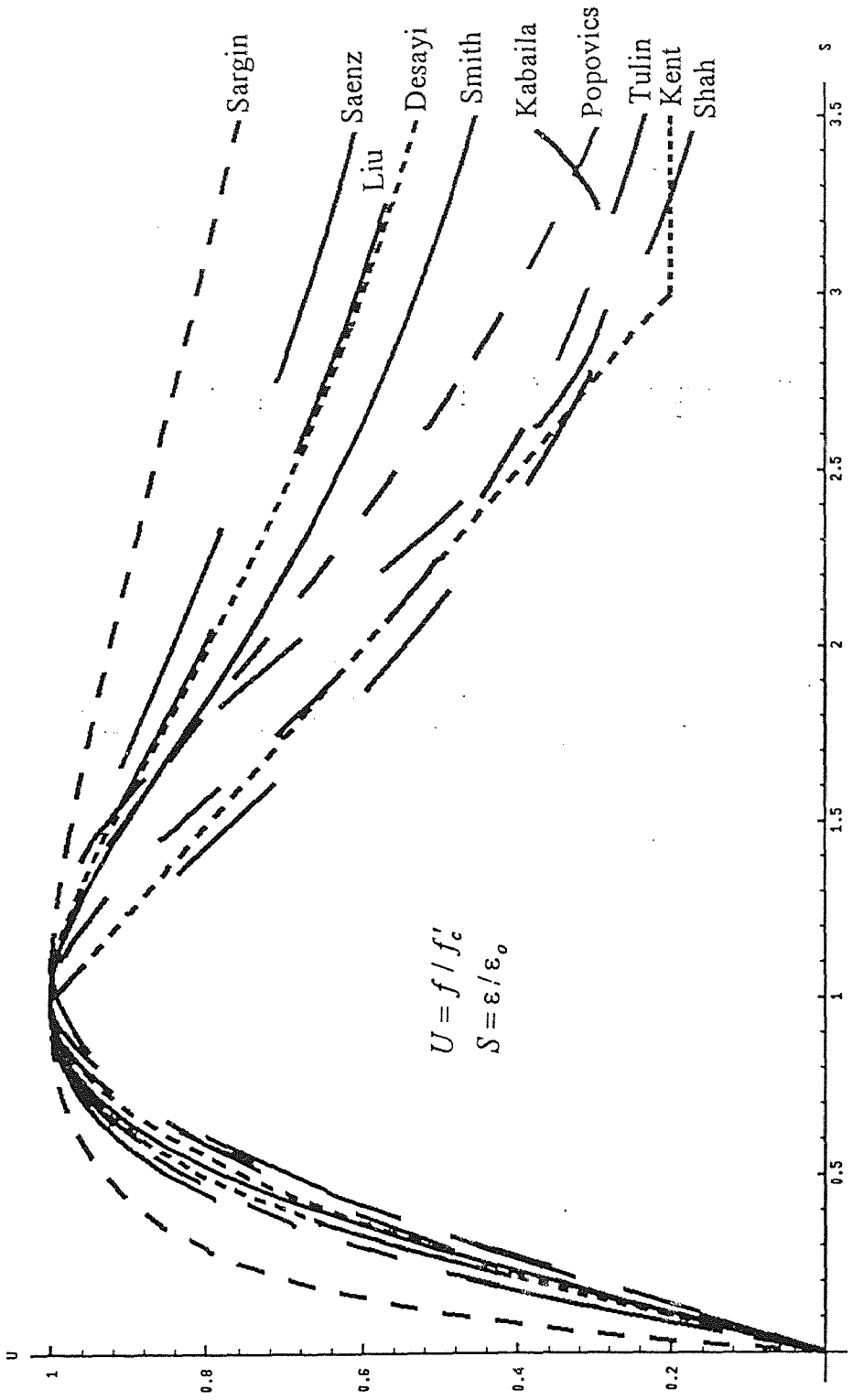

Figure 2.1 Comparison of Monotonic Stress-Strain Curves

that most empirical models of monotonic stress-strain curve for an envelope curve exhibit a more sensitive behavior in the descending branch than the ascending branch.

Common Point: The locus of points where the reloading curve of any cycle crosses the unloading curve is defined as common points and a closed hysteresis loop is formed in subsequent cycles. Karsan and Jirsa [1969] derived a mathematical expression for the common points .

This expression is in good agreement with an original envelope from which an initial mathematical formulation is developed as shown in Figure 2.2. However, when this expression is applied to other monotonic (envelope) stress-strain curve, it does not conform to a given model as shown in Figure 2.3. Thus it can be concluded that the common point limit depends on an adopted envelope curve. It is found that the mathematical expression of Karsan's common point model may have to be modified for other monotonic models of concrete. Furthermore, the location of common points has shown to vary with the type of loading applied in the present experimental investigation. Thus, it is concluded that the stress-strain relationships should be derived without using common points for a random cyclic loading which shows a more general loading pattern. But, in case of full unloading and reloading, the common point approach may be used, because it presents a more stable shape for each cycle with less sensitivity to the reloading strain through the present parametric study.

Plastic Strain: Nonrecoverable or plastic strains are defined as the strains corresponding to a zero stress level on the unloading or reloading stress-strain curve. During cyclic loading, the accumulation of plastic (residual) strain occurs for all type of loading regimes. There are no significant difference in the plastic strain between the confined and plain concretes. The trivial different formulation for both confined and unconfined concretes does not affect the overall shape of cyclic stress-strain curve.

The changes in the shapes of the cyclic stress-strain curves with increasing plastic strains suggests a relationship between the plastic strain and the nature of the unloading

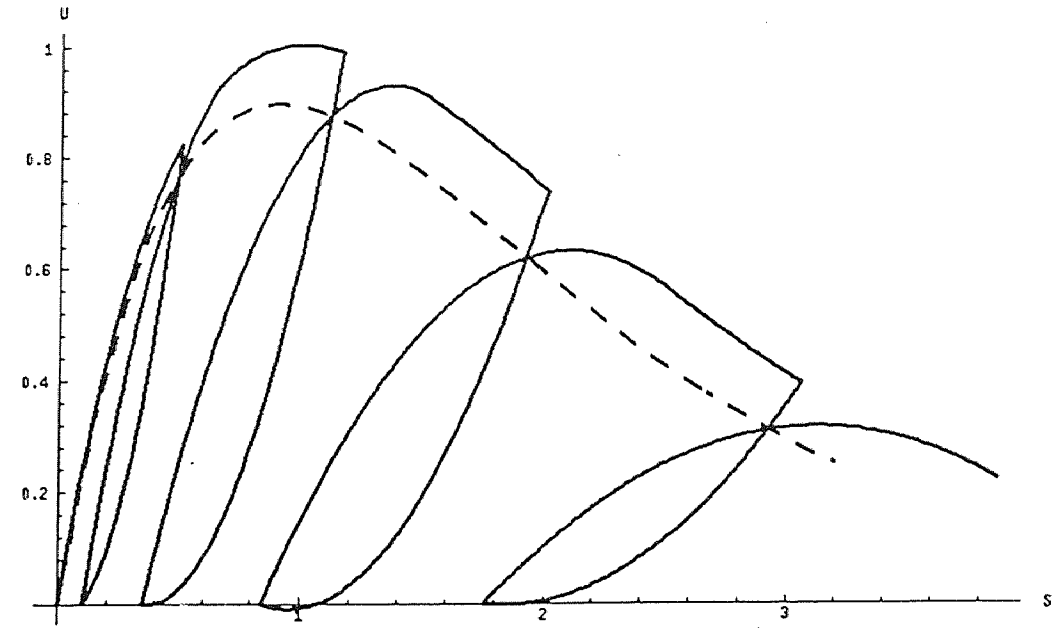

Figure 2.2 Karsan's Model with Original Envelope

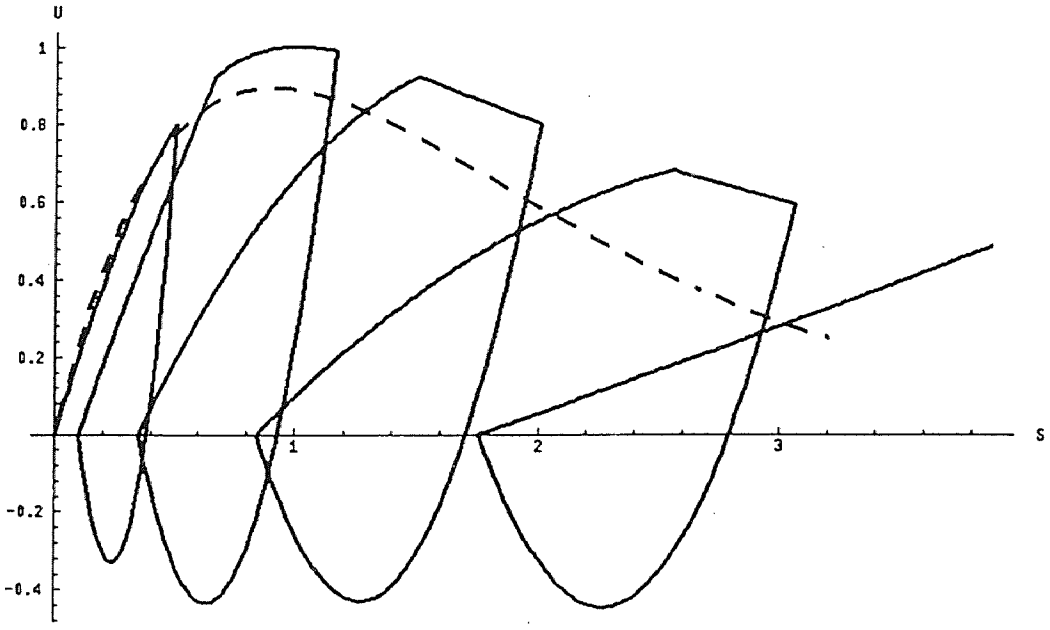

Figure 2.3 Behavior of Karsan's Model with Desayi's Envelope

and reloading curves. The previously developed expressions describe the low strain region satisfactorily, but show discrepancies with increasing strain.

Unloading and Reloading Curves: The unloading curve is characterized by its single curvature. The available unloading curve with different envelope curve which is not adapted in the developed models originally is presented in Figure 2.3. When a unloading curve is derived from a different envelope curve, physical contradiction can be developed. This phenomena may be caused by the highly nonlinearity of adopted mathematical equation type and/or severe asymptotic numerical behavior of formulation at near the plastic strain. Karsan's [1969] expression presents a unreasonable behavior in view of this physical sense. The predicting capability of such models is limited to the vicinity of the experimental data from which they are derived initially. This suggests a more physically motivated modeling is needed and argues for the formulation of an unloading curve that is less dependent on the envelope curve from which it is derived. Thus, the behavior of unloading curve may be simulated by the unified characteristics which are distributed through the reliable model.

The reloading curve is represented by a double curvature with mild curvature in the low stress level, and a sharp reversal in curvature just below the envelope curve. A similar phenomena is revealed when the expressions of reloading curve are applied with different envelope curve as shown in Figure 2.4. This unreasonable behavior of reloading curve is due to the severe asymptotic behavior at the vicinity of reloading strain on the envelope curve.

Through the extensive parametric study of previous work, the following important numerical and geometrical observations are attained. The numerical asymptotic behavior at near the major control points of cyclic stress-strain curve may present the unexpected manner and the complexity of adapted formulation is able to distort the overall shape of stress-strain curve under cyclic loading. The above mentioned phenomena can be developed when several different mathematical

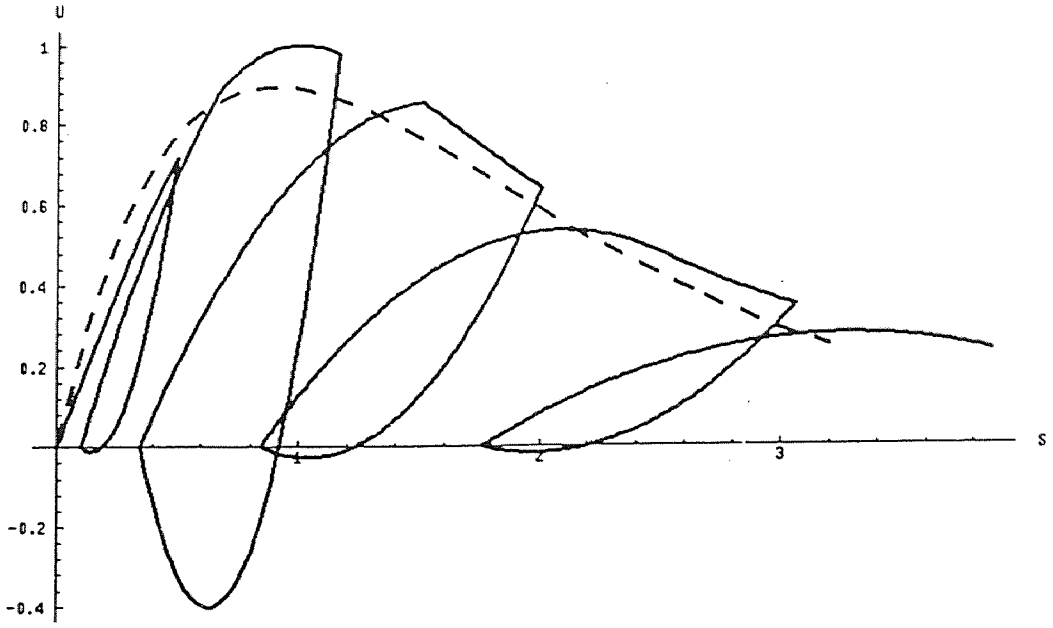

Figure 2.4 Behavior of Karsan's Model with Popovics's Envelope

expressions, those are highly nonlinear, should work together in a demanded direction. For example, infinitesimal change of unloading strain from the envelope curve causes the remarkable stress drop because of numerical sensitivity of selected equation type. And the concerned unloading cycle can not be controlled due to the rapid accumulation rate of reloading strain on the envelope curve.

Due to the above mentioned characteristics such as asymptotic behavior and complexity of mathematical formulation, the models previously developed for cyclic stress-strain relationships gives no flexibility to apply with certain experimental data and the previous models can not be responded to any future modifications. Thus, the strategy of mathematical formulation should be established to provide the flexibility of the model developed. In addition, more suitable type of equation for the each component of cyclic stress-strain curve have to be obtained to reflect the experimental characteristics of concrete under general cyclic loading patterns. The numerical behavior of adopted analytical expressions and the physical interpretation of mathematical terms should also be identified for the reliable cyclic model of concrete.

2.2 Physically Motivated Modeling

Analytical expressions of concrete behavior under cyclic loading may have to be recognized in view of both physical sense and numerical sensitivity. The following strategies of reliable modeling for cyclic stress-strain relationships are suggested through the intensive parametric study and theoretical simulations of related previous works.

Firstly, formulation of unloading and reloading curves should be independent or less dependent on mathematical expression of envelope curve which is adopted in the original model. Otherwise, the analytical model developed can not be applied with different monotonic stress-strain curves. This concept is directly related to applicability of the proposed model and flexibility of the mathematical formulation.

Secondly, the material behavior can be predicted more satisfactorily by a

physically motivated modeling that keeps the physical interpretation of the analytical terms for themselves.

Thirdly, the suitable equation types of each segment in the cyclic stress-strain curve may have to reflect not only the stable numerical behavior but also the growing change in graphical mode. Due to the sensitive numerical behavior of adopted equation types, overall shape of cyclic stress-strain curve for the proposed model may be distorted. Furthermore, the adopted functional shapes should reflect the dominant characteristics of concrete behavior in a different stress-strain path. Thus, it is important to identify a flexible equation types for different characteristics of concrete behavior under various loading patterns.

Based on the observations through parametric simulation and the test results of previous work, the flexibility of selected analytical expression seems to be essential to achieving the random cyclic stress-strain curve. The stress-strain curves obtained for cyclic loading tests will then be analyzed in the following sections, and an analytical model will be developed under the above mentioned strategies. The proposed model will be used to predict a yet untested stress-strain paths to examine the validity of the model developed.

2.3 Experimental Program

The purpose of the experimental program in this section is to investigate into the behavior of concrete under cyclic compressive uniaxial loading. The stress-strain curves obtained for 3 by 6 inches concrete cylinders under cyclic loading are presented and analyzed to calibrate the analytical model. A series of tests on the plain concrete cylinders are performed with four different loading patterns to be considered as the general loading types. The main test parameters are four different loading types under cyclic uniaxial compressions.

2.3.1 Test Specimens and Design of Test Parameters

The specimens are 3 inches in diameter by 6 inches in height cylinders of normal concrete. Photographs of instrumented concrete cylinder specimen are shown in Figure 2.5.

The concrete mix proportions are constant for all test specimens as shown below in weight ratio.

$$C : S : A : W = 1 : 2 : 2.5 : 0.55$$

The concrete is a blend of Type III Portland cement, local river sand, aggregate of 3/8 inches (maximum size), and water. The concrete was cast into a cylindrical mold and the concrete cylinders were kept at casting room for one day. Then they were cured under water for one week, and were left for drying after curing. Prior to testing the specimens were capped with sulphur compound at both ends.

Most of previous experimental researches focused on certain loading patterns. Patterns of loading may be classified into two categories based on the available test results and analytical models. The first one is that the unloading starts from the envelope to near zero stress level and then the reloading starts from near zero stress level to the envelope curve. The second one is that the unloading and reloading repeat themselves at the specified stress levels within the envelope curve.

However, behavior of various elements in a structural system may not fall into any of the above mentioned categories. For example, a loading may hit the envelope curve in a cycle and may not reach the envelope curve in the subsequent cycles. Such a behavior can be only presented by an empirical and/or mathematical model having a capacity to simulate random cyclic loading of a more general loading type. The stress-strain relationships under condition of general loading is necessary to reflect an observed behavior of the structural components.

To investigate into the stress-strain response of concrete under cyclic loading, four different loading regimes are employed in the following:

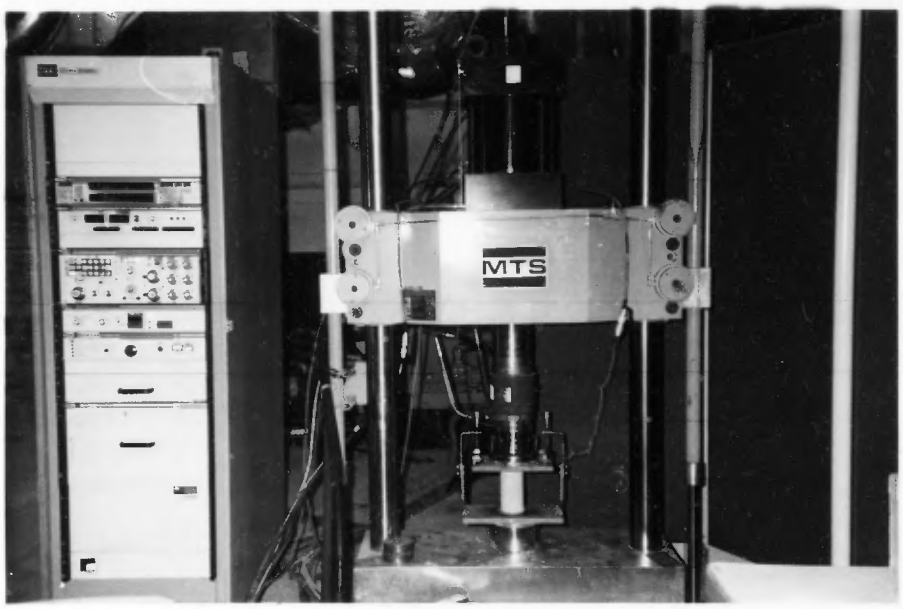

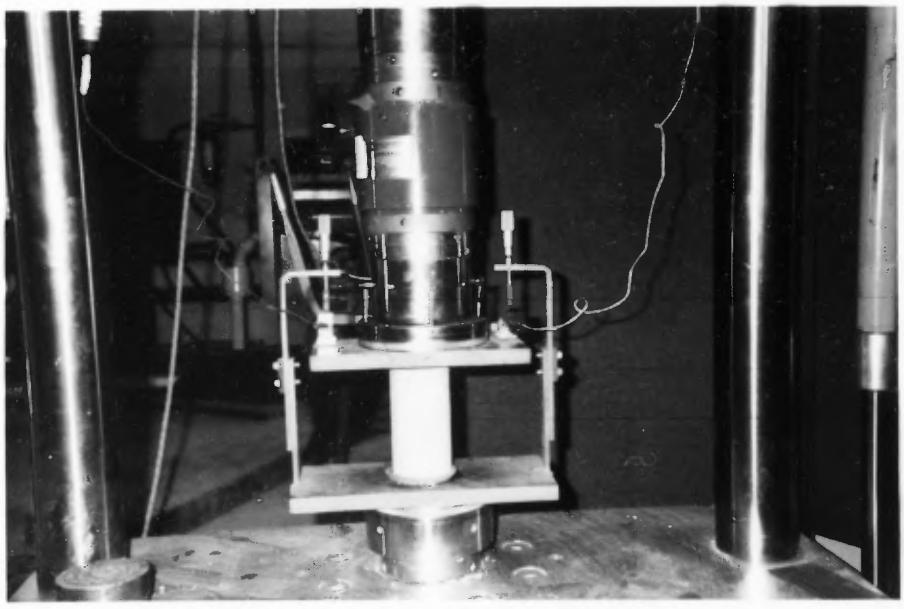

Figure 2.5 Set-up of Concrete Cylinder Test

1) Monotonic loading.

2) Cycles to envelope curve.

3) Cycles to common point.

4) Cycles with random loading.

Monotonic compressive tests are performed on concrete specimens with each batch and each applied loading type to determine the complete monotonic stress-strain curve, including the ascending part and descending part. These data are needed to determine the applicability of the envelope curve concept to concrete used in this tests.

The second cyclic loading scheme, cycles to envelope, is unloading to near zero load level, then reloading from the plastic strain at zero load. The resulting envelope curve will be compared with a monotonic stress-strain curve from the same batch. The empirical relationship between the unloading strain on the envelope curve and the plastic strain at the end of unloading will be studied.

The third cyclic loading pattern, cycles to a common point, is a repeated loading up to each common point and then unloading to zero load level. The common point is a location where the reloading curve crosses the unloading curve. This loading type is employed to study the accumulation rate of reloading strain from the end of unloading point to a common point because the slope of the reloading curve varies nearly linear but changes sharply after the common point.

The fourth cyclic loading regime, cycles with random loading, is involved with the combination of all possible loading patterns. There are full unloading and full reloading, full unloading and partial reloading, partial unloading and full reloading, and partial unloading and partial reloading. This loading pattern is a more general case than the above mentioned one and is selected to provide an additional information. This data may be found useful in calibration of the analytical model for the case of random cyclic loading.

These four different load patterns adopted are shown in Figure 2.6 through 2.9. It

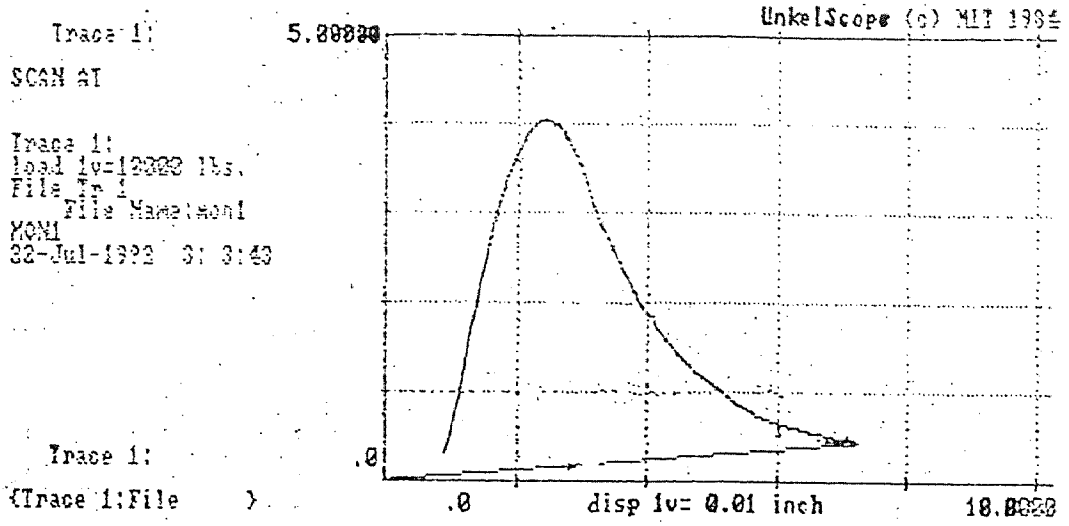

Figure 2.6 Load Type of Monotonic Loading

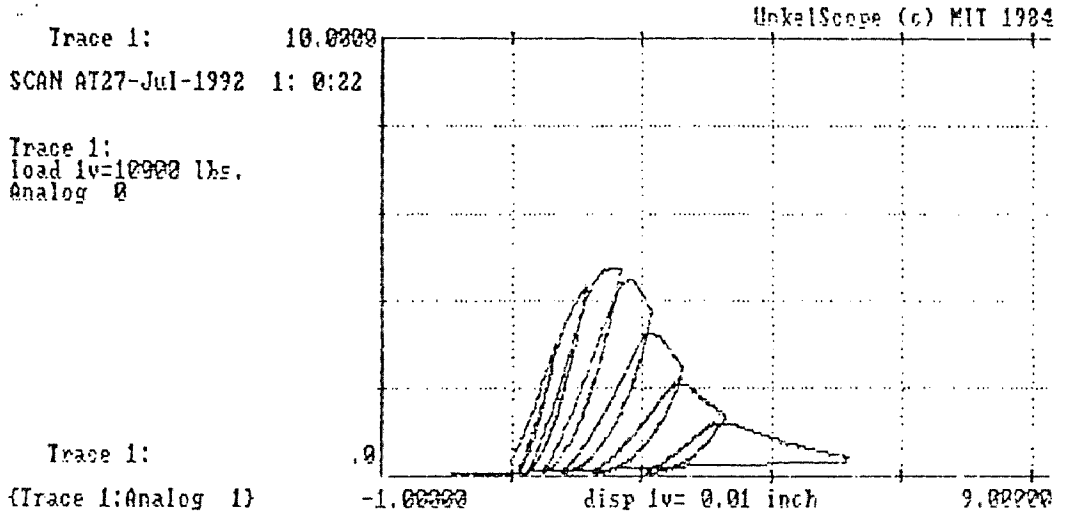

Figure 2.7 Load Type of Cycles to Envelope

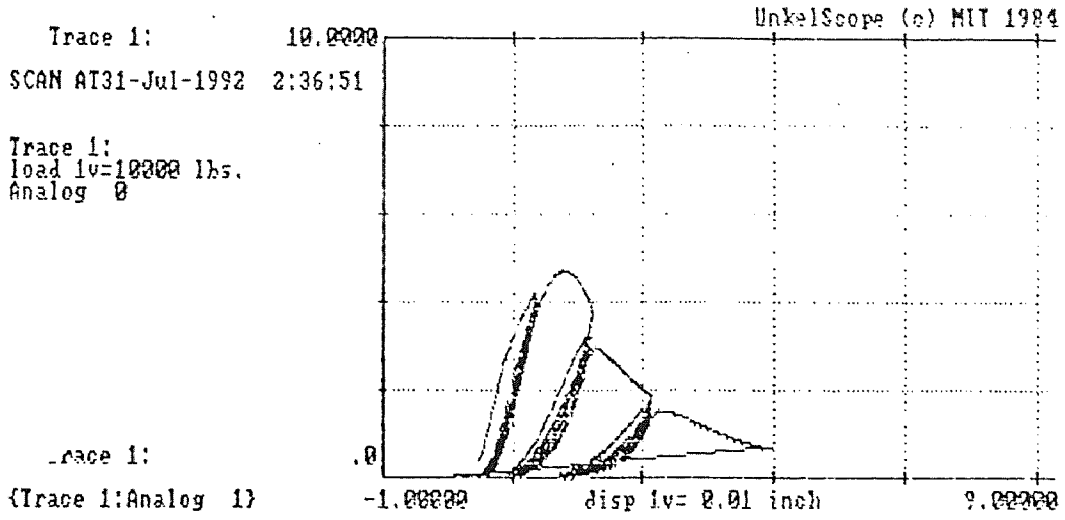

Figure 2.8 Load Type of Cycles to Common Points

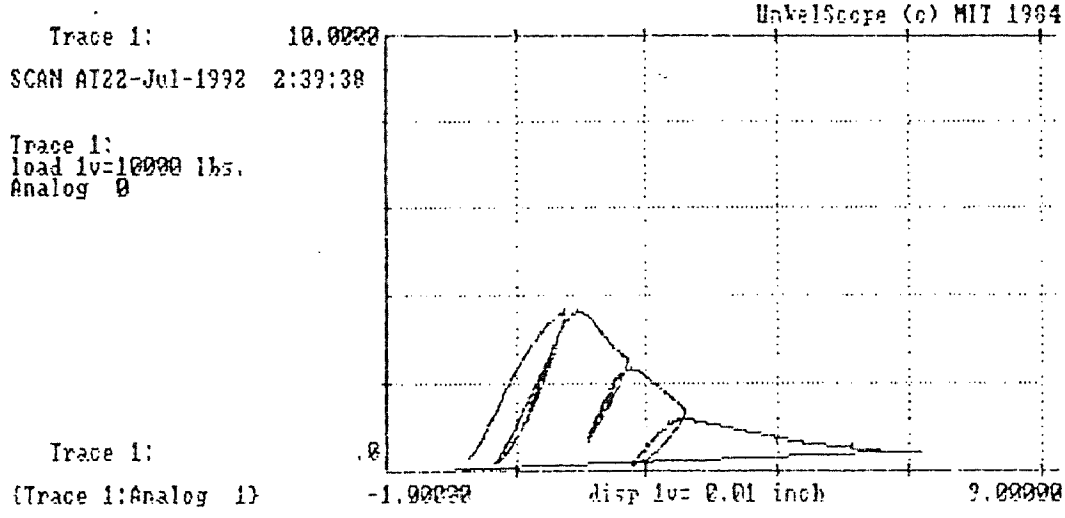

Figure 2.9 Load Type of Cycles with Random Loading

should be noted that Figures 2.6 through 2.9 present the results of an electron screen.

2.3.2 Test Control and Data Acquisition

The tests were carried out by a closed loop servo controlled material testing system (MTS) with a hydraulic capacity of 100 kips. During testing, the load and deformation data are recorded in the form of analog signal and stored by the data acquisition system. The data acquisition system consists of an IBM DACA converter which is installed in the personal computer and UnkelScope software. This DACA board converts an analog which is generated from the testing machine into the digital output and the sampling speed at 0.5 Hz is controlled by the setting of UnkelScope. The sampling rate of data can be adjusted according to the applied strain rate, so that the tests having thousands of data can be fully recorded. After the data is obtained, it is translated by the UnkelScope and is computed to obtain a real stress and strain quantity in order to produce stress-strain plot of the specimen. A procedure of present data acquisition can be found in Figure 2.10.

The testing machine has the capability to control test using load control, strain control, and stroke (displacement) control. All tests for different patterns of loading were performed under strain control to achieve both the prepeak and post peak ranges of stress-strain curve. The clip-on gage (MTS model 632.03B-20) are installed to measure the displacement of test specimen (see Figure 2.5). The working range calibrated for 10 volt full scale output from a MTS transducer conditioner is 0.20 inches for the gage used in this experiment. The strain rate used in this study is the static strain rate of 16.7 microstrain per second and the estimation of applied strain rate is in the following:

specimen height in loading direction: 6.0 inches

working range of gage: 0.20 inches

selected strain percentage: 50 %

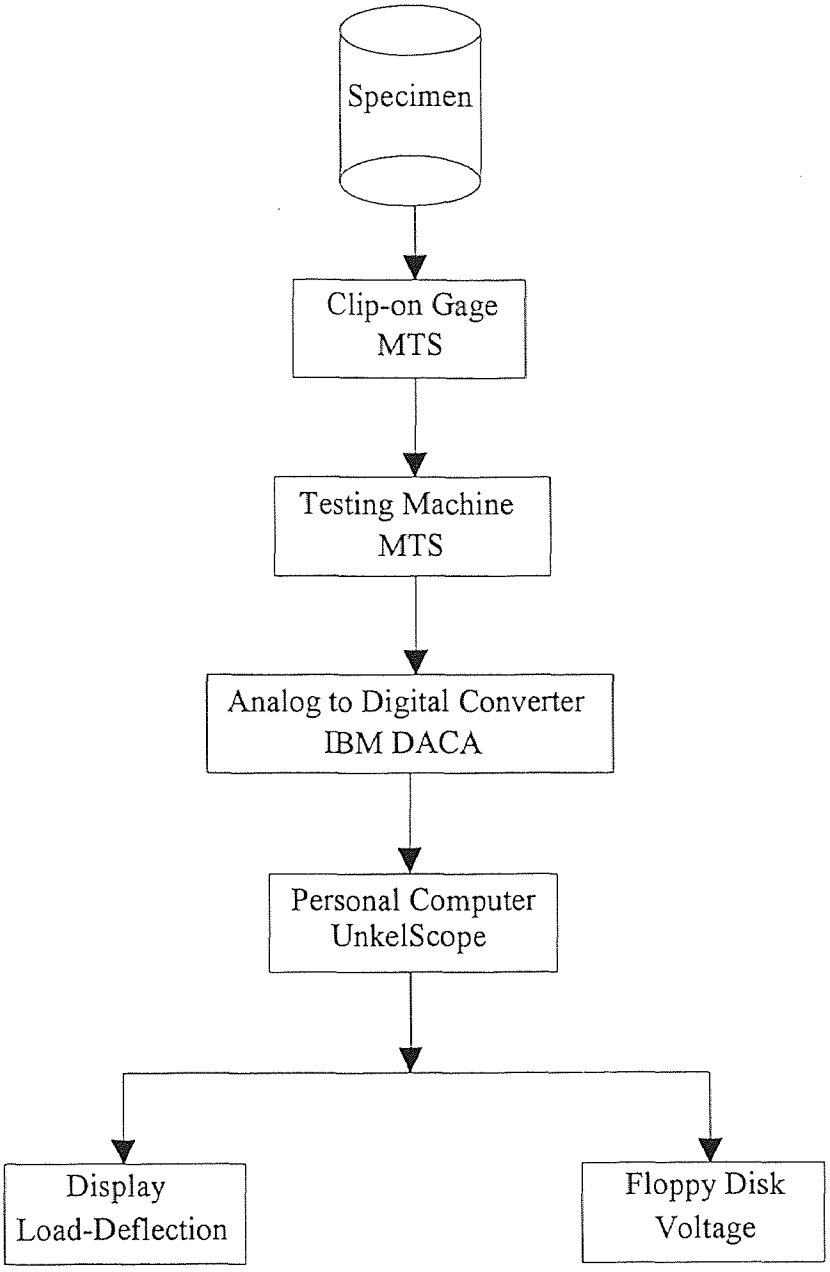

Figure 2.10 Procedure of Data Acquisition for Concrete Cylinder Test

selected frequency: 1.0x10^3 Hz = 1/(1.0 x 10^3) sec.

ε° = {(0.2 x 50/100) / 6.0} / (1.0x10^3)

= 1.67x10^-5 ε /sec = 16.7 με / sec.

It should be noted that the thickness of sulphur capping is neglected in determining the above strain rate.

The unloading and reloading are carried out at the interested load level by a digital function generator (model 410) which generates a wave form output. Other manual operation of MTS can not handle the extremely constant strain control during the different loading path of cyclic loading. The testing machine is controlled by a set-point until the load is near zero then reloading starts automatically by a function generator. A ramp wave form output is employed to generate the cyclic loading in this experiment.

2.4 Analysis of Cyclic Loading Test

This section describes the experimental results of concrete subjected to cyclic axial compressions. The deformation of specimens could not be taken directly from the recorded digital signal. The recorded data in the form of voltage corresponding to load and deflection were processed to convert it into the real mechanical quantity. The data processing scheme is shown in Figure 2.11. As mentioned in section 2.3, that four different loading patterns are used in this investigation.

The monotonic loading test was conducted for each series of specimens. In general, the stress-strain behavior observed is typical of that found in the concrete subjected to monotonically increasing axial compression. Figure 2.12 illustrates a typical response under monotonic load. Plain concrete usually fails in a brittle manner, caused by multiple failure planes. The asymptotic behavior of stress-strain curve shows in a very high strain range of the descending branch.

A generally accepted behavior for concrete under cyclic loading is that of an envelope curve, which provides a bound between the upper limit and lower limit for the

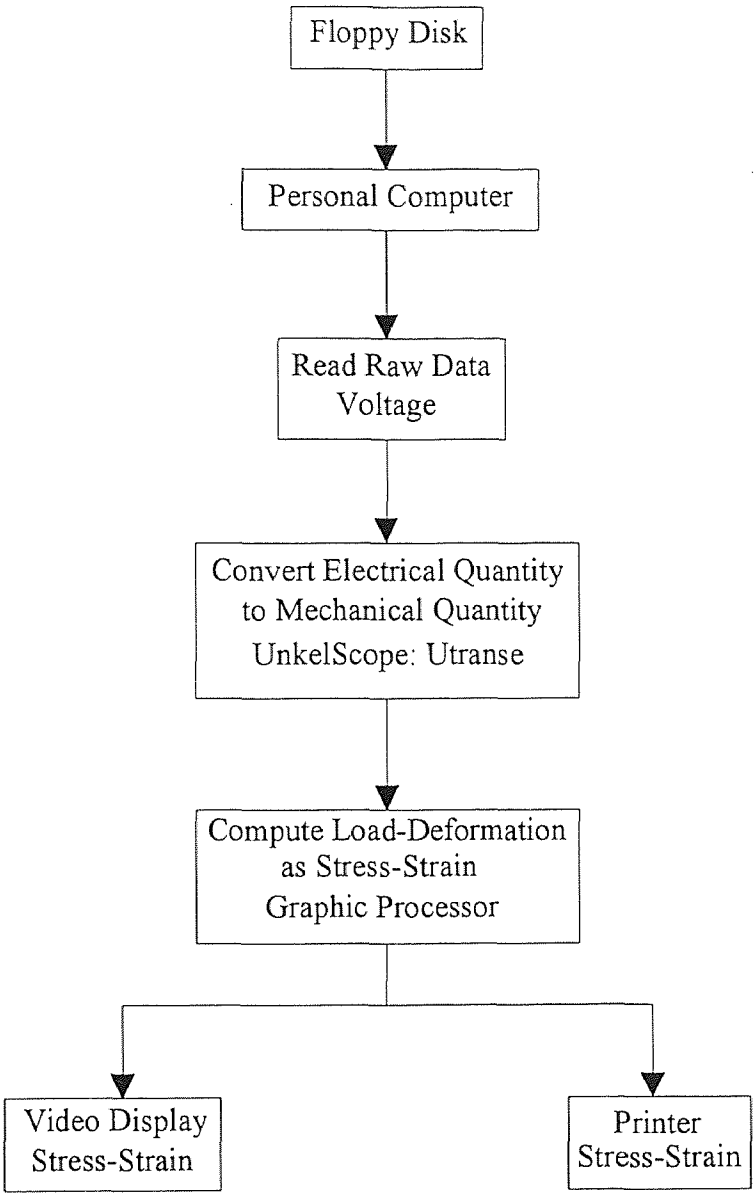

Figure 2.11 Data Processing Scheme

stress-strain curve, can be obtained under different loading paths. The existence of an envelope curve for a concrete can be studied by comparing the test results of cycles to envelope curve with the corresponding test results of monotonic loading. As shown in Figure 2.13, this suggests an existence of the envelope curve for a concrete subjected to cyclic axial compression and may be considered to coincide with the stress-strain curve under monotonic load.

Residual or plastic strains are defined as the strains corresponding to a near zero stress level on the unloading stress-strain path. The envelope unloading strains and plastic strains can be obtained by the load type of cycles to envelope curve. The observed changes in the shape of the stress-strain curves with increasing plastic strains suggest a relationship between the residual strain and unloading strain on the envelope curve. The increase in envelope unloading strain causes approximately the same increase in the accumulated residual strain.

In case of full unloading and full reloading, the common points limit shows a stable shape in the entire strain range of stress-strain curve. In the random cyclic loading, however, the position of common points depends on the stress level of previous unloading path as shown in Figure 2.13. In other word, the location of common points varies with the type of loading applied. This implies that the stress-strain relationships may have to be derived without using common points for a more general loading pattern.

The unloading and reloading curves obtained in tests do not coincide and are not parallel to the initial loading curve. The average slope of the unloading and reloading curves is inversely proportional to the plastic strain. This implies that there is a definite stiffness degradation for the entire strain range of stress-strain curve.

The reloading strain at common points after completion of the first full unloading is plotted against the envelope unloading strain in Figure 2.14. The envelope reloading strain versus envelope unloading strain curves are shown in Figure 2.15. The overall shapes of the curves in Figure 2.14 and 2.15 show the similar trend. This implies that the

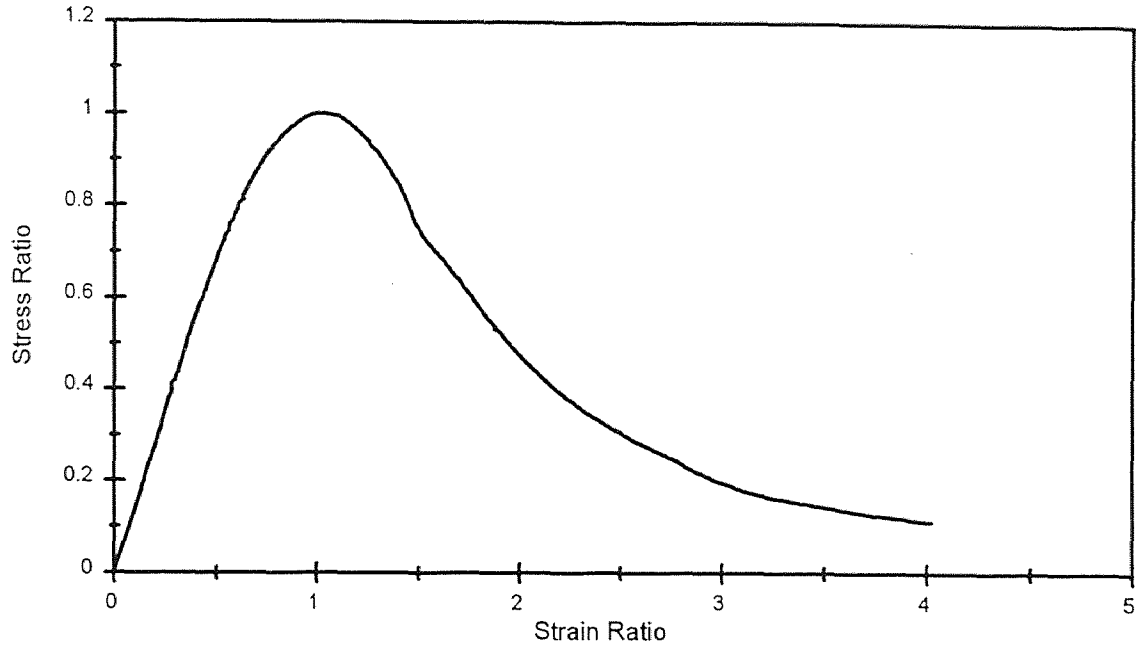

Figure 2.12 Stress-Strain Curve under Monotonic Loading

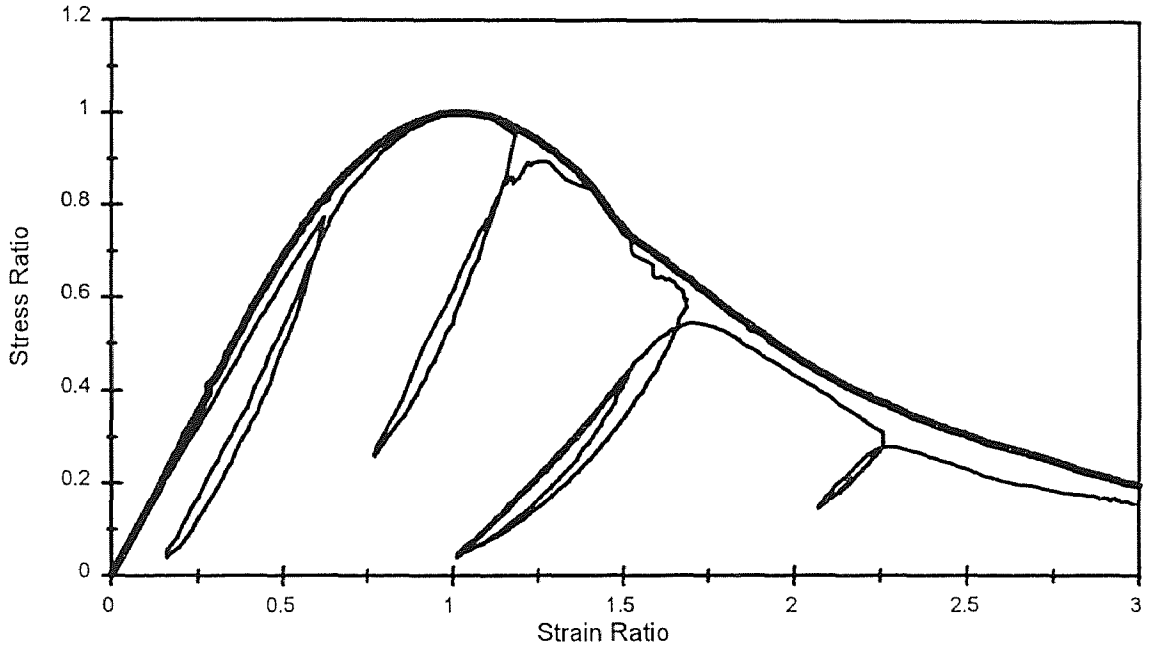

Figure 2.13 Cyclic Envelope Curve and Monotonic Stress-Strain Curve

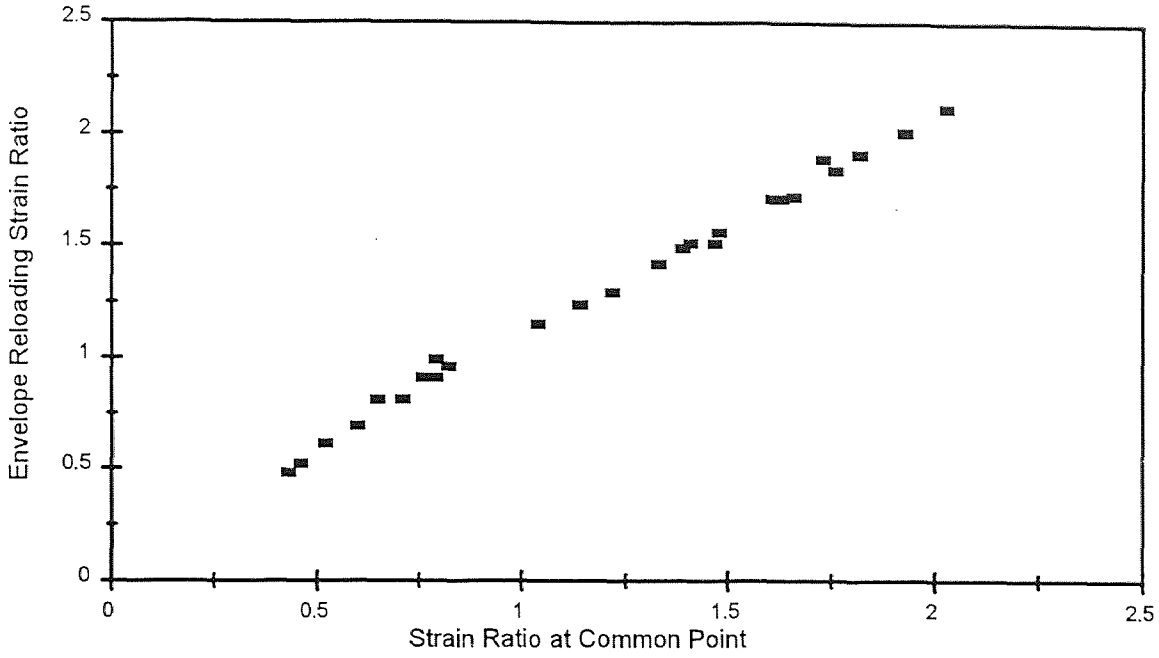

Figure 2.14 Relations between Common Strain and Envelope Reloading Strain

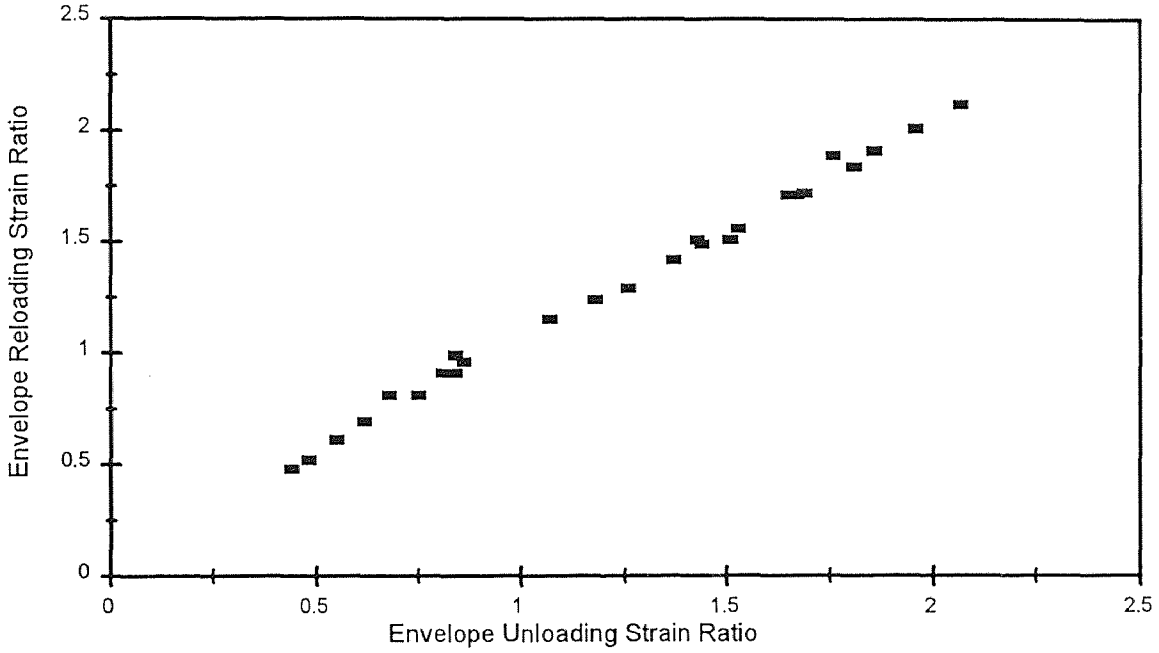

Figure 2.15 Relations between Envelope Unloading and Envelope Reloading Strain

accumulation rate of reloading strain can be defined regardless of different stress level in a reloading path. This observation through the random cycles enables to model the partial reloading curve. Therefore, it is possible to define the corresponding envelope reloading strain at the end point of certain stress level in the partial reloading path. However, in most previous research, it was generally accepted that the accumulation of reloading strain could be only defined at the maximum stress level, i.e. on the stress of envelope curve.

It is true that there are difficulties to obtain the actual point of reloading strain on the envelope curve due to the uncertainty of experimental data. It is not desirable to determine the relationship between the envelope unloading strain and envelope reloading strain solely based on the experimental data. Also, due to the highly nonlinearity of the cyclic stress-strain curve, the coefficient for this relationship may also be obtained through the theoretical simulation which gives a more reasonable overall shape of the stress-strain curve. Thus, the stress-strain relationships will be determined by a semi-empirical way.

It is necessary to consider the cases of partial unloading and partial reloading to predict the concrete behavior subjected to random load history as shown in Figure 2.16. In most previous work, the basic characteristics of concrete response were derived from the test results of full unloading and full reloading patterns. The test results of concrete under random cyclic loading are not yet available upto date. The test results of this type should also be employed to study any proposed mathematical expressions for random cyclic loading.

2.5 Modeling of Concrete under Cyclic Loading

This sections is devoted to developing the analytical expressions of stress-strain relationships for concrete subjected to cyclic compressions. The model developed is based on the results of parametric study and experimental data obtained for the present

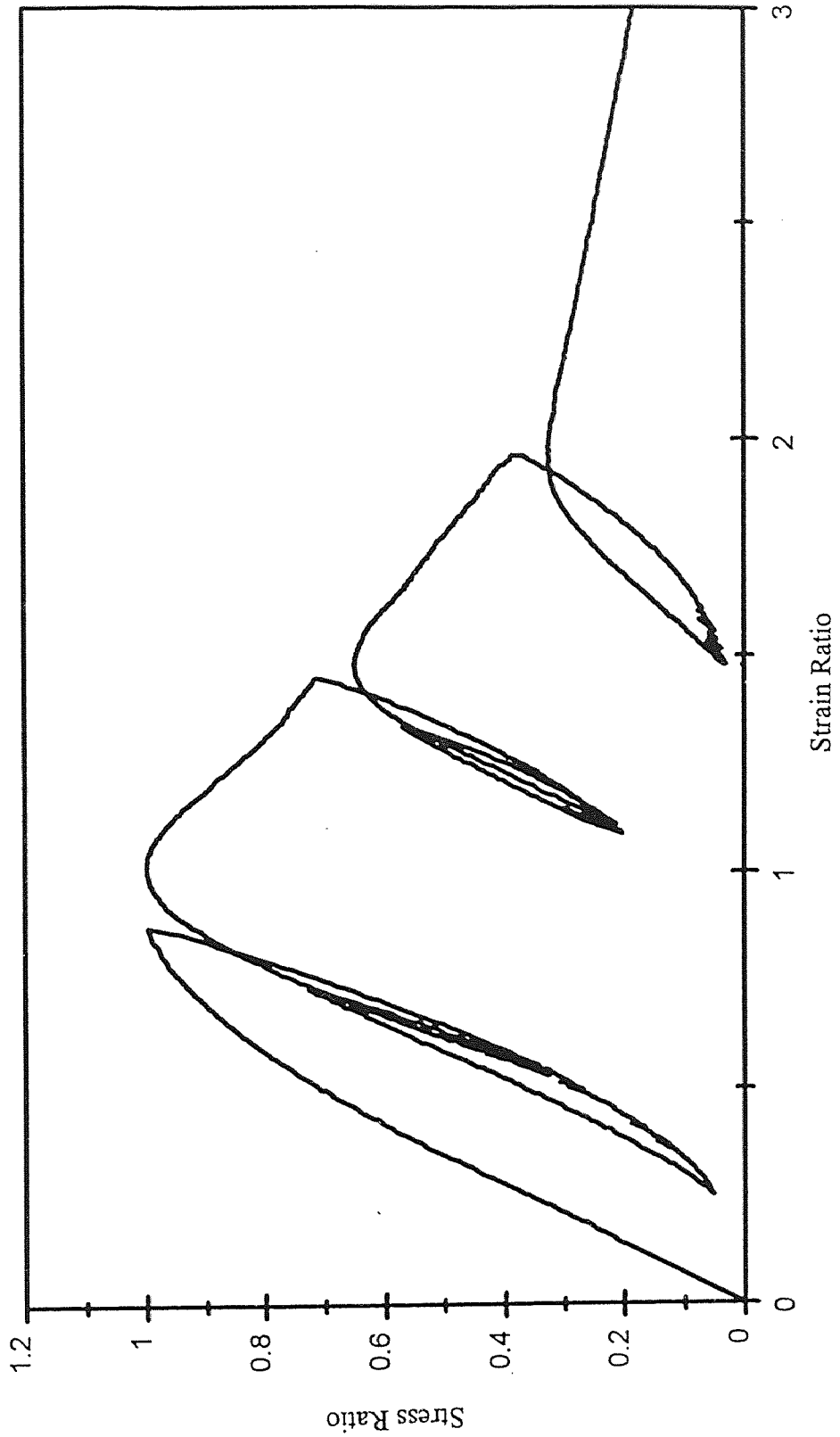

Figure 2.16 Stress-Strain Response to Random Cyclic loading

study. In order to predict the behavior of concrete under general loading patterns, each characteristic on the different stress-strain path should be incorporated into the mathematical formulations.

The model parameters are determined from both considerable amount of theoretical predictions and experimental data. It should be noted that certain test parameters for the cyclic loading can not be obtained clearly by the experimental results. Due to the variable nature of concrete behavior, it is more reasonable to provide the range of test results. Furthermore, this will give more flexibility to the developed concrete model for future modification. Thus the model developed is a semi-empirical one.

Numerical computations and graphical presentations are needed to determine a preliminary mathematical equation of the cyclic stress-strain curves. Procedures for the automatic generation of graphic stress-strain curves are needed to reduce the amount of work involved in the construction of stress-strain curves. For this purpose, new language MATHEMATICA, which is able to perform the symbolic operation and graphic presentation, is adopted.

Considering the highly nonlinearity of cyclic stress-strain relationships, the conventional procedures for curve fitting can not handle this problem. Furthermore, it is very difficult to develop the mathematical expressions by curve fitting that present a reasonable overall shape of cyclic stress-strain curves. Thus, a computer model for numerical and graphical simulation of analytical expressions has been developed here to analyze the experimental data and to predict the model parameters. This computer model may be linked to analyzing the reinforced concrete structure with appropriate interface. Also, it is possible to stand alone as a simulator for studying the stress-strain behavior of concrete under cyclic loading.

There is no need to develop a specific model for a monotonic stress-strain curve. It is because that the developed cyclic stress-strain relationships for general load patterns

can also be used for various monotonic stress-strain curves. Thus, the present analytical model provides a flexibility. The mathematical formulations, the flexibility of mathematical expressions, the physical interpretation of analytical terms and the identification of suitable equation type are discussed in the following.

At the present study, the flexible type of equations is defined as the one that the model parameters are corrected to fitting certain test results while the overall shape of cyclic stress-strain curve is preserved. Contrary to the flexible type of equation, the sensitive equation type is defined that if one or more parameters of the model is changed, the overall shape of stress-strain curve is distorted due to the locality of adopted test data. Thus it is very important to use the flexible equation type for each characteristics of concrete behavior under cyclic loading. The dominant characteristics of concrete behavior are the behavior of plastic strains, unloading curves, reloading strains and reloading curves for the entire range of strain regardless of full or partial unloading and reloading.

In this section, coordinates for stress and strain of the modeling procedure are nondimensionalized with respect to the maximum stress and peak strain corresponding to the maximum stress. The resulting normalized coordinates are $U = f / f_c'$ and $S = \varepsilon / \varepsilon_o$. Hereafter, the stress and strain are discussed as the ratio of stress and strain, respectively, in the normalized coordinates.

Plastic Strain: In the previous researches, most mathematical relationships between the envelope unloading strain and plastic strain were developed from the plasticity concept. A strain contains the elastic strain and plastic strain as shown in Figure 2.17. This means that the linear relationship between the unloading strain and residual strain is used. This concept may not be adequate to describe the descending branch of stress-strain curve due to the higher accumulation rate of plastic strain in a high strain range. In other word, the recoverable strain ($\varepsilon_e = \varepsilon_u - \varepsilon_p$) is greatly reduced when the envelope unloading strain is increased. Also, there is an asymptotic behavior of

$$\varepsilon_u = \varepsilon_e + \varepsilon_p$$

$$\varepsilon_p = \varepsilon_u - \varepsilon_e$$

$$\varepsilon_p = \varepsilon_u - f[\varepsilon]$$

ε_u = *Envelope Unloading Strain*

ε_e = *Elastic Strain* (Recoverable)

ε_p = *Plastic Strain* (*Nonrecoverable*)

$f[\varepsilon]$ = *Function of Strain*

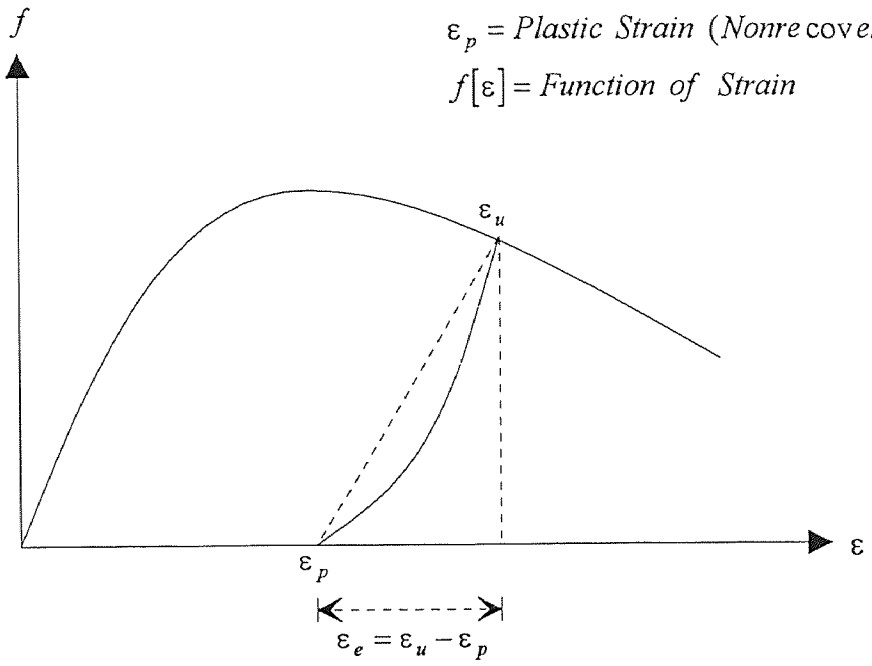

Figure 2.17 Plastic Strain and Recoverable Strain

plastic strain in the low strain region. As discussed previously, a suitable type of analytical expression can be used to reflect these characteristics directly.

Through the numerous simulation of different type in mathematical expressions, the power type equation is obtained for the relationship between the envelope unloading strain and plastic strain as shown Figure 2.18. Although a single term of a polynomial is not accurate as the multiple terms of a high order polynomial to predict the certain test data, the adopted single term expression does not sacrifice the above mentioned behavioral characteristic of concrete and its mathematical flexibility. The geometrical shape of adopted equation type also gives a reasonable shape with various parameters. This implies that the obtained equation type behaves reliably according to the provided experimental data. Thus, the proposed analytical relationships between the unloading strain and plastic strain can be written as:

$$S_{pu} = c_p (S_{eu})^{n_p} \tag{2.1}$$

Where S_{pu} is a unloading plastic strain ratio, S_{eu} is a unloading strain ratio on the envelope curve, c_p is a coefficient of plastic strain and n_p is an optimum order of proposed equation type in the concerned test data. The change of n_p will provide change in curvature of a curve shape for future modification.

The proposed equation also satisfies the theoretical boundary condition with which the plastic strain is always greater than zero or equal to zero in the range of compressive strain ($S_{eu} \geq 0$). A comparison of the above type equation with the test data of $S_{pu} - S_{eu}$ is shown in Figure 2.19. A constant of c_p is suggested as 0.30 based on the present test results for full unloading and reloading cycles and order of n_p is 2 which is an optimum for the present study. It is noted that the constant c_p will be modified for the cycle with random loading and a certain comparison. It is obvious that these coefficients can be adjusted to the certain experimental results.

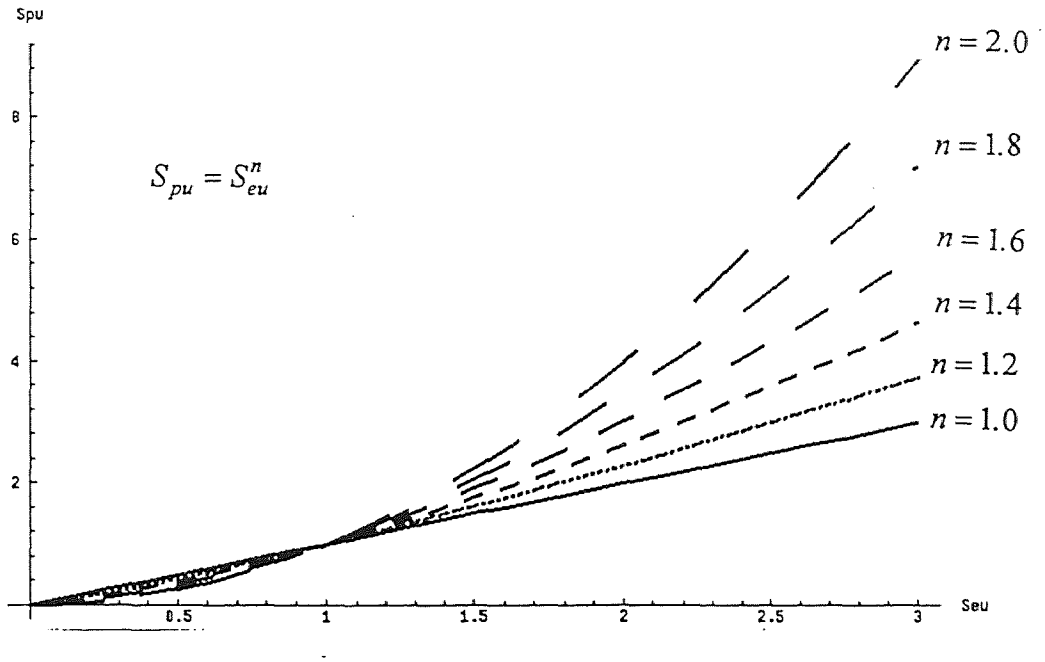

Figure 2.18 Adopted Power Equation Types for Plastic Strain

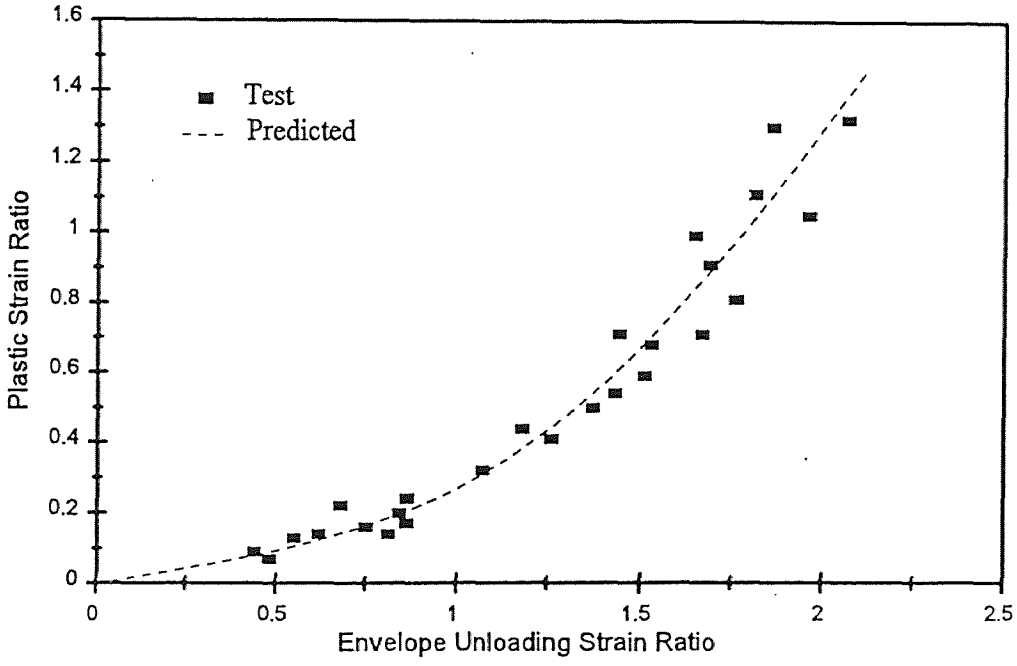

Figure 2.19 Relations between Plastic Strain and Envelope Unloading Strain

This analytical expression may be used for both plain or confined concrete. It is well known that the lateral confinements affect on the shape of envelope curves substantially but there was no significant difference in the plastic strain between the confined and plain concrete. This implies that the trivial different mathematical expressions do not affect the overall shape of cyclic stress-strain curve.

It should also be mentioned that the unloading plastic strain can be only obtained by full unloading from an envelope curve to the zero stress level in experiments. This suggests that the plastic strain can only be determined quantitatively by the unloading strain on envelope curve. This observation is very useful to obtain the plastic strain when the previous history of stress-strain path is of partial reloading. Thus, for the case of partial reloading, the proposed mathematical expression of plastic strain can be used at any stress level once the corresponding envelope unloading strain at the end point of partial reloading is found.

Reloading Strain: The reloading strain on the envelope curve can be formulated as either of the unloading strain or plastic strain. Observing the arbitrary single cycle of stress-strain curve, the envelope reloading strain is always greater than the envelope unloading strain. In case of partial unloading or partial reloading, the plastic strain at any stress level is always less than the reloading strain at any stress level on the reloading path that followed by full unloading. Because random cycles are a suitable combination of partial unloading and/or partial reloading stress-strain path, this observation enables to model the behavior of concrete subjected to random cyclic loading. Considering the highly asymptotic behavior of reloading curve near the envelope curve, a more accurate determination of envelope reloading strain may reduce the flexibility of mathematical formulation. Thus it is desirable to provide the reasonable range of experimental parameter rather than the value of specific test coefficient.

It is necessary to formulate the envelope reloading strain as a function of envelope unloading strain rather than the plastic strain. This leads to a unified

formulation because the plastic strain is expressed as a function of envelope unloading strain. For this purpose, the relation between the reloading strain and the unloading strain is shown in Figure 2.20. The results of tests can be approximated as:

$$S_{er} = S_{eu} + \delta S_{er} \tag{2.2}$$

Where S_{er} is a reloading strain on the envelope curve and δS_{er} is the difference between unloading strain and reloading strain on the envelope curve for full unloading and reloading cycles.

It is unavoidable to approximate the reloading strain due to the uncertainty of true reloading strain points on the envelope curve. In other word, the end points of reloading curves can not be obtained clearly in the test results. This implies that the reloading curve can be predicted in a comparatively simple shape. Observing the scatter is expanded when the unloading strain is increased, it is better to employ two parameters of δS_{er} in the prepeak range and post peak range of strain, respectively. The range of two parameters is between 0.05 and 0.12 and the specific coefficients are conformed to the observation of the overall shape of stress-strain curve.

For the case of random cyclic loading, the envelope reloading strain can be obtained by the end point of partial unloading. It is reasonable to suggest a unified reloading strain for both plain and confined concretes, due to the uncertainty and growing scatter of test results. Furthermore, the reloading strain can be determined from an arbitrary stress level of full or partial unloading that always exists below the monotonic (envelope) curve regardless of plain or confined concrete. The behavioral characteristics of confined concrete is tremendously affected by the shape of envelope curve.

Unloading and Reloading Curves: By observing the characteristics of unloading curve from the test results, numerous possible types of equation are presented

in Figure 2.21 through 2.23 for comparison. These tentative equation types are power function, polynomial and exponential types. The simplicity of formulation will be considered for a random cycle, although the obtained test results can be predicted by three different types of equation.

By observing these different types of mathematical expressions, it seems that the power type of equations gives a more stable curve shape with different parameters than those of polynomial and exponential types. It should be noted that the model flexibility is decreased as the number of functional terms and number of model parameters are increased. The experimental unloading curves show a noticeable sensitive behavior at the vicinity of envelope unloading points. Thus the power type of equation is employed to model the behavior of unloading curves in both ascending and descending branches of stress-strain curve. The adopted equation type should also be able to reflect the demanded curvature in the curve shape, because the degree of nonlinearity in the unloading curve are varied throughout the entire strain range of stress-strain curve.

The shape of unloading curve is strongly dependent upon the location of unloading plastic strain rather than the envelope unloading strain. Assuming that the unloading curve varies linearly from the envelope unloading strain to the plastic strain as shown Figure 2.24, the following linear relationships can be written as follows, where a point (S,U) is located at any location on the assumed straight line for unloading:

$$\frac{S - S_p}{S_{eu} - S_p} = \frac{U}{U_{eu}} \tag{2.3}$$

Where S_p is a plastic strain ratio, S_{eu} is a unloading strain ratio on the envelope curve and U_{eu} is a envelope unloading stress ratio at the corresponding strain ratio on the envelope curve.

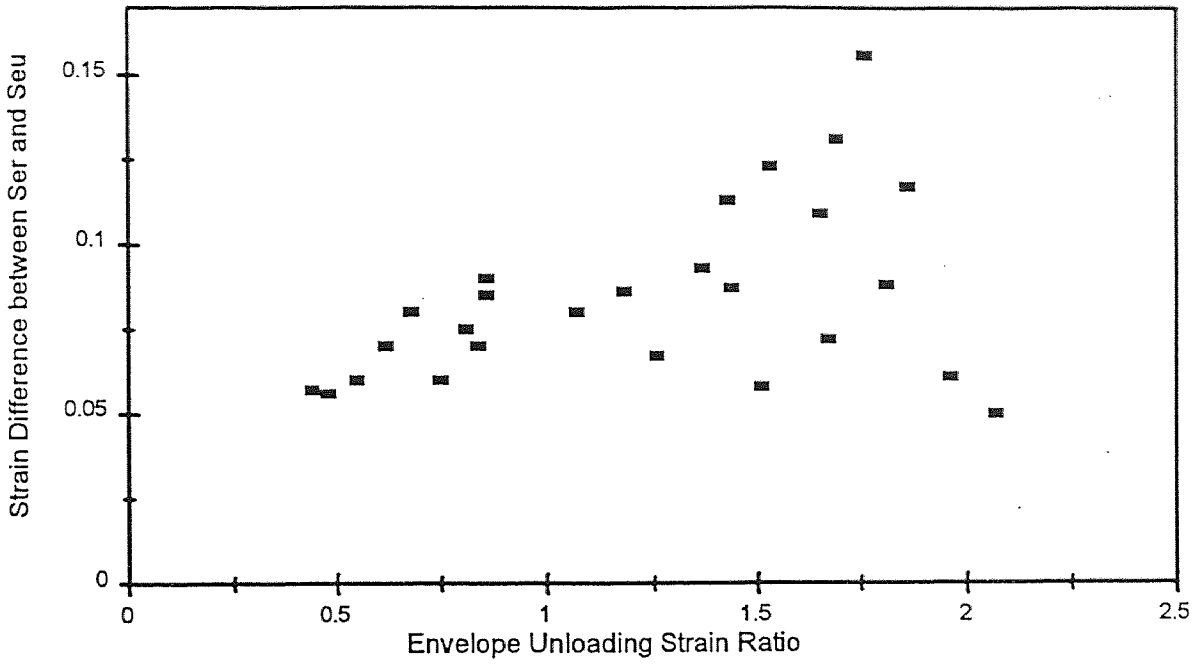

Figure 2.20 Envelope Reloading Strain and Envelope Unloading Strain

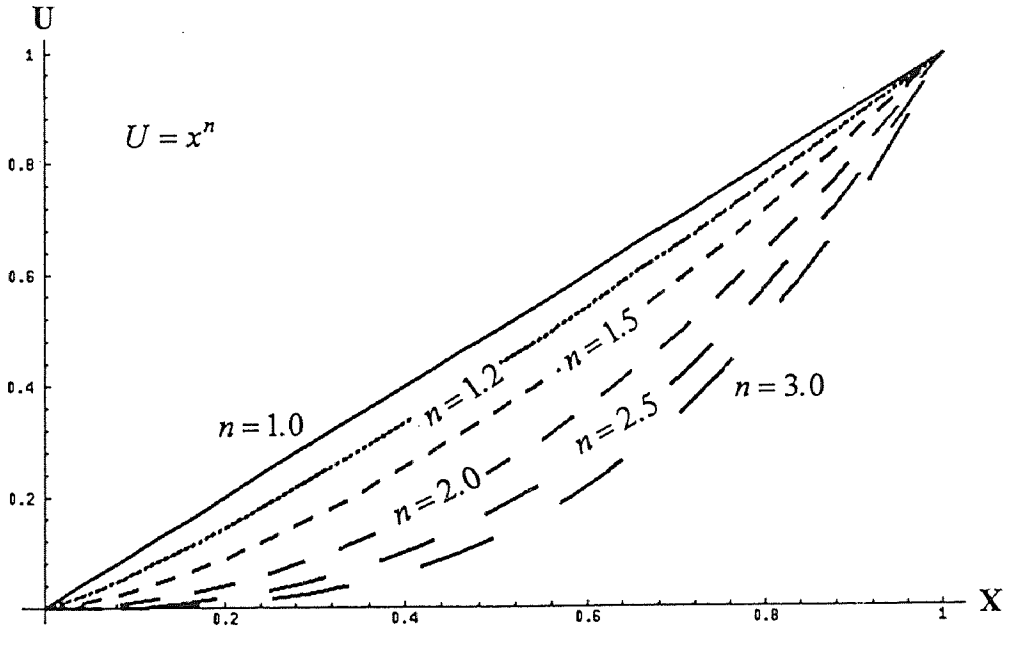

Figure 2.21 Power Function Types for Unloading Curve

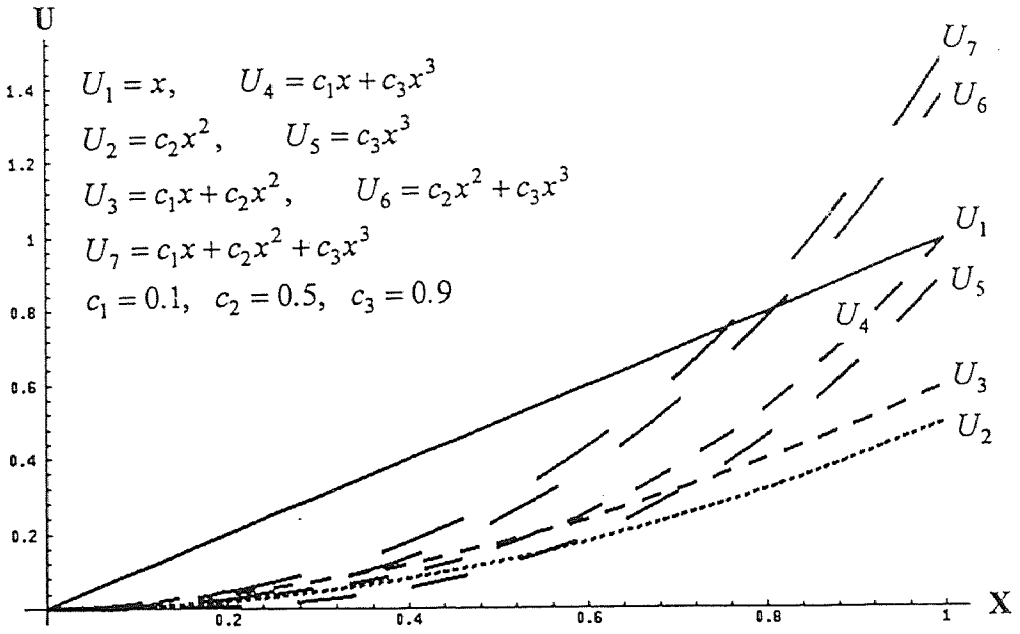

Figure 2.22 Polynomial Types for Unloading Curve

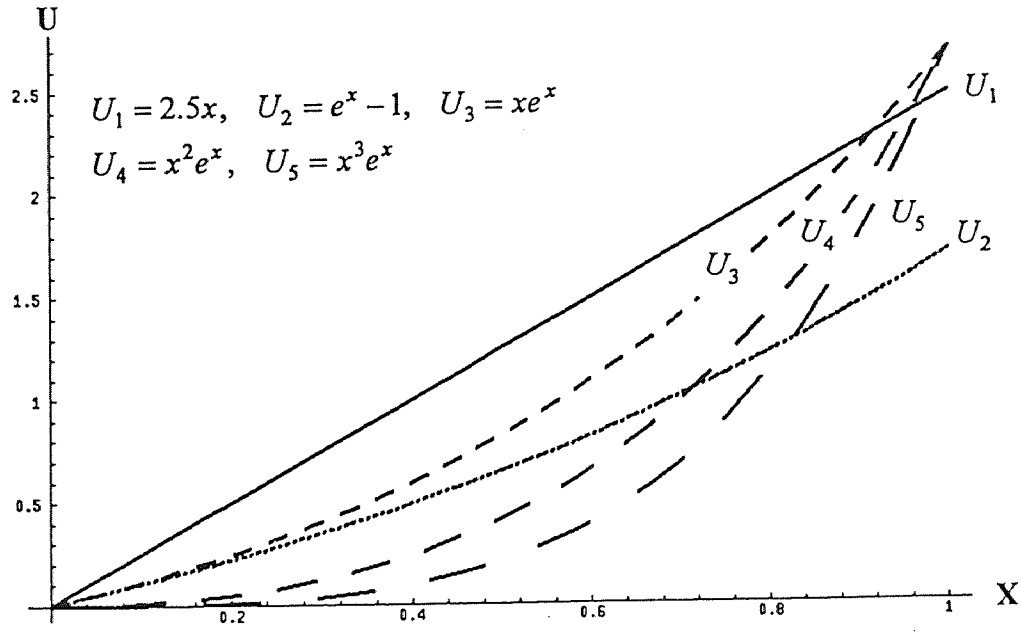

Figure 2.23 Exponential Types for Unloading Curve

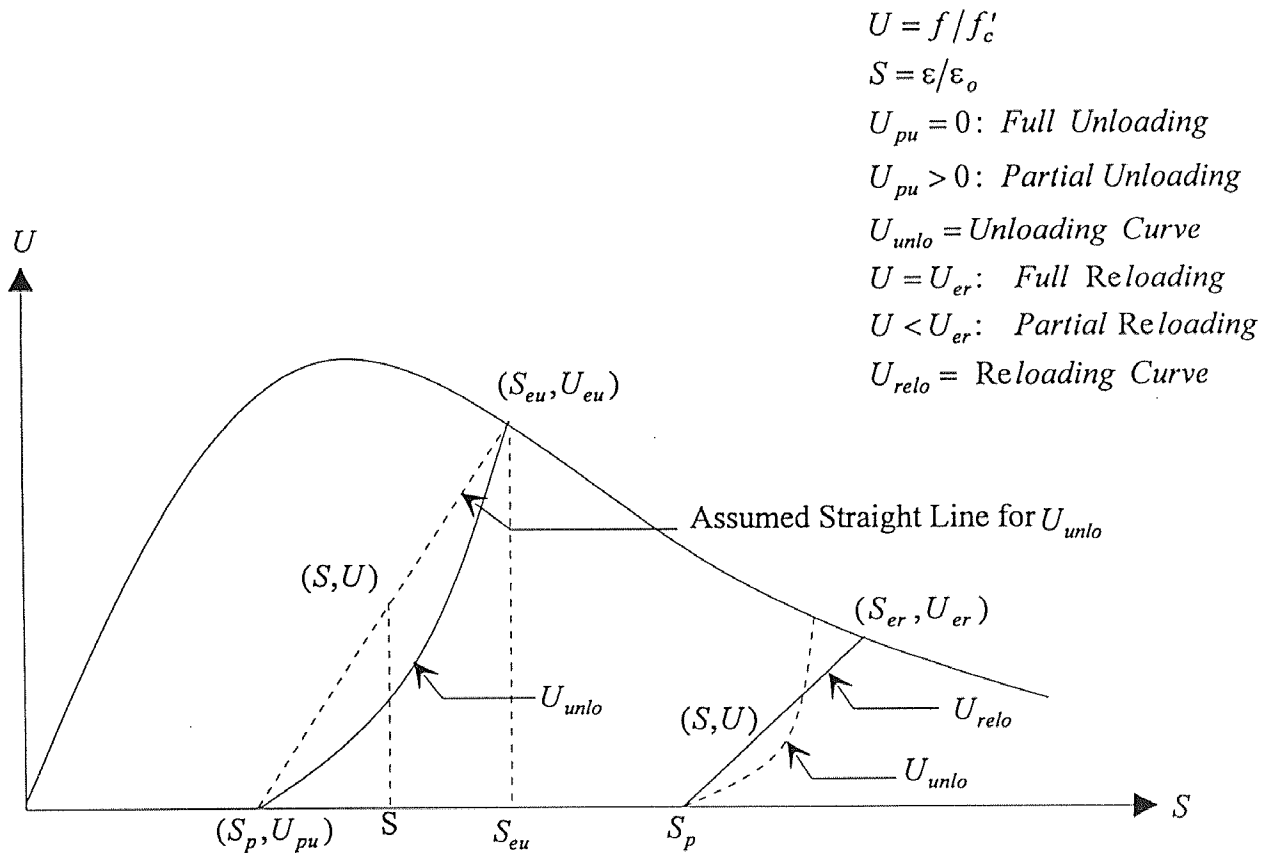

Figure 2.24 Unloading and Reloading Curves

Let $x = \dfrac{S - S_p}{S_{eu} - S_p}$, $\quad x = \dfrac{U}{U_{eu}}$, $\quad$ thus $\quad U = U_{eu}\, x$. Where x is a linear function.

A simplified straight line shown in Figure 2.24 is a special case of an actual behavior during unloading. Thus the analytical expression of unloading curve can be expressed as function of x to reflect the nonlinearity of actual shape of the unloading curve:

$$U_{unlo} = U_{eu}\, f[x] \tag{2.4}$$

Where U_{unlo} is a nonlinear function of unloading curve.

Substituting a linear function x into Equation 2.4:

$$U_{unlo} = U_{eu}\, f\left[\frac{S - S_p}{S_{eu} - S_p}\right] \tag{2.5}$$

The behavior of unloading curve can be predicted through the appropriate combination of basic linear function x which is discussed in above section. Considering the complexity of basic function x and envelope unloading stress ratio U_{eu}, a single term of the equation for unloading curve is at best proposed. It should be noted that the envelope unloading stress ratio U_{eu} must be determined from the adopted monotonic (envelope) curve for the applicability of the proposed model. When the number of terms in U_{eu} increases, the proposed mathematical expression becomes more dependent on the adopted monotonic curve. The envelope unloading stress ratio U_{eu} can be only defined on the envelope curve, and the resulting unloading equation is not analytical at the envelope unloading points if the term U_{eu} is eliminated from the proposed equation. Although the unloading equation without the term U_{eu} is completely independent on the adopted envelope curve, a envelope unloading stress have to be approximated by a

numerical iterations.

For an engineering analysis, it is not desirable to propose a concrete model that an iteration procedure is required to find an envelope unloading stress. Thus the type of power function is proposed here to characterize the concrete behavior of unloading. The mathematical expression of unloading curve is proposed in this study as follows:

$$U_{unlo} = c_u U_{eu} \left(\frac{S - S_p}{S_{eu} - S_p} \right)^{n_u} \tag{2.6}$$

Where c_u is a parameter of unloading curve and n_u is expressed as a function of the plastic strain.

Equation 2.6 is for the case of full unloading as shown in Figure 2.24 and Equation 2.6 is a more general expression than that of Equation 2.4. If the end point of unloading is not at zero stress level of U_{pu}, then the partial unloading stress U_{pu} should be added to Equation 2.6 and the term U_{eu} of the above equation must be replaced by $U_{eu} - U_{pu}$. Thus, for the case of partial unloading, that is a more general stress-strain path than a full unloading, Equation 2.6 can be written as:

$$U_{unlo} = U_{pu} + c_u (U_{eu} - U_{pu}) \left(\frac{S - S_p}{S_{eu} - S_p} \right)^{n_u} \tag{2.7}$$

The unloading coefficient c_u can not be determined by the simple fitting of test results at any specific point due to the variation of coefficients at each cycle. A trial and error approach of simulating the overall shape of stress-strain curve with the aid of test results is used to determine c_u. The ranges of parameter c_u is from 0.95 to 1.0 and 0.95 is adequate for the present study. The power term n_u can be expressed as a function of the plastic strain rather than the envelope unloading strain, because the curvature in

unloading curve changes sharply as a strain approaches to the plastic strain. Based on the concrete behavior during unloading in the present tests and the above mentioned preliminary shape of unloading curve, n_u is found to be greater than 1. It is found that n_u is $1.0+\sqrt{S_p}$ for the present study. The power term n_u shown in Equation 2.7 is used to characterize the nonlinearity of unloading curve as the unloading plastic strain increases.

Figure 2.25 shows a good agreement for the unloading curves obtained from the test results as compared with the proposed mathematical expression for unloading behavior. The experimental strain and stress at the envelope unloading points were required to simulate the proposed equation because the envelope curve was not involved in this comparison. The experimental unloading points were obtained from a large amount of the sampled data in the concrete cylinder test.

For the reloading strain as discussed previously, due to the uncertainty of reloading strain in the test results and a growing scatter of test data, the reloading curve will be approximately proposed. In this situation, a more accurate modeling may end up distorting the overall shape of cyclic stress-strain curve. Furthermore, to obtain a simple model which includes the partial reloading as a part of random cycle, the present study proposes a linear relationship for the reloading curve (see Figure 2.24). And a linear relationship may also be useful to define a stiffness in the reloading paths. Thus, the mathematical formulation of reloading curve can be expressed as:

$$U_{relo} = c_r U_{er}\left(\frac{S-S_p}{S_{er}-S_p}\right) \tag{2.8}$$

Where c_r is a reloading coefficient, S_{er} is a reloading strain ratio on the envelope curve and U_{er} is a corresponding envelope reloading stress ratio at the reloading strain ratio on the envelope curve.

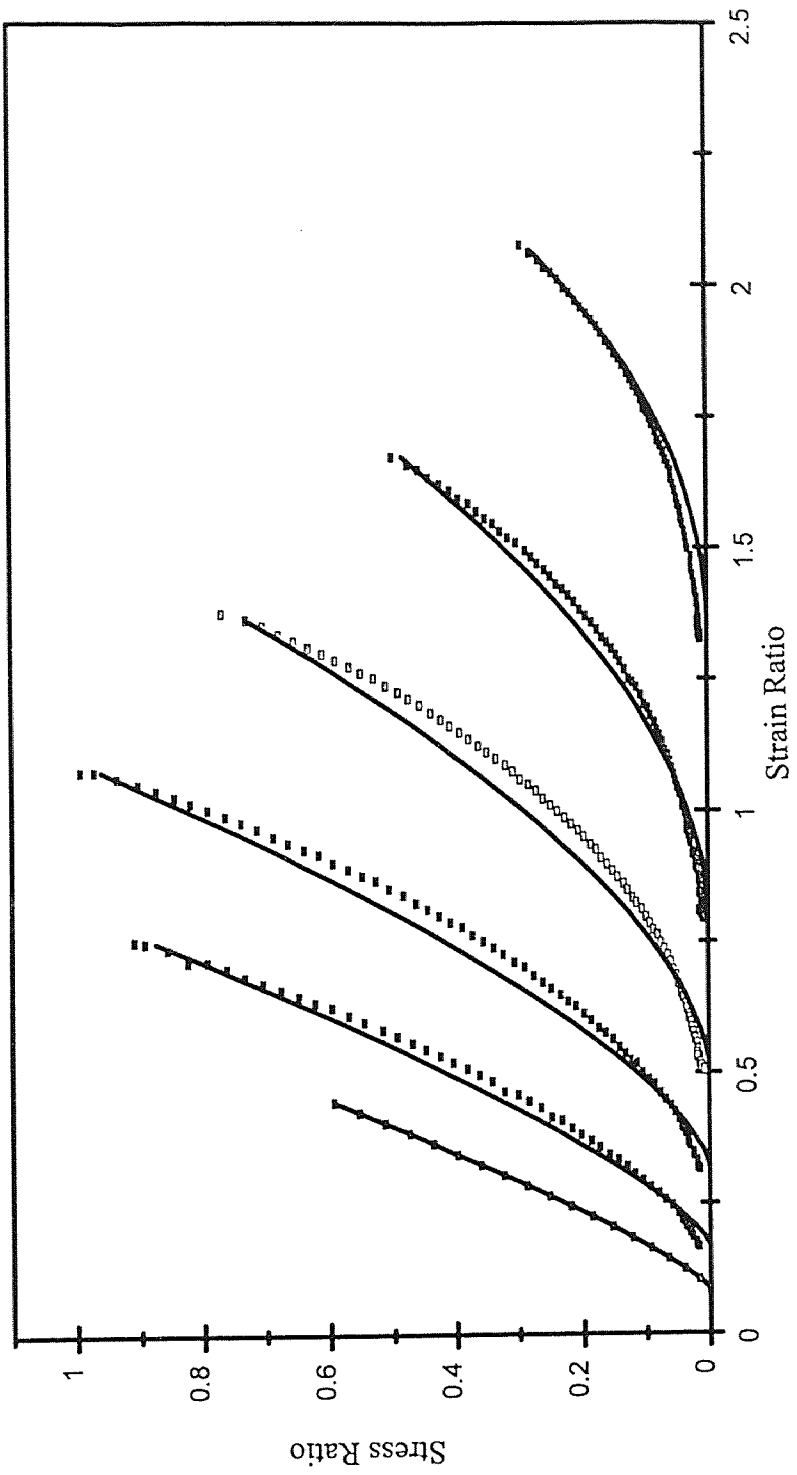

Figure 2.25 Comparison of Proposed Analytical Expression and Experimental Results for Unloading Curve

For a general analytical expression, the reloading curve may have to be considered with a history of unloading path (see Figure 2.28). Again, as in Equation 2.7, for the case of partial reloading with the history of partial unloading, the above equation can be written as:

$$U_{relo} = U_{ppu} + c_r (U_{erpu} - U_{ppu}) \left(\frac{S - S_{ppu}}{S_{erpu} - S_{ppu}} \right)^{n_r} \qquad (2.9)$$

Where the reloading coefficient c_r is equal to 1, n_r is equal to 1 for the present study, U_{erpu} is a envelope reloading stress ratio at the corresponding reloading strain ratio S_{erpu} and U_{ppu} is a partial unloading stress ratio at the corresponding partial unloading strain ratio in the history. U_{ppu} is equal to zero, when the full unloading previously occurs. In this case, Equation 2.9 is the same as Equation 2.8.

Partial Unloading and Reloading: In their pioneering work, Karsan and Jirsa [1969] proposed a non-uniqueness concept that the partial loading curve is not unique with respect to a given stress level. In addition, there is no additional strain accumulation in the partial reloading curve until the stress level exceeds a certain limit (stability limit). This concept is different from the uniqueness concept proposed by Sinha, et. al. [1964].

Validity of the above mentioned concepts may be confirmed from the test results of random cycles. A similar concrete behavior, which supports non-uniqueness concept, is also observed in the present test results. It is found that the current stress-strain response seems to be dependent upon the previous loading history. As shown in Figures 2.26 and 2.27, the test results of random cycles show the subsequent unloading paths that fall into either of the left side or the right side of previous unloading curves. These phenomena depend on the reloading stress level. The observations also support the non-uniqueness concept of stress-strain cycles. If the uniqueness concept of each cycle is assumed to be valid, the unloading behavior due to the partial reloading history in the

second cycle of Figure 2.26 can not be attained in the experiments. Thus, there is no guaranty that each subsequent cycle is able to construct a unique cycle in the stress-strain curve. Figure 2.27 shows a series of unique cycles.

The non-uniqueness concept and above observations provide a clue that the envelope reloading strain can be determined from the history of partial unloading. And the envelope unloading strain at a corresponding stress level can be obtained by the history of partial reloading.

Based on the present test results for full unloading and full reloading, and random cyclic loading, the envelope reloading strain is always greater than the envelope unloading strain regardless of partial or full unloading. Comparing the test results of a series of cycles to common points with the cycle of random loading, the unloading curve due to the history of partial reloading falls into the left side of the previous unloading curve when the stress level of the history of partial reloading is below a certain stress level. Consequently, the second cycle exists within the first cycle. Thus, it can be concluded that the accumulation of envelope reloading strain depends upon the stress level of unloading history and can be expressed as a function of envelope unloading strain.

A random cycle can be achieved by a suitable combination of partial unloading and partial reloading in the subsequent loading path. First of all, the possible and most general loading path should be identified. Figure 2.28 shows a schematic general stress-strain cycle and the possible loading paths. The pattern of load history and all possible stress-strain paths for random cycles are summarized in Table 2.1.

In the envelope, the possible and most general stress-strain path is the partial unloading. After partial unloading is finished at S_{ppu} (see Figure 2.28), partial or full reloading is followed. In this case, the envelope reloading strain S_{erpu} due to the history of partial unloading is required to obtain the reloading curve regardless of full or partial reloading. The envelope reloading strain S_{erpu} due to the history of partial unloading is

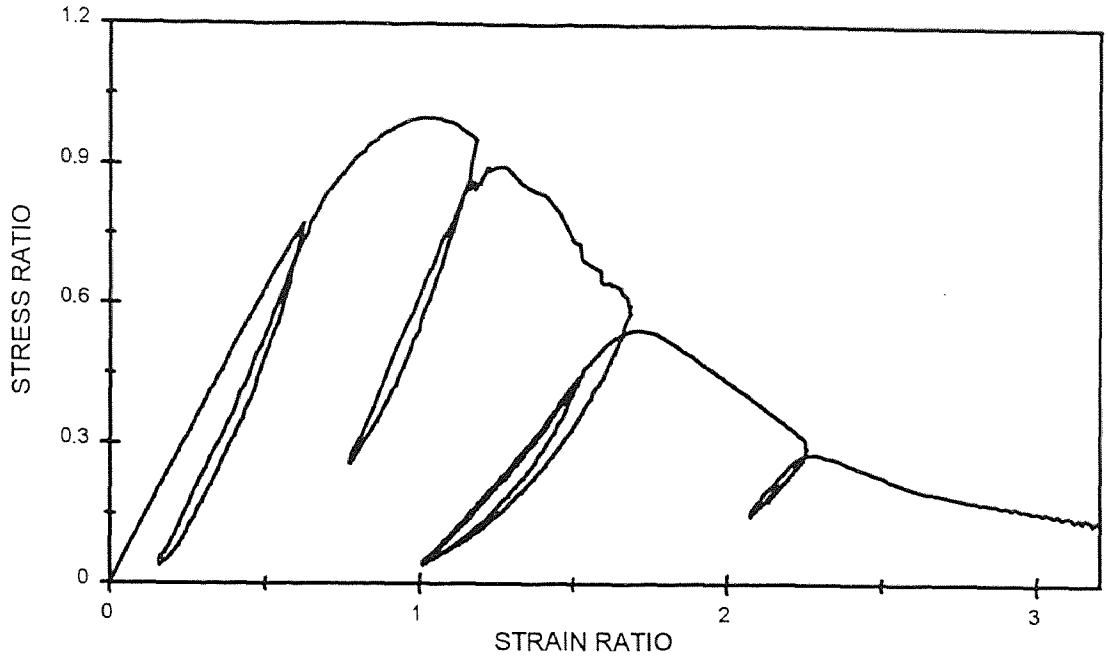

Figure 2.26 Non-unique Cycle of Unloading Curve

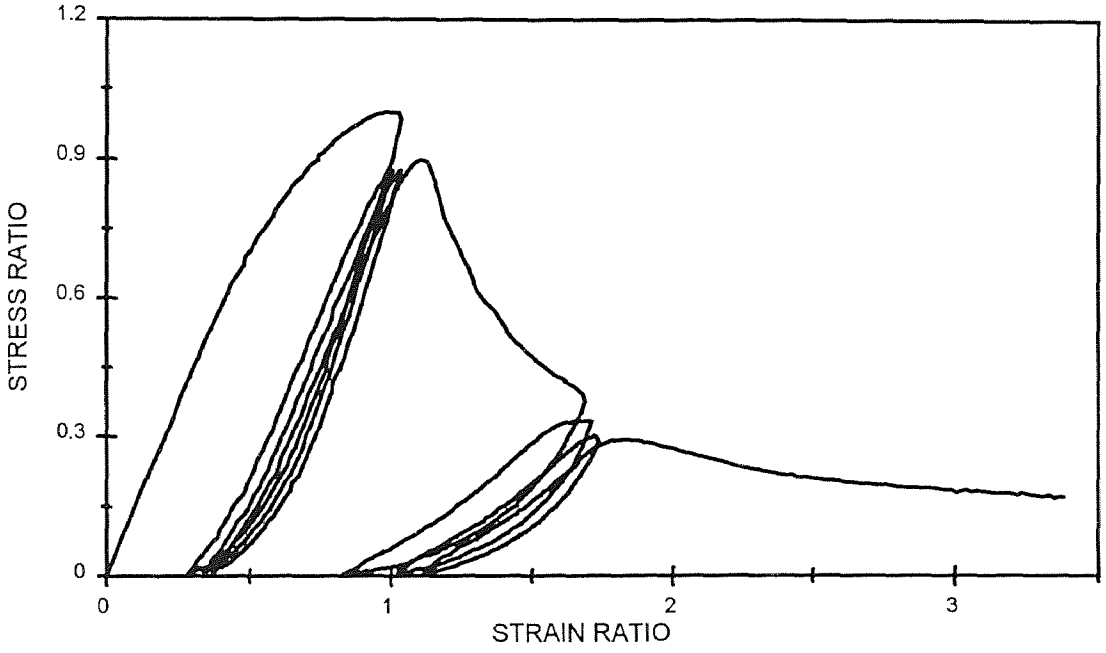

Figure 2.27 Unique Cycle of Unloading Curve

Partial Unloading; $S_{eu} - S_{ppu}$

Re*loading due to Partial Unloading*; $S_{ppu} - S_{rpr}$

S_{erpu}; *Envelope* Re*loading Strain due to Partial Unloading*

S_{ieupr}; Im*aginary Envelope Unloading Strain due to Partial* Re*loading*

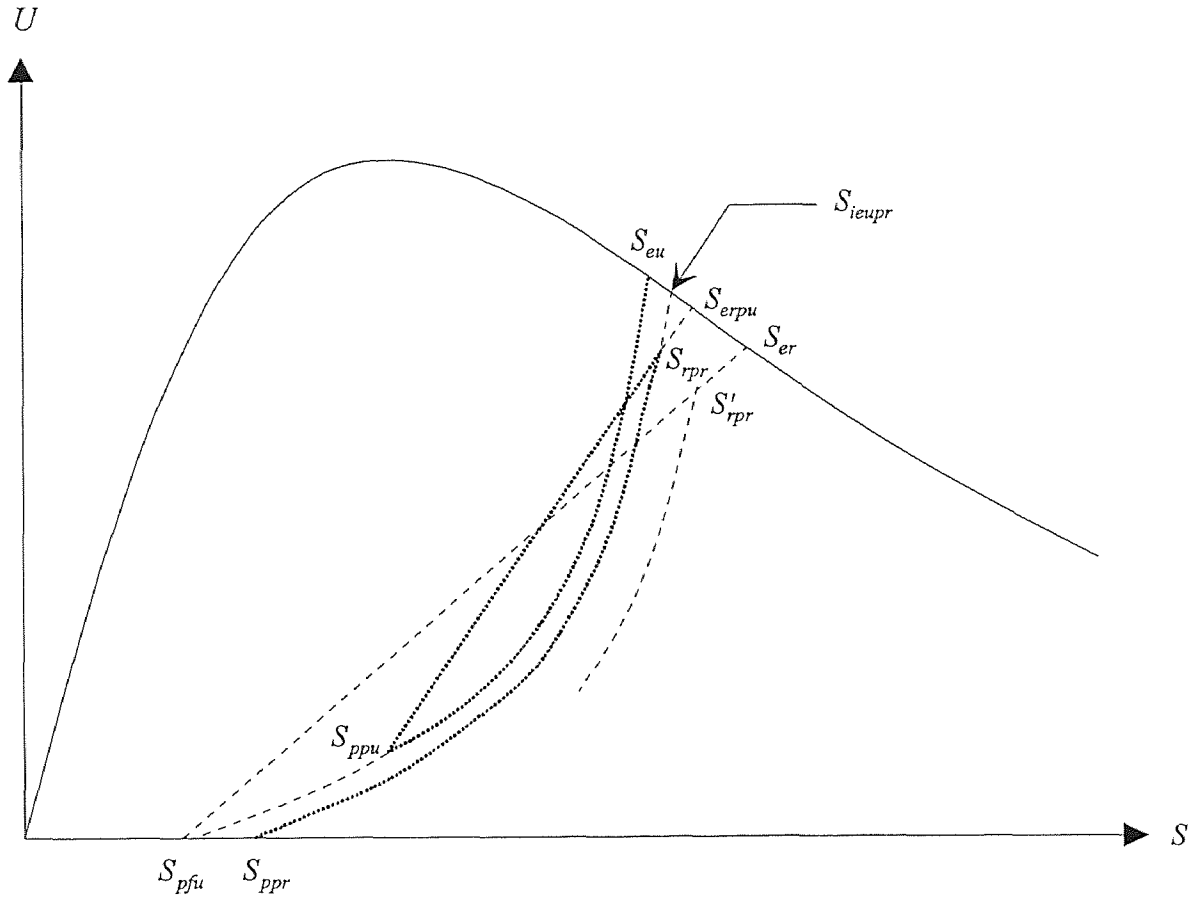

Figure 2.28 Schematic General Stress-Strain Cycles and Possible Loading Path

Table 2.1 Patterns of Load History and Possible Stress-Strain Path

Load Patterns	Stress-Strain Path *	Remark **
Full Unload	$S_{eu} \rightarrow S_{pfu}$	CEV, CCP, CRL
Full Reload	$S_{pfu} \rightarrow S_{er}$	CEV, CRL
Partial Unload with Full Reload	$S_{eu} \rightarrow S_{ppu} \rightarrow S_{erpu}$	CRL
Full Unload with Partial Reload	$S_{eu} \rightarrow S_{pfu} \rightarrow S'_{rpr}$	CRL
General Stress-Strain Path	$S_{eu} \rightarrow S_{ppu} \rightarrow S_{rpr} \rightarrow S_{ppr}$	CRL

* All notations can be found in section 2.5 and Figure 2.28.

** CEV, CCP and CRL are the applied load regimes in present experimental investigation:

CEV ; Cycles to Envelope.

CCP ; Cycles to Common Points.

CRL ; Cycles with Random Loading.

assumed that S_{erpu} exists between the envelope unloading strain S_{eu} and the envelope reloading strain S_{er} for full unloading and reloading. This assumption is based on the observation of experimental results in the partial unloading and full unloading (see Figure 2.13 and 2.16). For this purpose, the linear interpolation can be used to determine the arbitrary strain point between the envelope unloading strain S_{eu} and the envelope reloading strain S_{er} under a single cycle of full unloading and full reloading. Considering the relationships between the full unloading path and partial unloading path, the modified envelope reloading strain due to the history of unloading path can be determined as:

Accumulation of reloading strain ΔS_{er} due to the history of full unloading:

$$\Delta S_{er} = (S_{er} - S_{eu}) = (S_{er} - S_{eu})\left(\frac{U_{eu} - 0}{U_{eu}}\right) \tag{2.10}$$

Accumulation of reloading strain due to the history of partial unloading:

$$\Delta S_{er} = (S_{er} - S_{eu})\left(\frac{U_{eu} - U_{ppu}}{U_{eu}}\right) \tag{2.11}$$

Thus, the modified envelope reloading strain due to the history of partial unloading can be determined as:

$$S_{erpu} = S_{eu} + (S_{er} - S_{eu})\left(\frac{U_{eu} - U_{ppu}}{U_{eu}}\right) \tag{2.12}$$

Where, $U_{eu} = [U_{env}(s)]_{s=s_{eu}}$, $U_{ppu} = [U_{unlo}(s)]_{s=s_{ppu}}$.

The subscripts are: r = reload, u = unload, eu = envelop unload, er = envelope reload, pu = partial unload, and pr = partial reload, respectively. S_{pfu} is the plastic strain due to the history of full unloading and S_{ppu} is the plastic strain due to the history of partial

unloading path, respectively. $U_{env}(s)$ and $U_{unlo}(s)$ are the adopted envelope curve and history of unloading curve, respectively.

Equation 2.12 is a more general expression than that in Equation 2.2 to obtain the envelope reloading strain. In other word, if full unloading occurs, then the stress U_{ppu} at the end point of unloading path becomes zero and Equation 2.12 is the same as Equation 2.2. Determining the modified envelope reloading strain, the general reloading curve due to the history of partial unloading can be obtained by Equation 2. 9.

For a general unloading curve with previous partial reloading path, it is necessary to determine the unloading plastic strain under this history. It is assumed that this unloading path varies from an imaginary envelope unloading strain S_{ieupr} to the corresponding plastic strain S_{ppr} due to the history of partial reloading. The imaginary unloading curve ($S_{ieupr} \rightarrow S_{ppr}$) may or may not pass through the end point S_{rpr} of a previous partial reloading curve. It should be noted that the plastic strain can only be derived from the unloading strain on the envelope curve.

The imaginary envelope unloading strain S_{ieupr} due to the history of partial reloading can be obtained to estimate the corresponding plastic strain S_{ppr} due to the previous partial reloading. Once two points S_{ieupr} and S_{ppr} are obtained, the unloading path ($S_{rpr} \rightarrow S_{ppr}$) can then be determined at any arbitrary stress path. Due to the history of partial reloading, the stress level of this history is evidently below the envelop curve. Thus, it can be concluded that the imaginary envelope unloading strain due to the history of partial reloading exists somewhere between the previous envelope unloading strain S_{eu} and the envelope reloading strain S_{er}. Similarly, the imaginary envelope unloading strain S_{ieupr} can be expressed as:

Imaginary change of envelope unloading strain due to the history of partial reloading:

$$\Delta S_{eu} = (S_{er} - S_{eu})\left(\frac{U_{rpr} - U_{ppu}}{U_{er} - U_{ppu}}\right) \tag{2.13}$$

Thus, an imaginary envelope unloading strain due to the history of partial reloading:

$$S_{ieupr} = S_{eu} + (S_{er} - S_{eu})\left(\frac{U_{rpr} - U_{ppu}}{U_{er} - U_{ppu}}\right) \tag{2.14}$$

Where, $U_{er} = [U_{env}(s)]_{s=s_{er}}$, $U_{rpr} = [U_{relo}(s)]_{s=s_{rpr}}$

The subscripts are: pr = partial reload and er = envelope reload respectively. $U_{relo}(s)$ is the history of partial reloading curve.

The stress U_{rpr} at the end point of partial reloading path is always equal or greater than the first point of the previous partial reloading path. If the stress U_{rpr} is equal to U_{ppu}, this implies that the reloading does not start yet. Once an imaginary envelope unloading strain is obtained, the corresponding plastic strain can then be obtained from Equation 2.1. However, a constant c_p in Equation 2.9 is modified to give a close prediction of present test results for the random cycles. A constant c_p is calibrated as 0.18 for the test results of random cycles. The general unloading curve due to the history of partial reloading can therefore be determined by Equation 2.7 regardless of any stress level.

Discussion and Simulation of Proposed Model: Having the analytical expressions developed, the stress-strain behavior of concrete subjected to cyclic axial compression can be simulated successfully. A simulation program for the cyclic stress-strain response of proposed model is developed by using the new computer language MATHEMATICA. This computer program is implemented at SPARC workstation to give numerical and graphical presentations. Figure 2.29 shows the multiple cycles to the envelope with Smith's envelope curve and Figure 2.30 and 2.31 presents model behavior

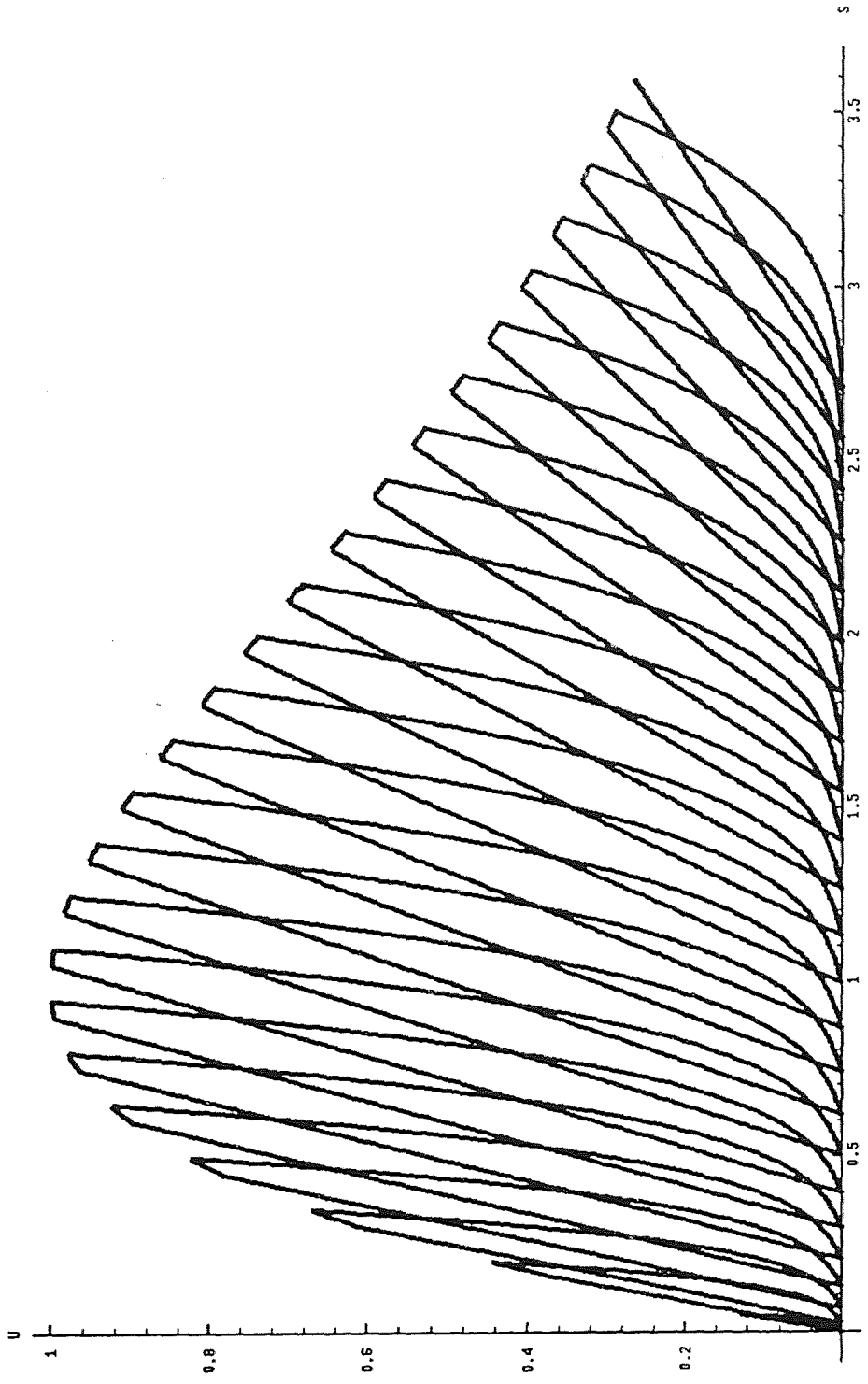

Figure 2.29 Simulation of Cycles to Envelope by Proposed Model

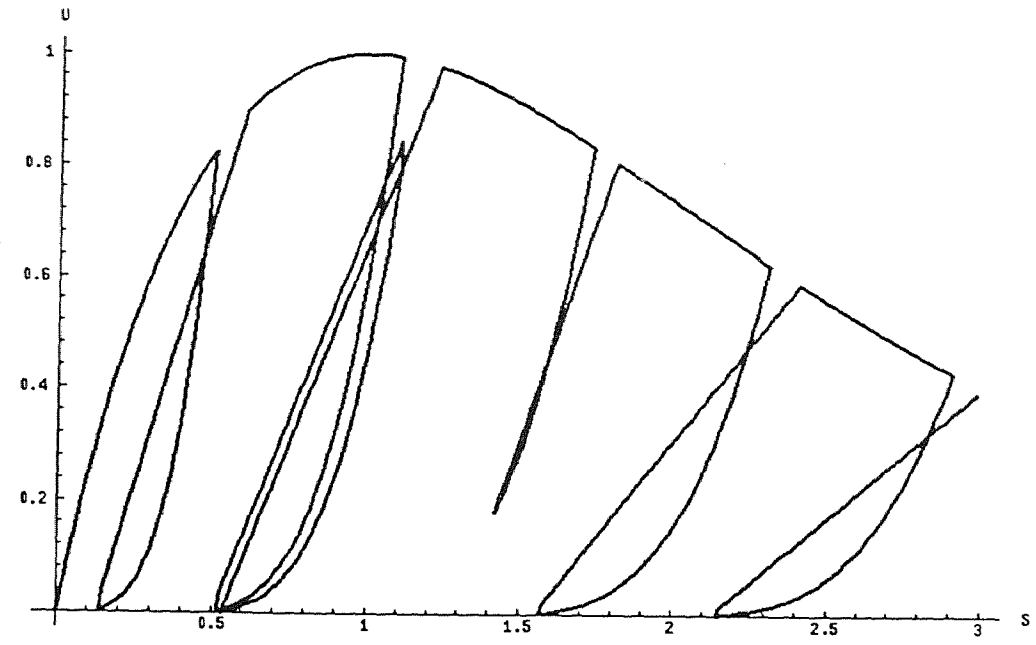

Figure 2.30 Random Cycles with Smith's Envelope by Proposed Model

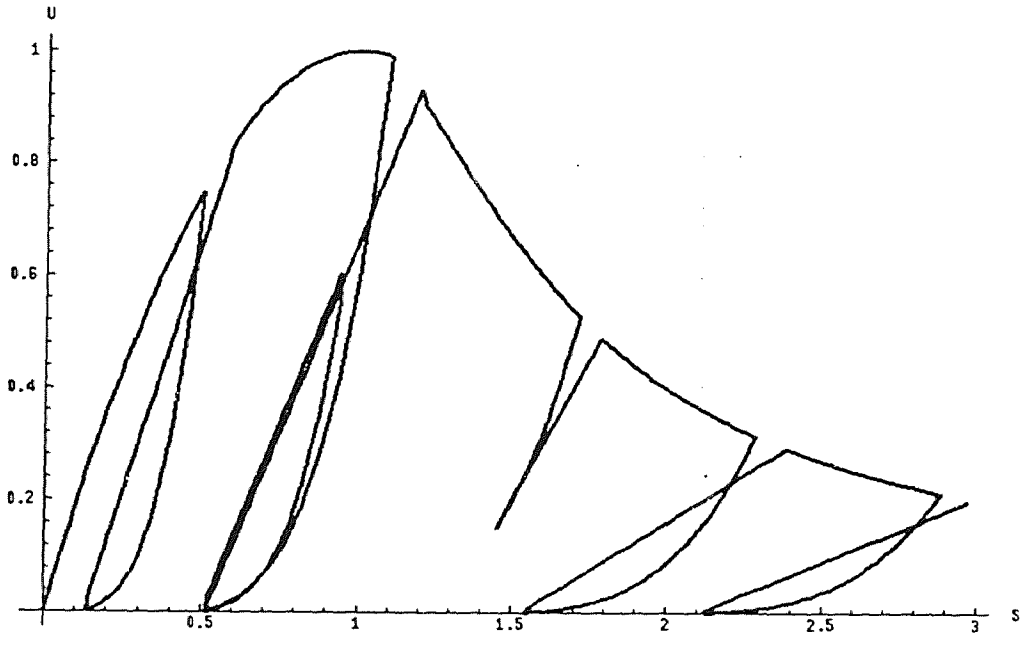

Figure 2.31 Random Cycles with Tulin's Envelope by Proposed Model

of random cyclic stress-strain curve with Smith's and Tulin's envelopes respectively.

The above simulations verify the validity of the proposed model. Comparing the simulations of Figures 2.30 and 2.31, they show that the proposed analytical expression reflects the non-uniqueness concept. These simulations are performed with different envelope curves, and they show the applicability and flexibility of the proposed mathematical expressions.

All model parameters, either an empirical or a semi-empirical, can be adjusted to a certain test results. The overall shape of stress-strain curve will not be distorted due to such minor modifications. Furthermore, the proposed model is less dependent upon the adopted envelope curve and this can be verified in the following section through the simulations with different envelope curves. Any specific monotonic stress-strain relationships of previous work are not involved in modeling procedure of cyclic stress-strain relationships. The proposed mathematical model is used here to simulate a typical cyclic behavior of concrete under all possible loading patterns. Some of them are untested stress-strain paths before this study. The preliminary results of using proposed model seems to be promising and the comparisons are made in the following section.

2.6 Comparison of Concrete Test and Proposed Model

A computer model based on the proposed analytical expressions has been developed to simulate the stress-strain behavior of concrete under various cyclic load regimes. The predictions of the proposed model are compared with experimental results on concrete subjected to cyclic axial compressions. The envelope unloading strain of analytical model can not be controlled exactly at the same unloading strain as in the test results. Thus, it is a more reasonable to compare the prediction of proposed model with the test results in view of the pattern recognition problem rather than the close comparison by curve fitting.

There are no any specific monotonic stress-strain relationships that are used for

envelope curve in modeling the concrete behavior under a cyclic loading. It is obvious that the proposed model will be able to give a close prediction of the test results by using the envelope curve which fits well the corresponding experimental envelope curve. However, such comparisons can not verify the validity of proposed model and they are only considered as a special case between the experimental results and the prediction of proposed model.

Thus, an arbitrary monotonic model for the envelope curve is employed here to compare the experimental results and the prediction of proposed model. As shown in Appendix A, a comparison of model prediction and test result is shown in Figures A.1 and A.2 for the load pattern of cycle to envelope. The overall stress-strain behavior of the proposed model and test result shows a similar configuration with each other.

Figures A.3 and A.4 compare the experimental and analytical behavior of concrete for cycles to common points. It is observed that the prediction of analytical model gives similar patterns as the ones shown in the experimental results. In the experimental results, the common points do not coincide exactly at the same point due to the determination of these points by a monitor display.

Figures A.5 and A.6 show the test results and simulation of proposed model for the random cyclic load pattern. A series of full unloading and reloading, partial unloading and partial reloading are presented. It depends on the stress level of current partial unloadings whether the current unloading curve falls on the left side or right side of the previous unloading curve. This observed behavior was previously discussed in section 2.5. It should be noted again that the location of current unloading curve due to the previous partial reloading is solely dependent on the stress level at the end point of previous partial reloading. There are no relations between the end point of partial reloading and the common point in the behavior of current unloading curve.

The proposed analytical model is less dependent upon an adopted envelope curve. The overall shape of stress-strain behavior of concrete under cyclic loading is not

distorted due to the employment of various monotonic stress-strain curves. The proposed analytical expression is used with the monotonic models proposed by Desayi, Smith and Young, Popovics and Shah, respectively. The flexibility and less dependency of proposed model are verified from a series of simulation as shown in Figure A.7 through A.10. For this purpose, the model behavior for random cycles is also presented in the previous section 2.5 (see Figures 2.30 and 2.31). Thus, the proposed mathematical model is able to simulate the stress-strain curve of concrete under various patterns of load history and it can also be used together with various monotonic stress-strain curves.

CHAPTER 3

ANALYSIS OF R/C COLUMNS UNDER CYCLIC AXIAL LOADING WITH BIDIRECTIONAL ECCENTRICITIES

This chapter discusses the behavior of slender reinforced concrete (R/C) columns under cyclic axial loading with bidirectional eccentricities. A brief discussion of conventional finite segment model is presented. Analysis of R/C column subjected to combined biaxial bending and axial load should be approached from the standpoint of a three dimensional problem.

Unlike the finite segment model, finite element model idealizes each structural members as an assemblage of a large number of finite elements. These elements can be of various types such as one dimensional and two dimensional elements, even three dimensional elements for concrete. The cost and time involved become prohibitive if three dimensional elements are used. In addition, there are some difficulties involved in implementing an idealized empirical concrete model in the finite element model. Thus, the conventional finite segment method is extended here to study the R/C columns under cyclic axial compression with bidirectional eccentricities.

3.1 Method of Column Analysis

3.1.1 Description of Column Analysis

The numerical procedures of the previous studies by Wang and Hsu [1990] and Tsao [1991], are based on the incremental deflection approach, where a deflection is assumed to be in a specific direction. In other word, this analytical procedure is good only to increase the strain at the divided areas of steel and concrete in column section under monotonically increasing load. The unloading in curvatures can not be considered

because the analytical formulations are expressed in terms of cross-sectional stiffness, strain at coordinate origin and deflections along the column. The convergencies are only confirmed for the strain at coordinate origin, axial force and deflections. After the deflections are determined, the corresponding curvatures are calculated from the finite difference method. Furthermore, the convergence criteria are difficult to reach the desired accuracy due to the feeding of simply increasing specific deflection for the subsequent stage of analysis. Thus, it can be concluded that a simple modification of previous numerical procedure can not handle the different loading paths needed in the present study.

Variations in loading can affect the stiffness and strength of the R/C column, especially when the loading and unloading occur. In addition, the axial load acting on a column section influences the flexural stiffness, the moment capacity, and the ductility of R/C column as well.

A finite segment method of analysis is extended here to predict the behavior of R/C slender columns under cyclic loading with bidirectional eccentricities. The numerical procedure is designed to consider increasing or decreasing of the strain at discrete elements in the column under cyclic loading. The rate of convergence in analysis depends on the proposed values of deflection and strain. The convergence of iterative procedures can be improved through the interpolation or the extrapolation method which utilizes the previous solutions.

The load-deflection curve, moment-curvature curve and ultimate load are predicted through the developed computer program. Computer model developed for the present study has the following capabilities:

1) General cross sections may be possible to enable consideration of any arbitrary shapes.

2) Complex loading conditions, including cyclic compression with bidirectional eccentricities.

3) Both material and geometrical nonlinearities can be considered.

4) Both ends of the column are assumed to be pinned-ended. However, it can be modified to accommodate other end conditions.

3.1.2 Idealized Stress-Strain Relations for Column Analysis

Once the strain in any discrete element is proposed, the corresponding stress can be obtained from the proposed cyclic stress-strain relationships as discussed in chapter 2. Generally, the complexity of the finite segment method in column analysis is a direct function of the material stress-strain relationships. The secant stiffness is defined as the secant slope of the stress-strain curve for a given strain. Here the secant stiffness is used to study the column behavior in both ascending and descending branches. It should be noted that, in the case of stress computation, the stiffness must be derived by considering the strain history at certain element of either loading or unloading paths in the stress-strain curve.

To determine a reasonable result, the element stiffness should be updated whenever any event occurs at an individual element. This, however, can be computationally unfeasible especially if a highly complex material model is adopted. Because of this reason, the material models should be idealized as simple as possible.

In this study, a kinematic hardening model [Chen and Han, 1988] is employed to describe the cyclic stress-strain relationships for steel reinforcement. The elastic range is assumed to be unchanged during strain hardening. The center of the elastic region is moved along the straight line aa' (see Figure 3.1). The envelope curve is characterized by the steel reinforcements in a tensile test until failure in a monotonically increasing load. The unloading and reloading curves follow along a stress-strain path that is generally assumed to be parallel to an initial elastic portion of the curve. Thus it is assumed that no stiffness degradation occurs as seen in Figure 3.1.

It is true that there is a considerable gap existed between the mathematical model of concrete and its use in an engineering analysis. It should be mentioned that there are many stiffness changes in the concrete model. The precise details of a concrete stress-strain curve do not greatly affect the overall behavior of a structural member. Hence, to accomplish implementation and to reduce the effort of computing, an idealized cyclic concrete model is proposed for the present column analysis. To simplify the proposed concrete model, several parametric studies are performed as discussed in chapter 2. The procedures of obtaining an idealized concrete model are conducted through a new intelligent language, MATHEMATICA.

First of all, an idealized concrete model should be able to represent the physical characteristics of stiffness on the envelope curve. In addition, the definition of stiffness on the unloading or reloading stress-strain paths must be reasonably established. The slope change of the unloading curve varies in a wide range from the envelope unloading point to the zero stress level. Thus the stiffness can not be adequately defined on the unloading stress-strain path. It can be concluded that the stiffness on the unloading or reloading stress-strain paths is defined somewhat of the slope on the reloading path of the cyclic stress-strain curve. The change in the slope of reloading stress path is more stable than the change in the slope of unloading path.

The envelope curve of an idealized cyclic stress-strain relationships is here modified from Hsu's [1974] monotonic stress-strain curve. The stiffness degradation of unloading or reloading path for concrete elements is well represented in the idealized model of the present study. In all cases a definite decrease in the average elastic modulus of the reloading curves with an increase in the plastic strain is shown in the present idealized stress-strain relationships of concrete (see Figure 3.2) for column analysis.

The stiffness degradation is an important feature for the analysis of the reinforced concrete structure. Several analytical expressions for the stiffness degradation have been proposed using three different approaches. The first is a slope of two points between the

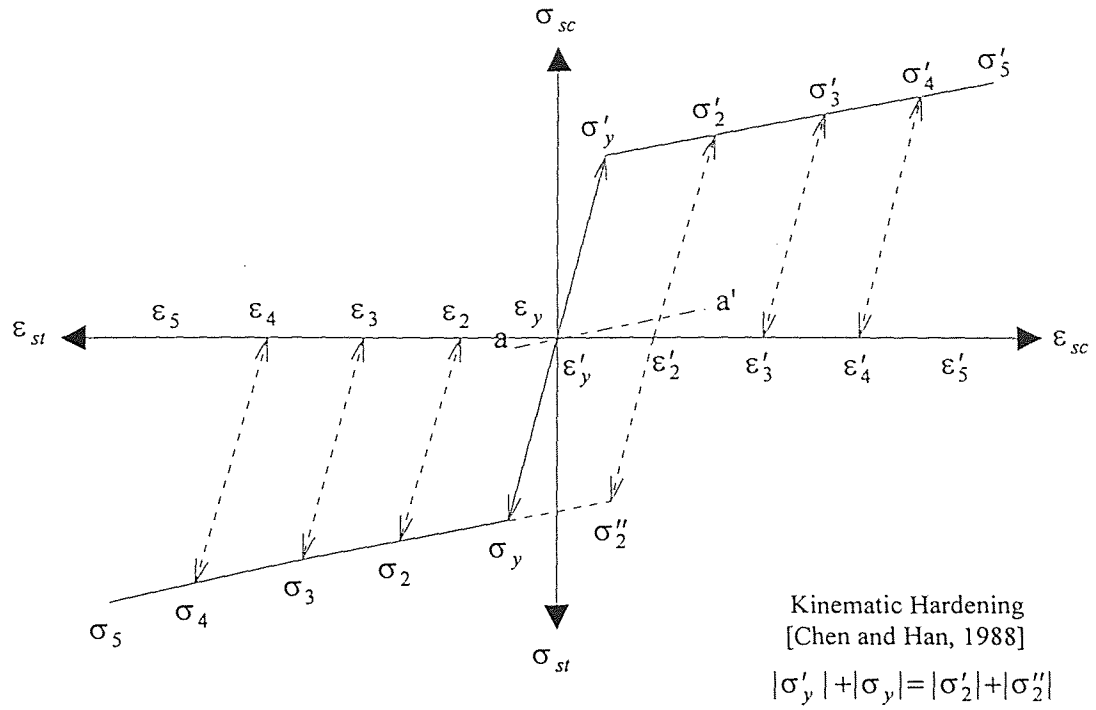

Figure 3.1 Idealized Cyclic Stress-Strain Curve for Steel

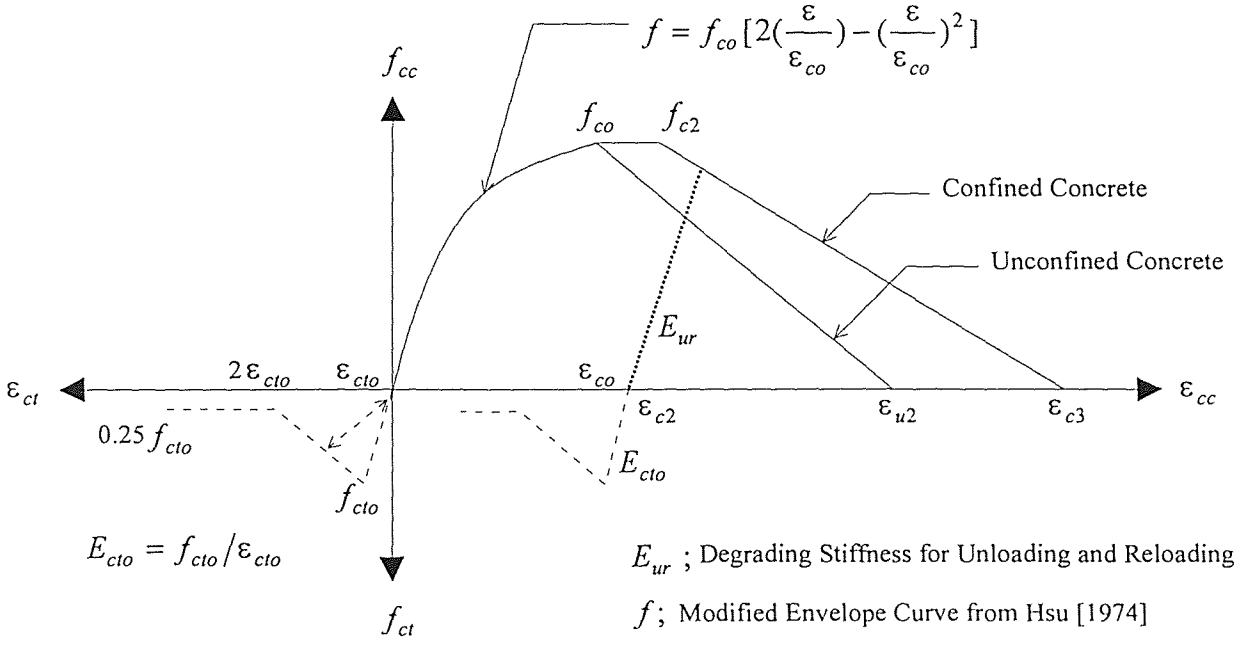

Figure 3.2 Idealized Cyclic Stress-Strain Curve for Concrete

plastic strain and reloading strain on the envelope curve. The second is derived from two points between the plastic strain and common point. The third is formulated by the plastic strain and the midpoint between unloading strain and reloading strain on the envelope curve. The changes of stiffness for the above mentioned three different approaches are presented in Figure 3.3.

Considering the behavior of a structural member which consists of a number of discrete elements, certain elements experience very different stress-strain paths. The common points and plastic strain points do not always exist in the consequent cycles of loading and unloading paths. Observing the random cyclic loading from the proposed concrete model as discussed in chapter 2 and the experimental results, the lowest stress point during partial unloading and the reloading point on the envelope curve are defined uniquely and these two points always exist. Thus it can be concluded that the stiffness of unloading or reloading stress-strain path can be defined by the above mentioned two points, namely, the plastic strain points, and envelope reloading points.

3.1.3 Extended Finite Segment Method for Cyclic Analysis

As shown in Figure 3.4, the column is considered as three dimensional structure after segmentation. The column section is divided into small elements of reinforcements and concrete in order to calculate each cross-sectional stiffness at different levels of strain. The analysis is based on the behavior of the cross-section at each segment point along the column.

The analysis has the following assumptions:

1) Plane sections remain plane before and after bending.

2) There exists a perfect bond between concrete and steel.

3) The effect of axial and shear deformations is negligible.

4) Envelope curve of an idealized cyclic stress-strain relationships is approximately same as the monotonic stress-strain curve.

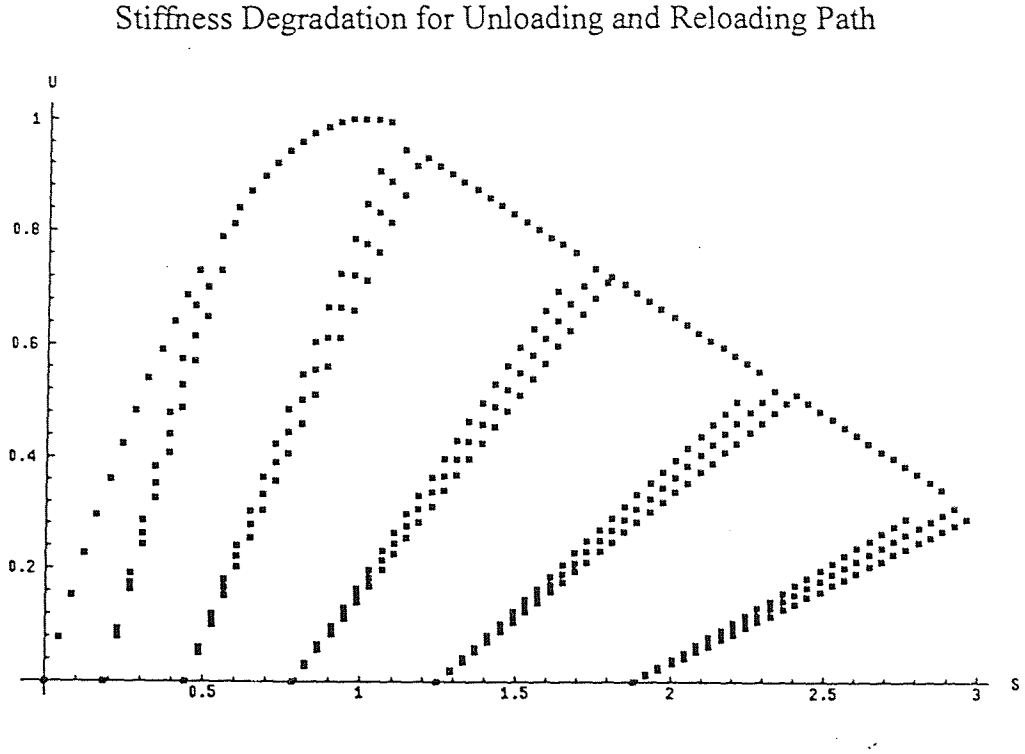

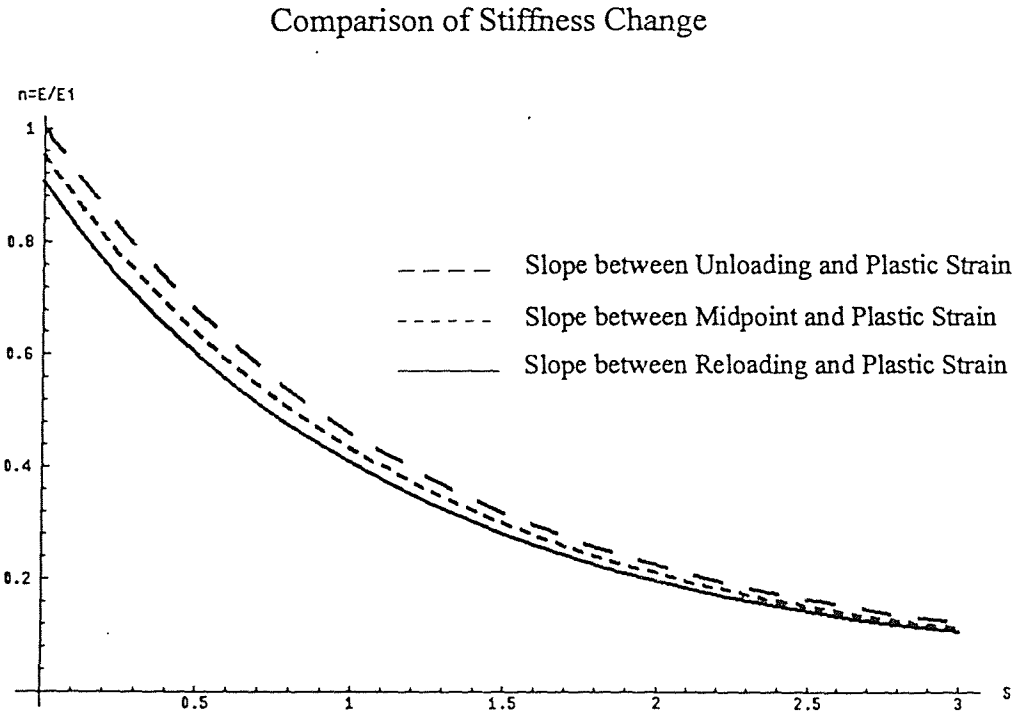

Figure 3.3 The Change of Stiffness Using Three Different Aproaches

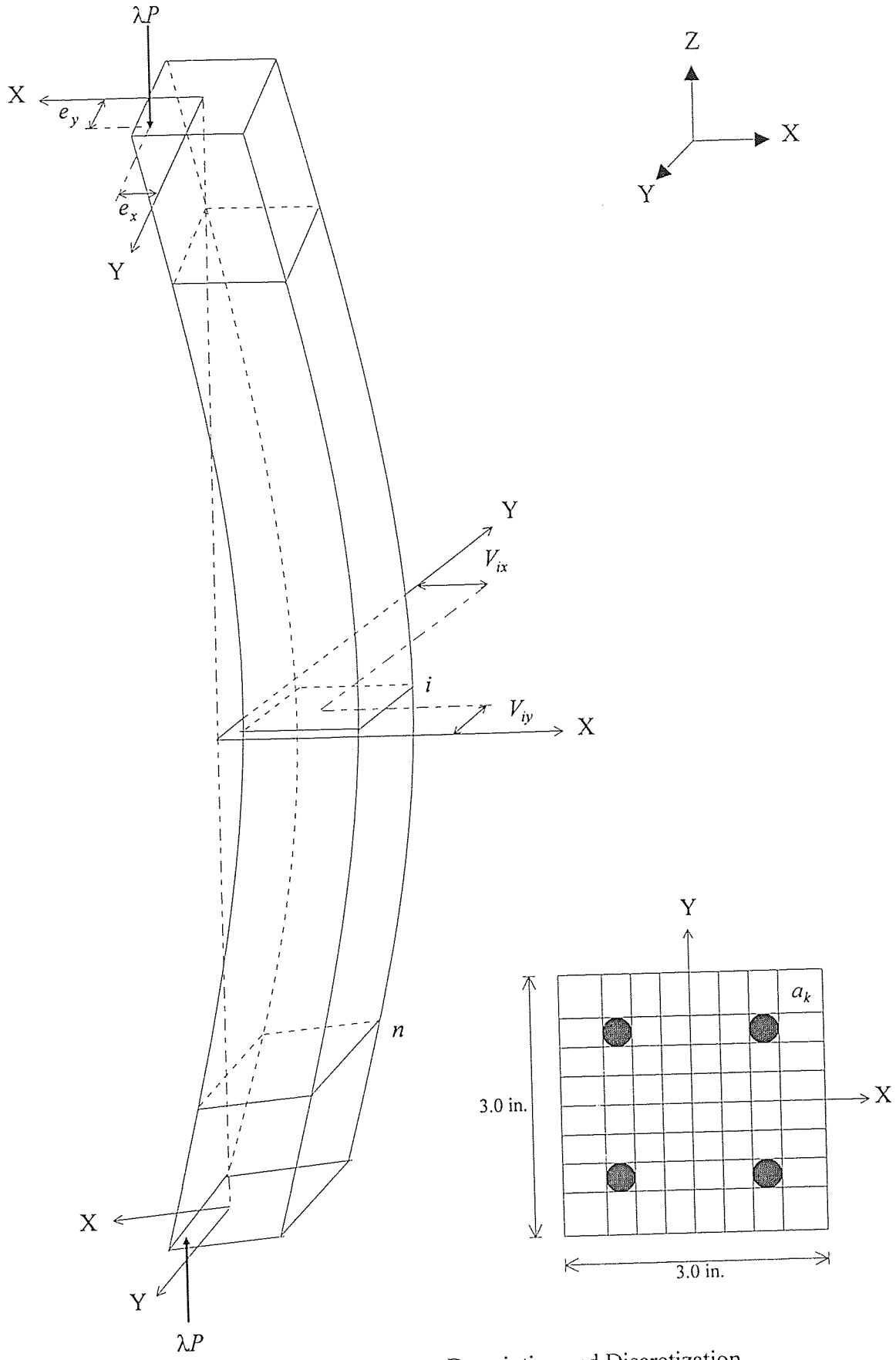

Figure 3.4 Column Description and Discretization

Using the assumption that plane section remains plane during bending, the strained plane in the cross-section can be described by the strain at the coordinate origin ε_o, curvatures ϕ_x and ϕ_y about both axes, respectively. They are shown in Figure 3.5. Thus the strain ε_k at any element k under combined biaxial bending and axial compression is given by [Hsu, 1974, Wang and Hsu, 1990]:

$$\varepsilon_k = \varepsilon_o + \phi_x y_k + \phi_y x_k \tag{3.1}$$

where

ε_o : strain at coordinate origin.

ϕ_x : curvature produced by bending moment M_x.

ϕ_y ; curvature produced by bending moment M_y.

M_x. and M_y ; moment about x-axis and y-axis, respectively.

x_k and y_k : coordinates of centroid of an element k from both principal axes X and Y, respectively.

The corresponding stress f_k and secant stiffness E_k are found by the idealized cyclic stress-strain relationships of steel reinforcements and concrete elements. When the elemental forces and moments in the column section are found, the calculated cross-sectional forces P_c, M_{xc} and M_{yc} are given by:

$$P_c = \sum_{k=1}^{n} f_k a_k \tag{3.2}$$

$$M_{xc} = \sum_{k=1}^{n} f_k a_k y_k \tag{3.3}$$

$$M_{yc} = \sum_{k=1}^{n} f_k a_k x_k \tag{3.4}$$

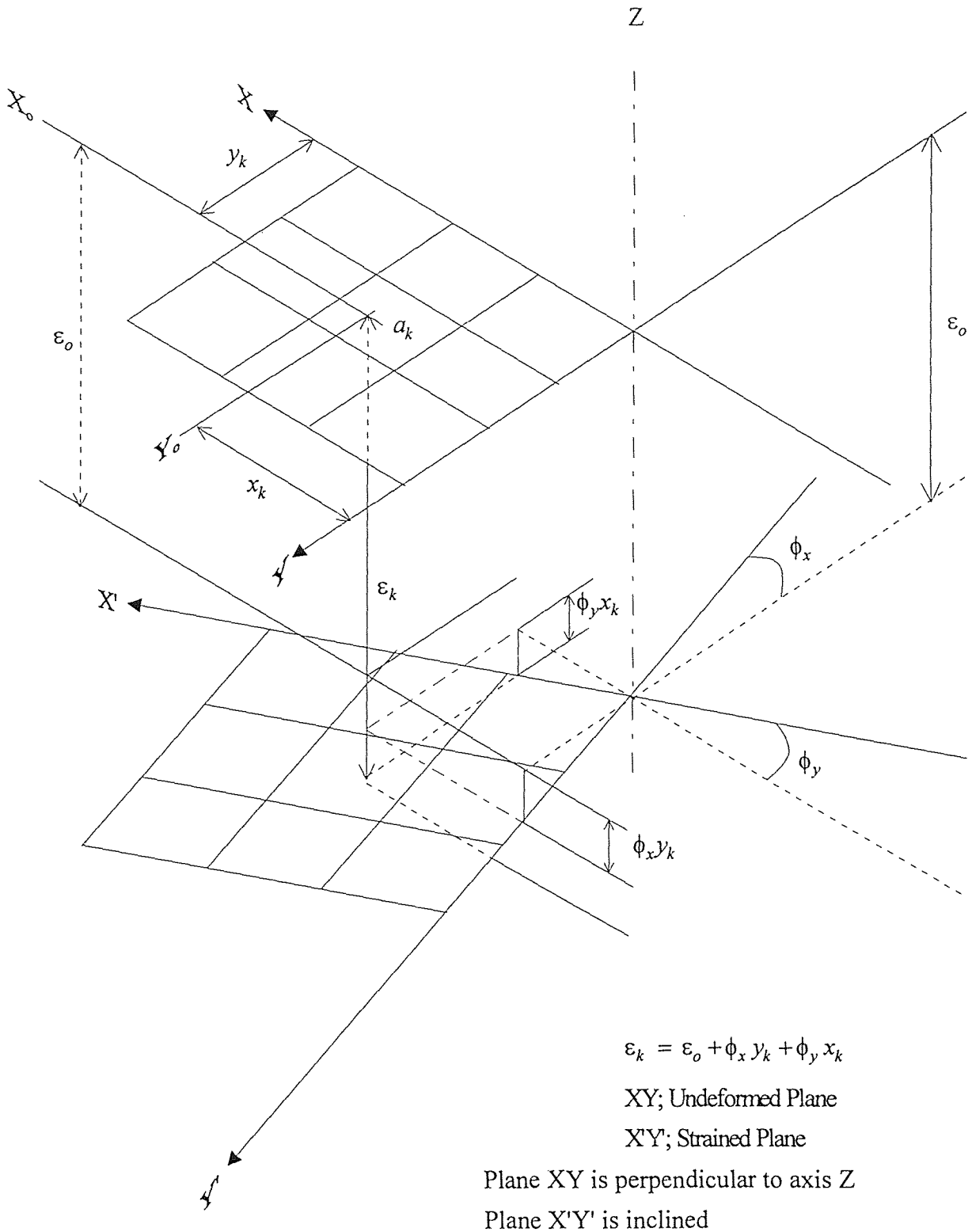

Figure 3.5 Strain Plane of Combined Biaxial Bending and Axial Load

where a_k is a small area of discrete element k and subscript c denotes the calculated values.

Considering Equations 3.3 and 3.4 for calculated moments M_{xc} and M_{yc}, the formulas are only valid when the areas of divided elements are comparatively small. This implies that the mechanical behavior of a unit element should be estimated more accurately. Thus Equations 3.5 and 3.6 are used here to reduce an accumulation of error when the coarse mesh is used for analyzing the column section.

$$M_{xc} = \sum_{k=1}^{n} f_k \, a_k \, y_k + \sum_{k=1}^{n} \phi_x \, E_{sk} \, I'_{x_o k} \tag{3.5}$$

$$M_{yc} = \sum_{k=1}^{n} f_k \, a_k \, x_k + \sum_{k=1}^{n} \phi_y \, E_{sk} \, I'_{y_o k} \tag{3.6}$$

Where $I'_{x_o k}$ and $I'_{y_o k}$ are the moments of inertia (second moment) of an element k about elemental centroidal x_o and y_o axes parallel to both reference x and y axes, respectively.

The moments of inertia of each element $I'_{x_o k}$ and $I'_{y_o k}$ were suggested by Menegotto and Pinto [1977] to calculate the moments of inertia I_{xk} and I_{yk} about a coordinate system. Two additional terms in Equations 3.5 and 3.6 represent the effect of inclined elemental plane on the computed moments M_{xc} and M_{yc}, respectively (see Figure 3.5). The additional terms involving the moment of inertia of each element enable the number of elements to be reduced. It should be noted that for elements where unloading occurs, the curvatures ϕ_x and ϕ_y in Equations 3.5 and 3.6 must be replaced by $(\phi_x - \phi_{xh})$ and $(\phi_y - \phi_{yh})$, where ϕ_{xh} and ϕ_{yh} are the curvatures corresponding to the solution at which a updated strain history ε_{kh} for the particular element. This procedure of using a updated strain history saves a considerable amount of memory space in the computer implementation and the details of computer algorithm will be explained later in this chapter.

The relationship among the axial load, moment and curvature for the uniaxial case was obtained by Gurfinkel and Robinson [1967]. Through the numerous researches, this thrust-moment-curvature relationships were expanded to the incremental stiffness matrix (3 x 3) of the cross-section for biaxial bending [Hsu, 1974]. The detailed formulation, which is in the form of partial derivative, of the cross-sectional stiffness matrix can be derived by considering the effects of finite changes $\delta\varepsilon_o$, $\delta\phi_x$, $\delta\phi_y$ in ε_o, ϕ_x and ϕ_y on P_c, M_{xc} and M_{yc}.

The small change of strain due to an axial load, $\delta\varepsilon_o$, produces a corresponding stress change, δf_k, at an element k which is corresponding to $E_{sk}\delta\varepsilon_o$. The resulting changes of force components from Equations 3.2, 3.5 and 3.6 can be obtained, thus δP_c, δM_{xc} and δM_{yc} can be expressed as:

$$\delta P_c = \sum_{k=1}^{n} a_k E_{sk} \delta\varepsilon_o$$

$$\delta M_{xc} = \sum_{k=1}^{n} a_k y_k E_{sk} \delta\varepsilon_o \qquad (3.7)$$

$$\delta M_{yc} = \sum_{k=1}^{n} a_k x_k E_{sk} \delta\varepsilon_o$$

The finite change of a curvature about x-axis, $\delta\phi_x$, introduces a stress change, $E_{sk}\delta\phi_x x$, and the resulting change of force components from Equations 3.2, 3.5 and 3.6 can be determined. Thus δP_c, δM_{xc} and δM_{yc} are given by:

$$\delta P_c = \sum_{k=1}^{n} x_k a_k E_{sk} \delta\phi_x$$

$$\delta M_{xc} = \sum_{k=1}^{n} x_k^2 a_k E_{sk} \delta\phi_x + \sum_{k=1}^{n} I'_{x_o k} E_{sk} \delta\phi_x \tag{3.8}$$

$$\delta M_{yc} = \sum_{k=1}^{n} x_k y_k a_k E_{sk} \delta\phi_x$$

Similarly, the finite change of a curvature, $\delta\phi_y$, generates a stress change, $E_{sk}\delta\phi_y y$, and the resulting change of force components δP_c, δM_{xc} and δM_{yc}, can be written as:

$$\delta P_c = \sum_{k=1}^{n} y_k a_k E_{sk} \delta\phi_y$$

$$\delta M_{xc} = \sum_{k=1}^{n} x_k y_k a_k E_{sk} \delta\phi_y \tag{3.9}$$

$$\delta M_{yc} = \sum_{k=1}^{n} y_k^2 a_k E_{sk} \delta\phi_y + \sum_{k=1}^{n} I'_{y_o k} E_{sk} \delta\phi_y$$

It is a must that the stress resultants P, M_x and M_y satisfy both the equilibrium and compatibility conditions. Referring the strained plane (Figure 3.5) under combined biaxial bending and axial load, the stress resultants P, M_x and M_y can be expressed as functions of ε_o, ϕ_x and ϕ_y :

$$P = P_c(\varepsilon_o, \phi_x, \phi_y)$$

$$M_x = M_{xc}(\varepsilon_o, \phi_x, \phi_y) \tag{3.10}$$

$$M_y = M_{yc}(\varepsilon_o, \phi_x, \phi_y)$$

Expanding Equation 3.10 about ε_o, ϕ_x and ϕ_y by Taylor's series and retaining linear terms:

$$P = P_c + \frac{\partial P_c}{\partial \varepsilon_o}\delta\varepsilon_o + \frac{\partial P_c}{\partial \phi_x}\delta\phi_x + \frac{\partial P_c}{\partial \phi_y}\delta\phi_y + \ldots$$

$$M_x = M_{xc} + \frac{\partial M_{xc}}{\partial \varepsilon_o}\delta\varepsilon_o + \frac{\partial M_{xc}}{\partial \phi_x}\delta\phi_x + \frac{\partial M_{xc}}{\partial \phi_y}\delta\phi_y + \ldots \tag{3.11}$$

$$M_y = M_{yc} + \frac{\partial M_{yc}}{\partial \varepsilon_o}\delta\varepsilon_o + \frac{\partial M_{yc}}{\partial \phi_x}\delta\phi_x + \frac{\partial M_{yc}}{\partial \phi_y}\delta\phi_y + \ldots$$

Rearranging Equation 3.11 in a matrix form, an incremental stiffness of small cross-section can be written as:

$$[K_{sc}] = \begin{bmatrix} \frac{\partial P_c}{\partial \varepsilon_o} & \frac{\partial P_c}{\partial \phi_x} & \frac{\partial P_c}{\partial \phi_y} \\ \frac{\partial M_{xc}}{\partial \varepsilon_o} & \frac{\partial M_{xc}}{\partial \phi_x} & \frac{\partial M_{xc}}{\partial \phi_y} \\ \frac{\partial M_{yc}}{\partial \varepsilon_o} & \frac{\partial M_{yc}}{\partial \phi_x} & \frac{\partial M_{yc}}{\partial \phi_y} \end{bmatrix} \tag{3.12}$$

The components of cross-sectional stiffness matrix $[K_{sc}]$ can be given from the prescribed Equations 3.7, 3.8 and 3.9. Thus, the incremental stiffness matrix of a cross-section for numerical analysis can be given as:

$$[K_{sc}] = \begin{bmatrix} \sum_{k=1}^{n} a_k E_{sk} & \sum_{k=1}^{n} a_k x_k E_{sk} & \sum_{k=1}^{n} a_k y_k E_{sk} \\ \sum_{k=1}^{n} a_k x_k E_{sk} & \sum_{k=1}^{n} (a_k y_k{}^2 + I'_{x_o k}) E_{sk} & \sum_{k=1}^{n} a_k x_k y_k E_{sk} \\ \sum_{k=1}^{n} a_k y_k E_{sk} & \sum_{k=1}^{n} a_k x_k y_k E_{sk} & \sum_{k=1}^{n} (a_k x_k{}^2 + I'_{y_o k}) E_{sk} \end{bmatrix} \quad (3.13)$$

It is required to express an equilibrium equation in an incremental (difference) form for numerical analysis from the analytical (differential) form ($dF = K_{sc} dD$). Thus the incremental form of equilibrium equation is given for small changes of force, δF , and strain, δD, as follows:

$$\{\delta F\} = [K_{sc}] \{\delta D\} \quad (3.14)$$

The resultant force and strain vectors under combined biaxial bending and axial compression at any segment point along the column are defined as:

$$\{F\} = \{P, M_x, M_y\}^T \quad (3.15)$$

$$\{D\} = \{\varepsilon_o, \phi_x, \phi_y\}^T \quad (3.16)$$

The difference between the proposed and calculated forces at any segment point is given by:

$$\{\delta F\} = \{F_c\} - \{F_p\} \quad (3.17)$$

If the proposed force vector is not close to those obtained from the calculated values of forces, corrections to strain $\{\varepsilon_o, \phi_x, \phi_y\}^T$ is required to reduce the difference in next iteration. Thus a finite change of strain due to the obtained difference in force can be written from Equation 3.14 as:

$$\{\delta D\} = [K_{sc}]^{-1}\{\delta F\} \tag{3.18}$$

Due to finite difference of force components, a small quantity of strain components $\{\varepsilon_o, \phi_x, \phi_y\}^T$ updates actual strain ε_k at each element to reduce the force difference in the next iteration. This work is remarkably robust because the procedure must be carried out at both individual element and each segment points along the column.

The deflections at each segment points along the column are determined by the double integration of both curvatures corresponding to the converged force vectors previously. In other word, the deflection is equal to the fictitious moment [Timoshenko and Gere, 1963] through the consecutive points on fictitious loading curve (curvature diagram). The deflections are calculated starting with the pinned end and the calculated deflection at segment point i is given by:

$$V_{ic} = V_{ic-1} + A_{i-1} L_i + \frac{L_i(2\phi_{i-1} + \phi_i)}{6} L_i \tag{3.19}$$

$$\text{where } A_i = A_{i-1} + \frac{L_i(\phi_{i-1} + \phi_i)}{2}$$

Equation 3.19 is based on the assumption that the curvature varies linearly within a segment along the column as shown in Figure 3.6.a. This implies that the area of fictitious load is apparently underestimated. Furthermore, the curvature has an abrupt change at the midheight of a column as the hinging region develops there. Hence, it can

be concluded that the calculated deflection should be modified to give a better approximation by adopting the nonlinear variation of curvature between the segment points. The curvature diagram can be represented by a second order parabola. The parabola is determined so as to pass through three consecutive points on the fictitious loading curve as shown in Figure 3.6.b. The extended formulation of deflection can be expressed in the following form as:

$$V_{ic} = V_{ic-1} + A_{i-1} L_i + \frac{L_i(\phi_{i-1} + 10\phi_i + \phi_{i+1})}{12} L_i \tag{3.20}$$

$$\text{where } A_i = A_{i-1} + \frac{L_i(\phi_{i-1} + 2\phi_i)}{3}$$

Where the subscript i is recursive, V_{ic} is a calculated deflection at segment i, A_i is an area of fictitious load at segment i and L_i is a length of segment i.

After the deflections are calculated, the compatibility conditions should be examined through the provided tolerance and the incompatibility. The incompatibility ζ is defined as (see Figure 3.7):

$$\zeta = V_{ic} - V_{ip} \tag{3.21}$$

Where V_{ip} is a proposed deflection at segment i.

The compatibility conditions should be checked at the control segment point in control direction either in x-direction or y-direction because the externally controlled deflection is only concerned with one direction. If the difference between the calculated deflection at the control segment point and the proposed deflection at control point is not below a given allowable tolerance, this implies that the applied axial load with

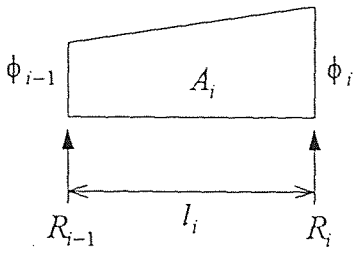

$$A_i = A_{i-1} + \frac{l_i(\phi_{i-1} + \phi_i)}{2}$$

$$R_{i-1} = \frac{l_i}{6}(2\phi_{i-1} + \phi_i)$$

$$R_i = \frac{l_i}{6}(\phi_{i-1} + 2\phi_i)$$

(a) Linear Distribution of Curvature

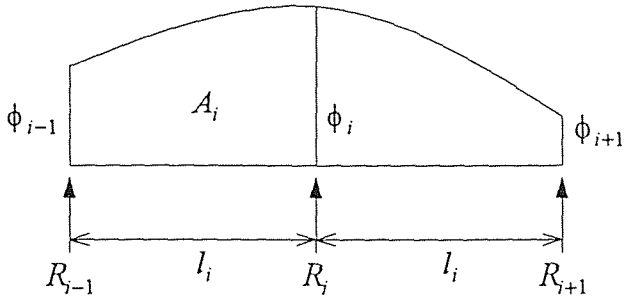

$$A_i = A_{i-1} + \frac{l_i(\phi_{i-1} + 2\phi_i)}{3}$$

$$R_i = \frac{l_i}{12}(\phi_{i-1} + 10\phi_i + \phi_{i+1})$$

(b) Nonlinear Distribution of Curvature

Figure 3.6 Variation of Curvature in a Column Segment

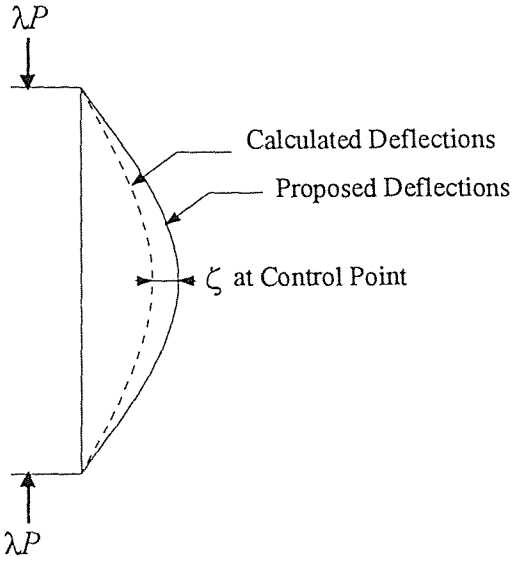

Figure 3.7 Modifed Iterations for Deflection at Control Point

bidirectional eccentricities is less or greater than the required axial load to produce a deflection close to the proposed deflection. Thus, an axial load factor λ must be used to modify the applied axial load and the modified axial load will generate the adjusted control deflection in the next iteration (Figure 3.7).

In the previous study, the procedure was repeated until the difference between the calculated and proposed deflections within an allowable tolerance through successive iteration method. However, this algorithm can not handle the case of unloading. Furthermore, the convergence may not be achieved in some cases as illustrated in Figure 3.8. Such situation of convergence problem may be caused by an approximation of cross-sectional stiffness when the strain enters into the inelastic range of stress-strain curve. In particular, such a small change in resultant strain near the envelope unloading point is able to cause a remarkable change in stress. Such numerical sensitivity has also been observed when the proposed model is simulated for the concrete under cyclic loading (see section 2.5 and 2.6). Thus, a more sophisticated method is needed to achieve the convergence. Also, this method is required to handle the different loading paths for the present study.

In the derivation of incremental cross-sectional stiffness, Taylor's series was used to approximate the force components. Taylor's expansion exhibits the characteristics that all the information used in the approximation concentrates on the expanded points in ε_o, ϕ_x and ϕ_y. It should be mentioned that the primary use of Taylor's expansion in a numerical analysis is not for approximation purpose, but for the derivation of numerical technique. Therefore, there is a need to develop a forecasting procedure of a more reasonable proposed value and an advanced modification procedure of the applied axial load in this study. These are particularly needed to achieve a solution in the descending branch of load-deformation curve. The reason is that the cross-sectional stiffness has been approximated as the strain enters into the nonlinear range of stress-strain curve. In other word, an inadequate difference in the strain components may cause the

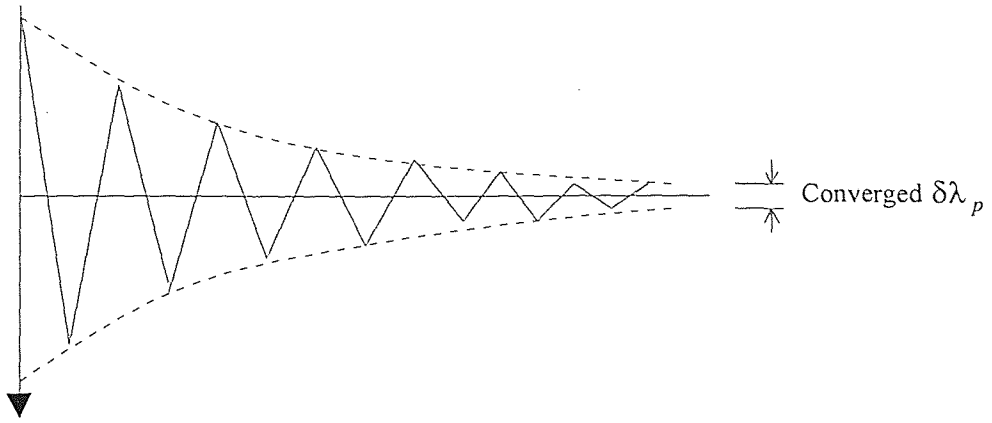

(a) General Case

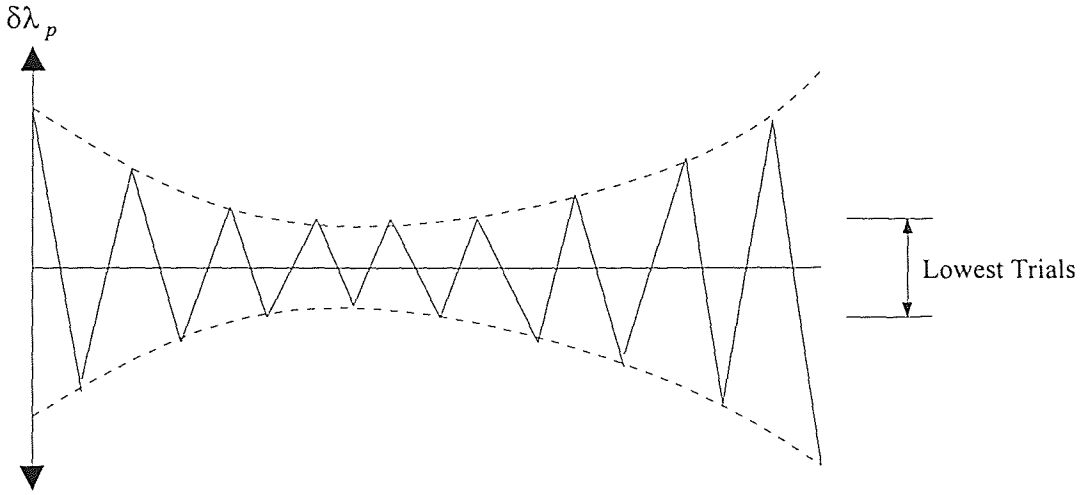

(b) Perturbation in High Strain Range

Figure 3.8 Behavior of Load Factor for Modification Procedure

considerable change of stress in the stress-strain curve. Due to the above mentioned characteristics of incremental stiffness in the cross-section, the numerical behavior of load factor is perturbed in some instance.

The modification of proposed load factor can therefore be determined by considering the effect of unit change in the proposed load factor λ_p. The unit change in load factor λ produces the corresponding axial force with bidirectional eccentricities at certain discrete element k as:

$$\begin{aligned} (P_k)_{\lambda=1} &= P \\ (M_{xk})_{\lambda=1} &= P\, e_y + P\, y_k \\ (M_{yk})_{\lambda=1} &= P\, e_x + P\, x_k \end{aligned} \tag{3.22}$$

Equation 3.22 shows the axial force and moments when λ is equal to unit. The corresponding strain vector $\{D\}$ at the individual element can then be obtained by:

$$\begin{Bmatrix} (\varepsilon_{ok})_{\lambda=1} \\ (\phi_{xk})_{\lambda=1} \\ (\phi_{yk})_{\lambda=1} \end{Bmatrix} = \left[K_{sc} \right]_k^{-1} \begin{Bmatrix} (P_k)_{\lambda=1} \\ (M_{xk})_{\lambda=1} \\ (M_{yk})_{\lambda=1} \end{Bmatrix} \tag{3.23}$$

After the changes in curvature are obtained at each element, the changes are integrated to find the corresponding changes in the calculated deflections. Differentiating Equation 3.21 with the proposed load factor λ_p, the calculated deflection due to a unit load factor can be determined as:

$$\frac{\delta\zeta}{\delta\lambda_p} = \frac{\delta(V_{ic} - V_{ip})}{\delta\lambda_p} = (V_{ic})_{\lambda=1} \tag{3.24}$$

The term $\delta(V_{ic} - V_{ip})/\delta\lambda_p$ corresponds to the calculated deflection due to a unit load factor, because V_{ic} is the calculated deflection when the applied eccentric load is $\lambda_p P$ and V_{ip} is a proposed deflection at the control point which can be controlled externally. Thus, the modification quantities, $\delta\lambda_p$, can be obtained by rearranging the above Equation 3.24 and $\delta\zeta$ from Equation 3.21:

$$\delta\lambda_p = \frac{\delta\zeta}{(V_{ic})_{\lambda=1}} = \frac{(V_{ic})_{\lambda=\lambda_p} - V_{ip}}{(V_{ic})_{\lambda=1}} \tag{3.25}$$

Since $\delta\zeta$ changes from the incompatibility ζ of the first iteration to a very small value which is almost zero. Therefore the change in incompatibility, $\delta\zeta$, is equal to the first incompatibility ζ .

The modification quantity of load factor is added to the proposed load factor λ_p to give new proposal value for the next iteration. The calculated deflection due to the new proposed load factor is therefore adjusted. It should be noted that the quantity of updated λ_p depends on the sign of $\delta\lambda_p$ to adjust the applied eccentric axial load.

The above procedure for modifying the load factor is not enough to secure the convergence as the material behavior enters into an inelastic strain range. The cross-sectional stiffness in this range become an approximated value even though the discrete element is designed to be a sufficient small to achieve an uniform stress. In certain analysis stage, an infinitesimal change in load factor may produce a comparatively large difference in strain of each element. Consequently, the change in magnitude of the resultant forces may never falls into the specified tolerances.

There are cases where the solution diverges in the descending branch of load-deformation curve. For this case, it is observed that the required modification quantity of a load factor, which is able to give converging solution, exists between two trials as

shown in Figure 3.8. Once this numerical behavior is found in the modification procedure, the modification quantity of a load factor should be restricted within two trials instead of using the above mentioned modification procedure. The two trials are selected as the lowest values. However, the procedure consumes more computing time by using an infinitesimal change of modification quantity of a load factor.

In order to deal with loading or reloading and unloading, it is necessary to maintain a strain history for all the discrete elements along the column segments. As each successive solution is found, the strain in each element should be calculated and compared with the latest value in the strain history. If the current magnitude of strain is less than the strain history value, the unloading has developed as shown in Figure 3.9.b and the current strain should not be stored as the strain history for optimum algorithm. If the magnitude of calculated strain is greater than the strain history value, the loading has developed and the strain history is replaced by the current strain. This implies that the strain history can only be updated by the strain on the envelope curve. During the present numerical analysis, if the magnitude of the proposed strain at any element ε_k is less than the magnitude of the strain history value at the corresponding element ε_{kh}, then the unloading stress f_k at element k can be obtained by:

$$f_k = f_{kh} - E_{unlo}(\varepsilon_{kh} - \varepsilon_k) \tag{3.26}$$

where f_{kh} is the stress corresponding to strain history ε_{kh} and E_{unlo} is the slope of the unloading curve as described in section 3.2.1.

Equation 3.26 is valid in both ranges of compressive and tensile strains. In addition, this mathematical expression is effective in both unloading and reloading stress-strain paths while the magnitude of current strain ε_k is less than the stored value of strain history ε_{kh}. The proposed concept for the strain history can reduce the consumed memory space in the practical computer implementation. The required memory space in

$\varepsilon_k < \varepsilon_{kh}$; $f_k < f_{kh}$; *Unload* ; $f_k = f_{kh} - E_{unlo}(\varepsilon_{kh} - \varepsilon_k)$

$\varepsilon_k > \varepsilon_{kh}$; $f_k < f_{kv}$; Re*load* ; $f_k = f_{kh} - E_{unlo}(\varepsilon_{kh} - \varepsilon_k)$

$\varepsilon'_k > \varepsilon_{kh}$; $f'_k > f'_{kv}$; *Load* ; $f_k = f'_{kv}$ *from envelope*

Update Strain History at Every Converged Solution

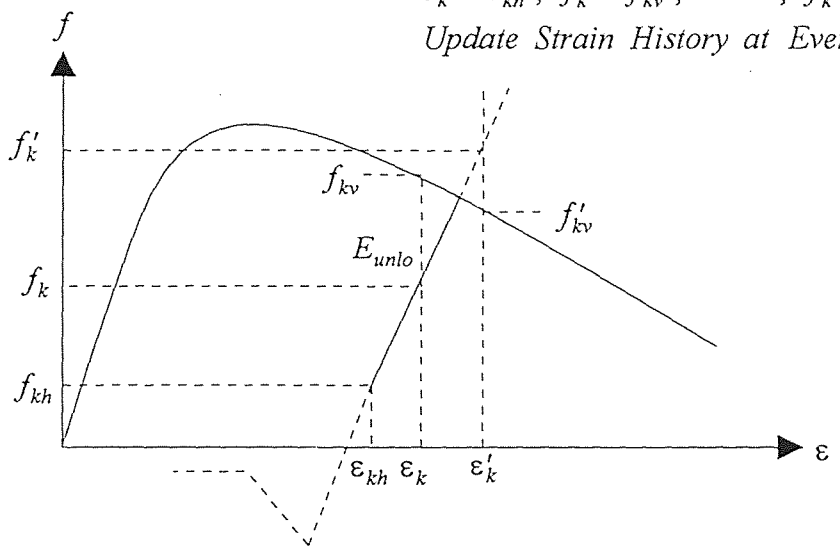

(a) Conventional Strain History

$|\varepsilon_k| < |\varepsilon_{kh}|$; *Unload or* Re*load* ; $f_k = f_{kh} - E_{unlo}(\varepsilon_{kh} - \varepsilon_k)$

$|\varepsilon'_{kh}| > |\varepsilon_{kh}|$; *Load* ; $f_k = f'_{kh}$ *from envelope*

Update Strain History; $|\varepsilon_k| > |\varepsilon_{kh}|$ *at Converged Solution*

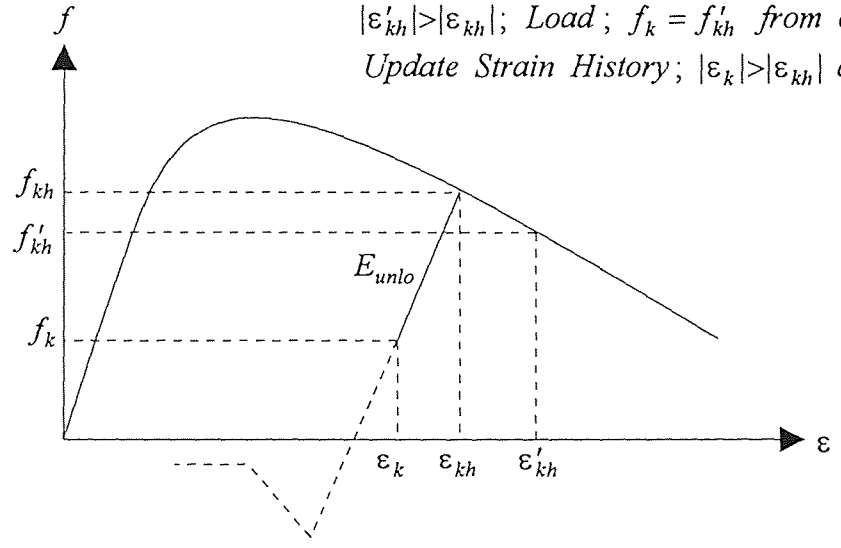

(b) Present Strain History

Figure 3.9 Unloading Behavior of a Discrete Element

the conventional algorithm (see Figure 3.9.a) is remarkably large to decide the status of stress-strain path at the individual element along the column segments.

3.1.4 Discussions of Accuracy and Convergence

It should be noted that the small change of strain components $\delta\varepsilon_o$, $\delta\phi_x$ and $\delta\phi_y$ have to be sufficiently small in order to satisfy the basic assumption of Taylor's series expansion about ε_o, ϕ_x and ϕ_y. Equation 3.11 was expanded using the Taylor's series about ε_o, ϕ_x and ϕ_y to approximate the resultant force components P, M_x and M_y. This implies that the proposed values of strain components ε_{op}, ϕ_{xp} and ϕ_{yp} should be close enough to ε_o, ϕ_x and ϕ_y respectively. Consequently, the proposed values of strain components have achieved convergence. In other word, if the proposed values of strain components exist outside of certain range, there is no guarantee that the proposed value converge to a solution regardless of number of iterations.

The following allowable tolerances have been found: 10^{-6} for force and moments, 10^{-3} for deflections. The allowable incompatibilities can be reduced slightly by using double precision, but the numerical results are not affected significantly.

Generally the present proposed procedures converges rapidly, especially where solutions being sought are in the ascending branch of load-deformation curve. Although the rate of convergence to give a solution is dependent on several conditions, it is desirable to provide the reasonable proposed values for the load factor, strain vector at each element and deflections at all segment points before the iterations for converging solution. Thus, the second order Lagrange Polynomial is used to forecast a better proposal from the last three proposals corresponding to the converged solutions. If the required forecasting point x exists beyond the range $[x_o, x_2]$, the polynomial is an extrapolation function. Otherwise, the polynomial is approximated as an interpolation, and x locates within range $[x_o, x_2]$ as shown in Figure 3.10. Of course, the accuracy of

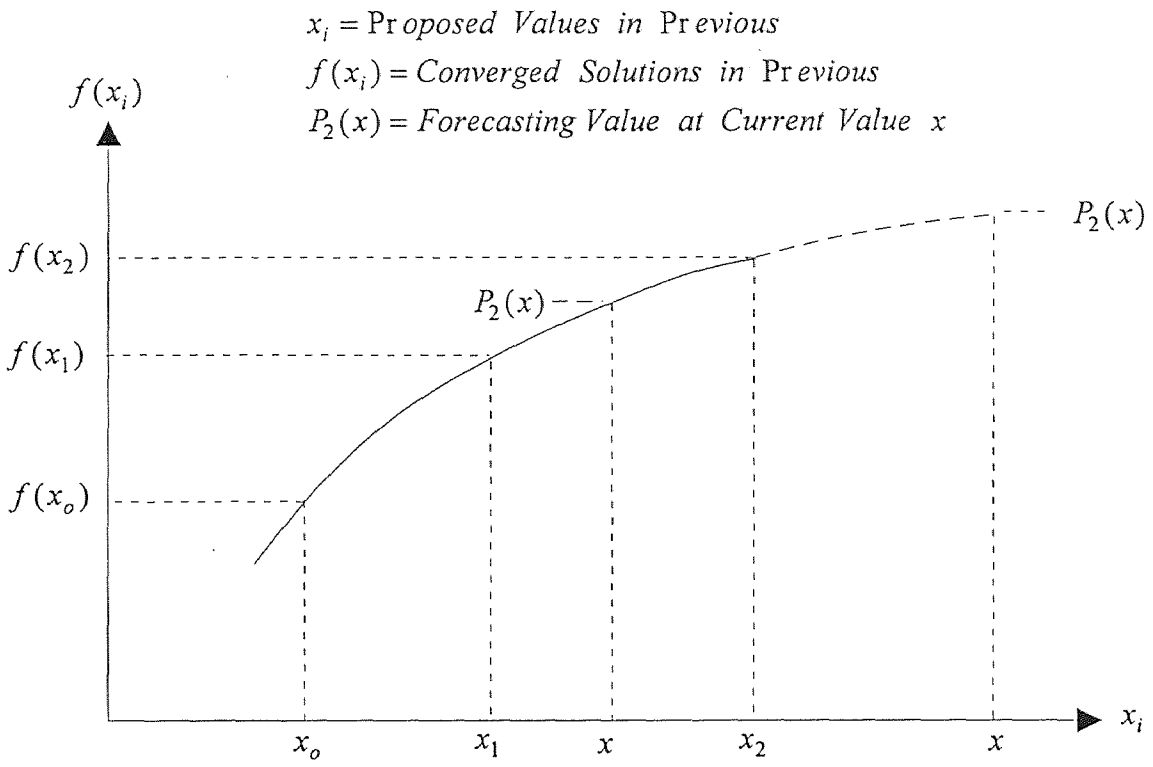

Figure 3.10 Forecast of Reasonable Proposal

forecast in the extrapolation is decreased because the Lagrange Polynomial is able to give more accurate values in the interpolation.

Consider x_o, x_1 and x_2 as the deflections at control segment point for the previous three solutions and $f(x_o)$, $f(x_1)$ and $f(x_2)$ as the values of converged solutions in the previous solutions. Now let x be the current control deflection for which a solution is being sought. The forecasting value $P_2(x)$ for x is written as:

$$P_2(x) = \sum_{n=o}^{2} f(x_n)\, L_n(x)$$

$$= f(x_o)\, L_o(x) + f(x_1)\, L_1(x) + f(x_2)\, L_2(x) \qquad (3.27)$$

Where coefficient polynomials are $L_o(x)$, $L_1(x)$ and $L_2(x)$:

$$L_o(x) = \frac{(x-x_1)\ (x-x_2)}{(x_o-x_1)\ (x_o-x_2)}$$

$$L_1(x) = \frac{(x-x_o)\ (x-x_2)}{(x_1-x_o)\ (x_1-x_2)}$$

$$L_2(x) = \frac{(x-x_o)\ (x-x_1)}{(x_2-x_o)\ (x_2-x_1)}$$

The forecasting procedure reasonably provides the first trial and this routine contributes to reducing the number of iterations to a converged solution. The forecasting procedure for each new solution stage can be applied to both loading and unloading paths through the extrapolation and interpolation.

3.2 Procedure of Numerical Analysis

Computer implementation of analytical model discussed in section 3.1 is described in this section. The computer model developed consists of both preprocessor and analysis procedure. FORTRAN 77 is used to implement the extended analytical model at VAX system.

Preprocessor: This routine generates the coordinates and area of discrete elements for each segment points along the column . There is a subroutine INPUTGEN.

Analysis Procedure: This procedure contains thirteen major subroutines as follow: STATEMENT, MOMENT, CLEAR, STEEL, CONCRETE, ACCUMU, SOLVER, SAVE, INTEGRA, LAMDA, HISTORY, SHIFT, FORECAST.

1) STATEMENT: This routine gives definitions of numerous variables used in the program and does not perform any calculations.

2) MOMENT: This routine calculates moments at each segment points along the column from the proposed axial load with eccentricities including the second order effect at each iteration.

3) CLEAR: This routine erases the previous calculated force vector at each segment point and the cross-sectional stiffness matrix of an individual element along the column at the first iteration.

4) STEEL: This routine gives corresponding stress and secant modulus at the proposed strain on a specific stress strain path for steel elements along the column segments. The unloading, reloading and loading stress-strain paths are solely dependent upon the stored strain history at corresponding elements along the segment of a column.

5) CONCRETE: This routine is similar to the subroutine STEEL. The idealized cyclic stress-strain curve is implemented.

6) ACCUMU: This routine accumulates the calculated elemental forces and elemental cross-sectional stiffness matrix to build the force vector and its resultant stiffness on the specific segment point.

7) SOLVER: This routine solves the equilibrium equation to obtain a strain vector due to the force difference between the calculated and proposed ones.

8) SAVE: This routine saves the converged force vector and corresponding strain vector and corresponding resultant stiffness matrix at each segment points along the column.

9) INTEGRA: This routine integrates the converged curvatures of a strain vector from the subroutine SAVE to give the calculated deflections at each segment points

10) LAMDA: If the calculated deflection dose not satisfy with the proposed deflection at the control segment point, this routine should be performed to modify the load factor of an eccentric axial load which is able to produce a closer deflection to the proposed control deflection for the next iteration. And the load factor is traced in this routine to find a numerical behavior of the modification quantity in load factor.

11) HISTORY: This routine updates the strain history at each element along the column through the concept discussed in the previous section 3.1.3 once a solution is obtained.

12) SHIFT: After the solutions are found, the load factor, strain vector and segment deflections are restored and these stored informations will be used to forecast a new proposal for the next solution.

13) FORECAST: This routine forecasts the load factor, strain vector and deflections at each segment points to provide closer proposals to the next solution.

A detailed flow chart for an analysis of reinforced concrete column under cyclic axial compression with bidirectional eccentricities is presented in Figure 3.11. A computer model developed is based on the extended finite segment method as described in section 3.1.3. It should be noted that the present computer analysis assumes that both ends of the column are pinned-ended. However, this computer program can be easily modified to accommodate other end conditions.

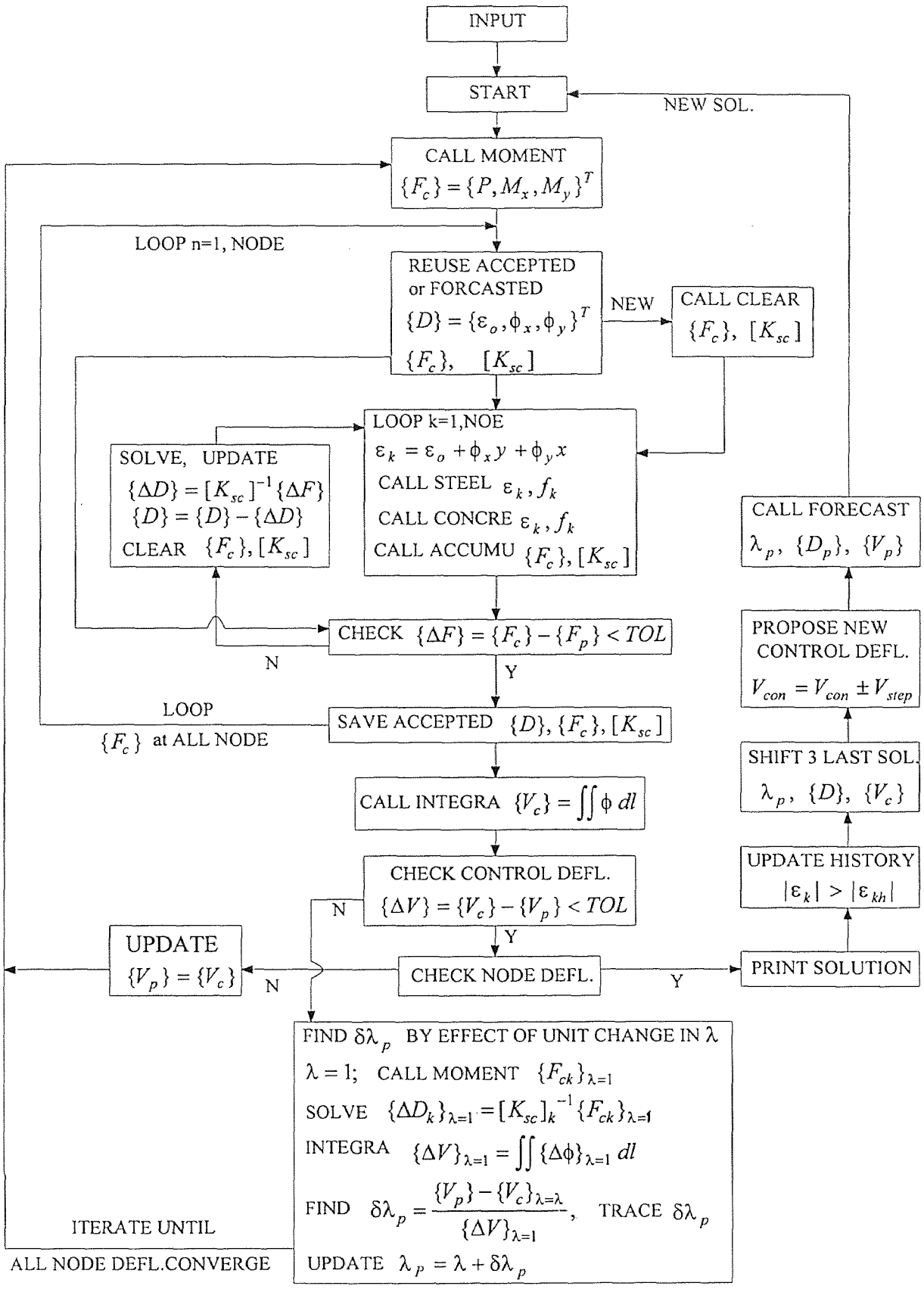

Figure 3.11 Flow Chart for Analysis of R/C Columns

CHAPTER 4

EXPERIMENTAL PROGRAM AND PREDICTION OF COLUMN ANALYSIS

An experimental investigation was carried out on slender reinforced concrete (R/C) columns to compare the ultimate load, load-deflection and moment-curvature predicted by the proposed numerical method with those obtained experimentally. For the present study, eight slender R/C columns were tested under cyclic axial compression with bidirectional eccentricities. The columns had the pinned end at both ends.

The test parameters of column specimens were bidirectional eccentricities and its angle to the reference axis. Eccentricities used in this experimental study were 1.0 inch and 2.0 inches, respectively. The angles used were 45 and 22.5 degrees as shown in Table 4.1. It should be mentioned that the cyclic compressive loading with bidirectional eccentricities is in the longitudinal direction, not in the transverse direction, with respect to the column axis.

4.1 Test of R/C Columns under Cyclic Axial Compression with Bidirectional Eccentricities

4.1.1 Preparation of Column Specimens

All columns had a nominal cross section of 3.0 by 3.0 inches in both sides, four feet long and the brackets at both ends to enable axial load to be applied outside of the column section for the required biaxial eccentricities. The reinforcement consisted of four #3 deformed steel bars which were tied by 12 gage steel wire as a stirrup at spacing 3.0 inches. The details of column geometry and reinforcements are shown in Figure 4.1.

The concrete materials consisted of Type III Portland cement, sand, aggregate and water. Each column specimen and five control cylinders were cast from the same

Table 4.1 Test Outline of Column Specimens

Specimen	Main Bars	f_y (ksi)	f_c' (psi)	s (in.)	e_x (in.)	e_y (in.)	θ (deg.)	l (in.)
C1	4-#3	61	4700	3.0	0.707	0.707	45.0	48.0
C2	4-#3	61	4800	3.0	0.765	1.848	22.5	48.0
C3	4-#3	61	5900	3.0	0.383	0.924	22.5	48.0
C4	4-#3	61	6500	3.0	1.414	1.414	45.0	48.0
C5	4-#3	61	5500	3.0	0.707	0.707	45.0	48.0
C6	4-#3	61	7100	3.0	0.707	0.707	45.0	48.0
C7	4-#3	61	5200	3.0	0.707	0.707	45.0	48.0
C8	4-#3	61	5400	3.0	1.414	1.414	45.0	48.0

f_y = Yield stress of Main Bars.

f_c' = Maximum Strength of Concrete.

s = Spacing of Stirrups.

e_x and e_y = Eccentricities along X-Axis and Y-Axis, respectively.

l = Total Length of Column Specimens.

$\theta = \tan^{-1}(e_x / e_y)$.

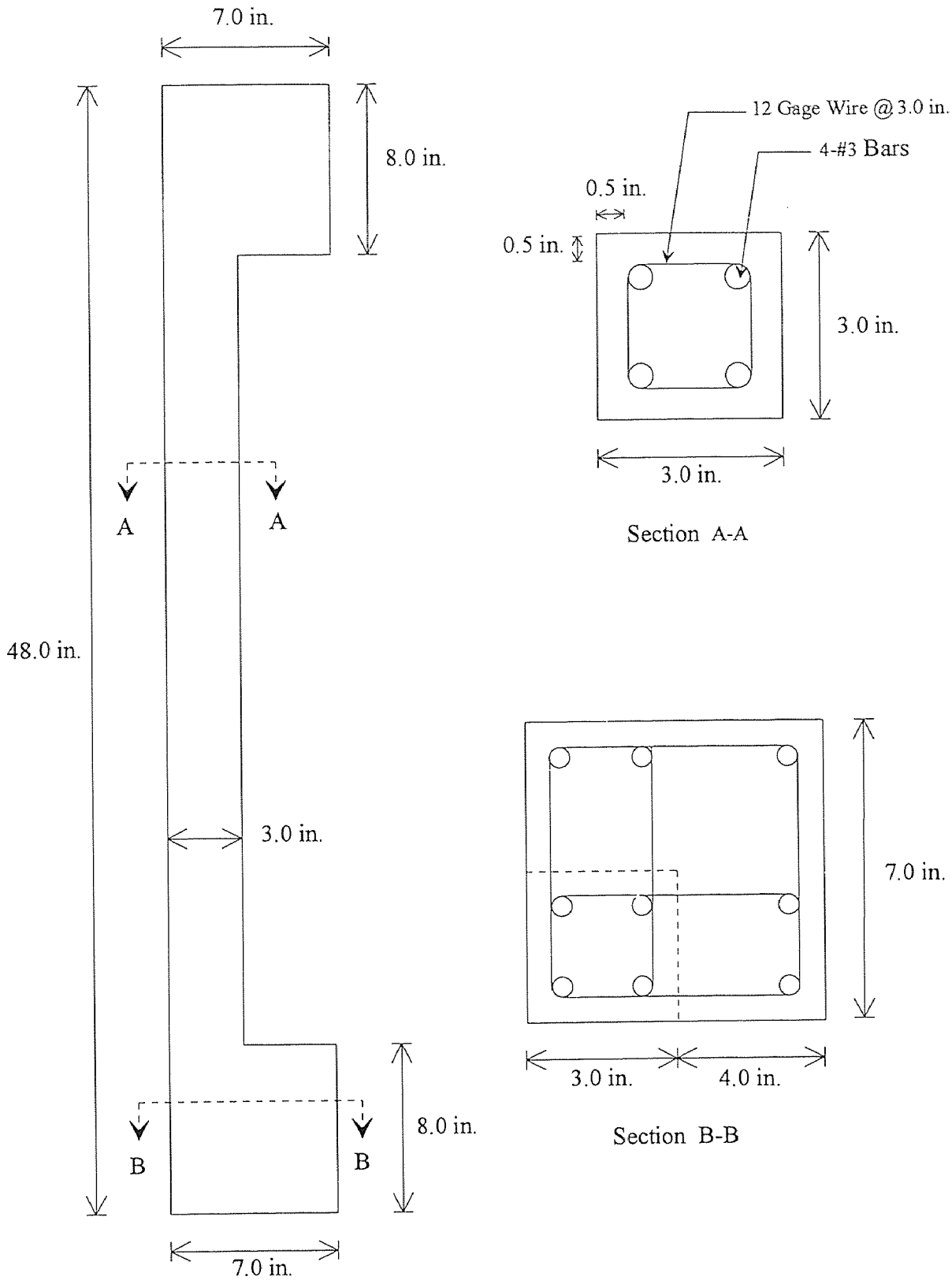

Figure 4.1 Geometry and Reinforcements of Column Specimens

batch of concrete. And all columns were cast horizontally using the electrically driven vibrator and steel rod. The columns and cylinders were stripped approximately 24 hours after casting and both specimens were under moisture curing period of 7 days. Both column specimens and control cylinders were exposed under the same curing condition until the tests were conducted.

4.1.2 Details of Column Test

The tensile tests for #3 steel reinforcements were performed by Tinus & Olsen testing machine and its typical stress-strain curve for #3 reinforcement is shown in Figure 4.2. Five control cylinders with standard size (3.0" x 6.0") for each column specimens were tested to obtain the corresponding ultimate strength of concrete. The tests of concrete cylinders were conducted on the same day as the corresponding column specimens were tested.

The column tests were conducted by an electro-hydraulic closed loop servo controlled material testing system (MTS) under stroke control (stroke rate=0.05 in./min.) to achieve both ascending and descending branches of load-deformation curve. The unloading and reloading were accomplished at an interested load level or a deflection point by a digital function generator (model 410) which enables to generate the loading and unloading with a constant stroke rate. Other manual operation of MTS can not handle the constant displacement control during the different loading path of cyclic loading. Adequate data sampling points were decided by monitoring the results of X-Y RECORDER (model 431) which were generated from the built-in LVDT (linear voltage differential transducer) of the testing machine.

It should be noted that testing machine will shut off automatically when the set-point control at minimum load level is unable to keep holding the column specimen during the entire testing procedure. Because of this difficulty, a number of preliminary tests with imaginary specimens were performed to eliminate the loss of column

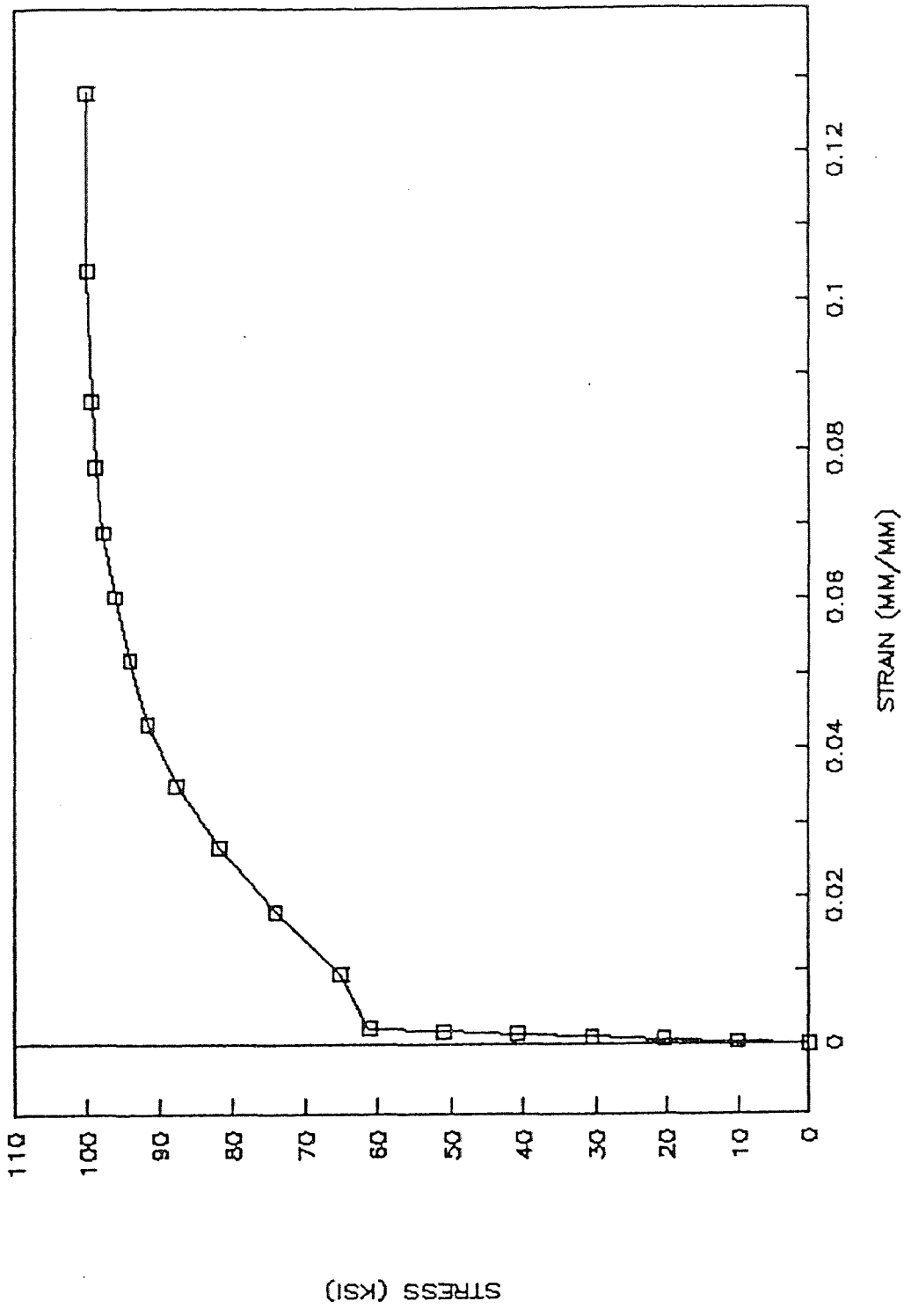

Figure 4.2 Monotonic Stress-Strain Curve for #3 Reinforcement

specimens by this manmade condition.

The desired eccentricities were obtained by moving the ball bearings to the proper position relative to the end plates which were mounted on the both ends of column specimen. The column specimens were adjusted so that the center line of the end bearing facing the load cell coincide with its center line. Subsequently, a small load was applied to keep the specimens in place. An outline of column test programs is presented in Table 4.1.

Several couple of dial gages were used to measure the deflection at the beginning of brackets and at mid-height of column in both X and Y directions. The initial length of mechanical gages were measured before and after setting the column specimens into the testing machine. The initial measurements were repeated several times to ensure the actual length of initial mechanical strain gages. This initial gage length is the basic quantity to calculate the strains and curvatures at each loading steps after all test data are acquired. The deformations at mid-height of column were measured by four pairs of mechanical strain gages to obtain the strains about both X and Y directions, as shown in Figure 4.3. The deflections were measured by AMES dial gage which can measure upto 1/10000 inches.

The setup of column test is presented in Figure 4.4. Data readings from the measuring devices were repeated at certain sampling points when those measured quantities were not stable. The corresponding data samplings were terminated by unavoidable experimental conditions that local failure occurred either at the location of mechanical gages or the hinging region was developed far from the mid-height of column. The reason is that the collected data can not be considered as good results when the noticeable failure occurs beyond the range of mechanical strain gages.

4.1.3 Analysis of Test Results for Columns

The applied axial load can be obtained directly from MTS and the moments Mx and My

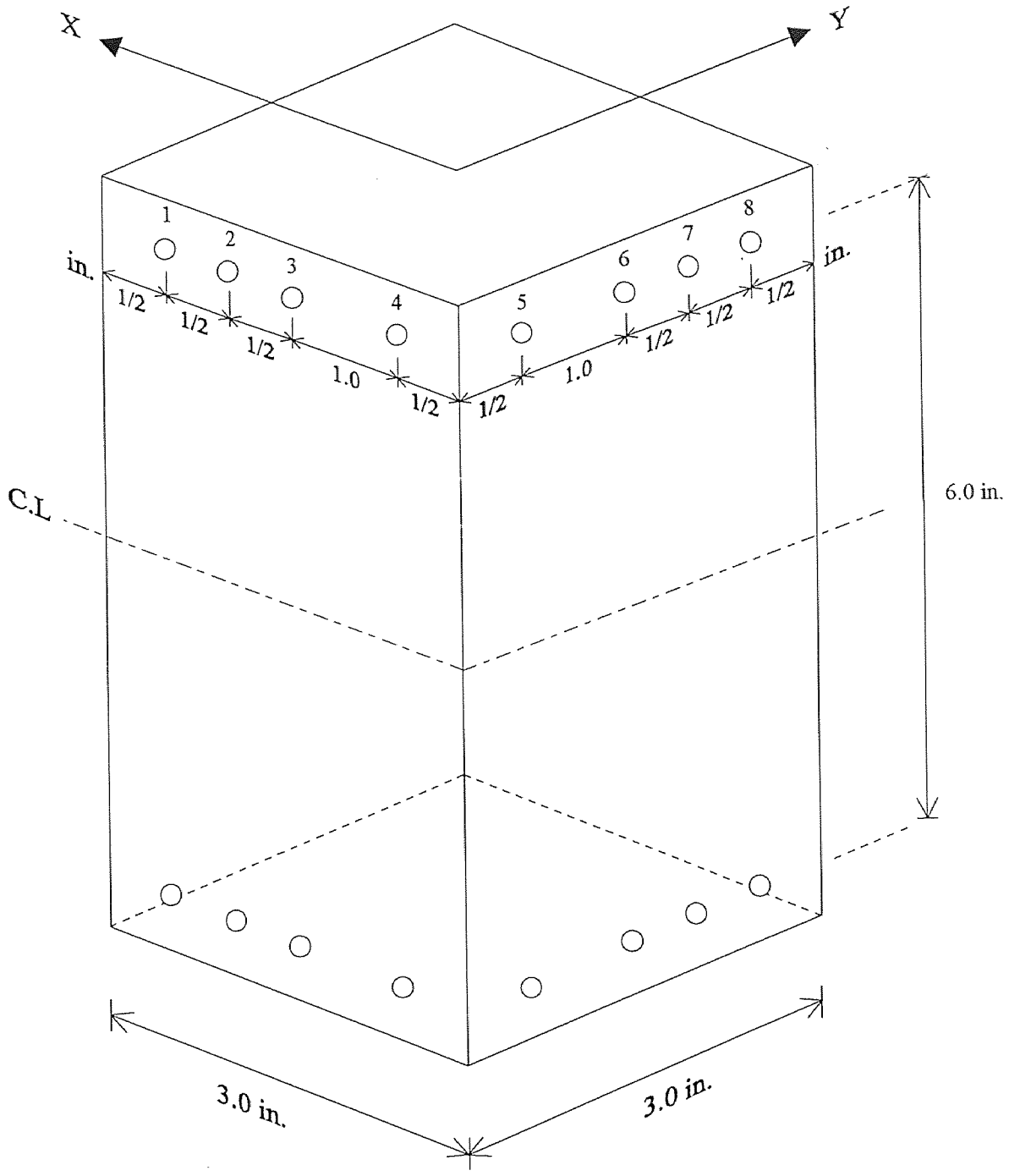

Figure 4.3 Arrangement of Mechanical Strain Gage over Column Segment

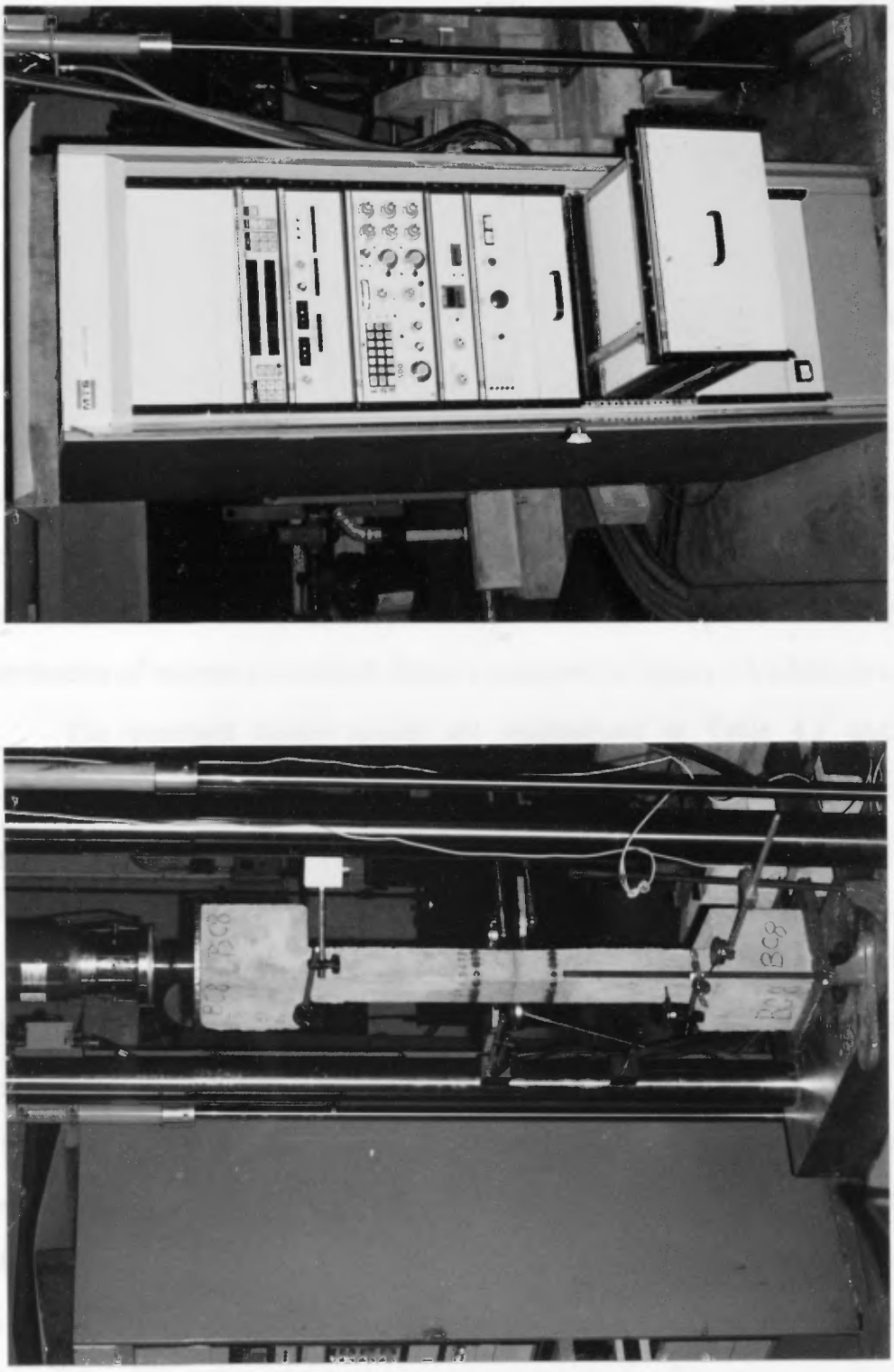

Figure 4.4 Set-up of Column Test

at mid-height of column can be determined from the applied eccentric load, the provided eccentricities and the measured deflections at each load step. These experimental results of maximum axial load and moments are presented in Table 4.2. The ultimate strengths of control concrete cylinders show a scatter due to the different age of concrete column specimens that were tested. Five control cylinders of concrete for each column specimens were tested as the same day as the column test was conducted.

The strains can be calculated by the ratio of difference between an initial gage length and the current gage length to an initial gage length. The curvatures are determined by the slope between the horizontal line and piece wise linear line from the obtained strains at mid-height of the column as shown in Figure 4.5. Extending the nonlinearity of strain value, a linear regression is used to get a more stable value of curvature. The remarkably deviated value of a strain from the remaining three strain data can be excluded in the regression instead of four data points. The typical strain distribution of column on the both faces is presented in Figure 4.6 which is a part of data.

The observed failure modes are summarized in Table 4.3 and Figure 4.7 illustrates the deformed column specimens after testing. For columns with symmetric eccentricities, the crushed concrete in compression zone usually occurs at the corner of both compression faces as shown in Figure 4.8. From these observations of failure mode, it shows that there is a large deformation in the diagonal direction. The failure of concrete seems to be dependent on the magnitude of the maximum load level at each cycle.

It is observed that there is a difference between the current test series and previous studies [Tsao, 1991] on biaxial bending columns under monotonic loading. For the previous study, the location of hinging region was not as predictable as would be desired. But in the present experiments, the hinging region is mostly formed near the mid-height of the columns except one column specimen. The reason for this trend is that an even distribution of cracking due to the stress relaxation of the repeated loading and

Table 4.2 Test Results of Maximum Axial Load and Moments

Specimen	P (lbs)	Mx (lb-in)	My (lb-in)	Number of Cycle *	
C1	18530	22180	21440	1	1
C2	11610	28310	13180	2	2
C3	21110	27740	14630	3	2
C4	12730	23220	23090	2	2
C5	20090	21240	21440	2	2
C6	23110	23500	23730	3	N.A
C7	19340	20640	20440	1	3
C8	11670	22100	21990	1	3

* Denotes Numbers of Cycles in the Ascending and Descending Branches of Load-Deflection Curves respectively.

N.A; Hinging Region of Specimen C6 occured outside the Range of Mechanical Strain Gages.

Note that the unloading points for each test are not necessary to be the same points.

Table 4.3 Observed Failure Mode of Column Specimens

Specimen	Location of Plastic Hinge	Length of Plastic Hinge	Exposed Main Bar	Remark
C1	corner of midheight	5 ~ 6 in.	yes	within gage length
C2	side face of midheight	4 ~ 5 in.	yes	within gage length
C3	side face of upper midheight	3 ~ 4 in.	yes (severely)	noticeable bent
C4	corner of midheight	3 ~ 4 in.	yes	noticeable bent
C5	corner of lower midheight	4 ~ 5 in.	yes (barely)	noticeable bent
C6	below upper bracket	5 ~ 6 in.	yes	beyond gage length
C7	corner of midheight	3 ~ 4 in.	yes	within gage length
C8	corner of upper midheight	3 ~ 4 in.	yes (severely)	within gage length

* Plastic Hinges for all Columns are located within the length of Mechanical Strain Gage except Specimen C6.

* For all Column Specimens, the Cracks are well distributed along the Columns.

* The failed columns show that all reinforcing bars are not buckled.

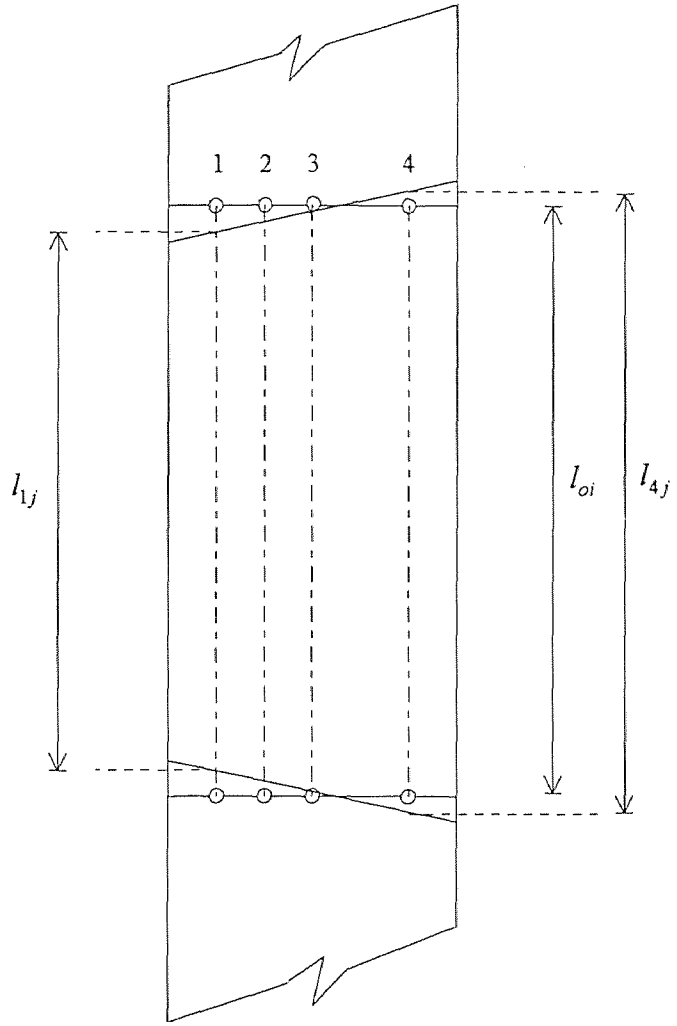

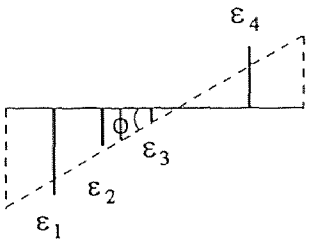

$$\varepsilon_{ij} = \frac{l_{ij} - l_{oi}}{l_{oi}}$$

ϕ = Slope of Linear Regression (3 or 4 Points)

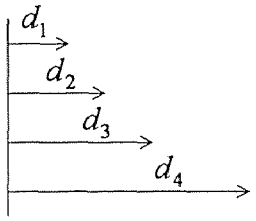

d_i ; Strain Depth at Gage Number i

i ; Gage Number (1 ~ 4)

j ; Load Stage

l_{oi} ; Length of Initial Gage

l_{ij} ; Length of Deformed Gage

ϕ ; Approximated Curvature

Figure 4.5 Analysis of Experimental Strain and Curvature

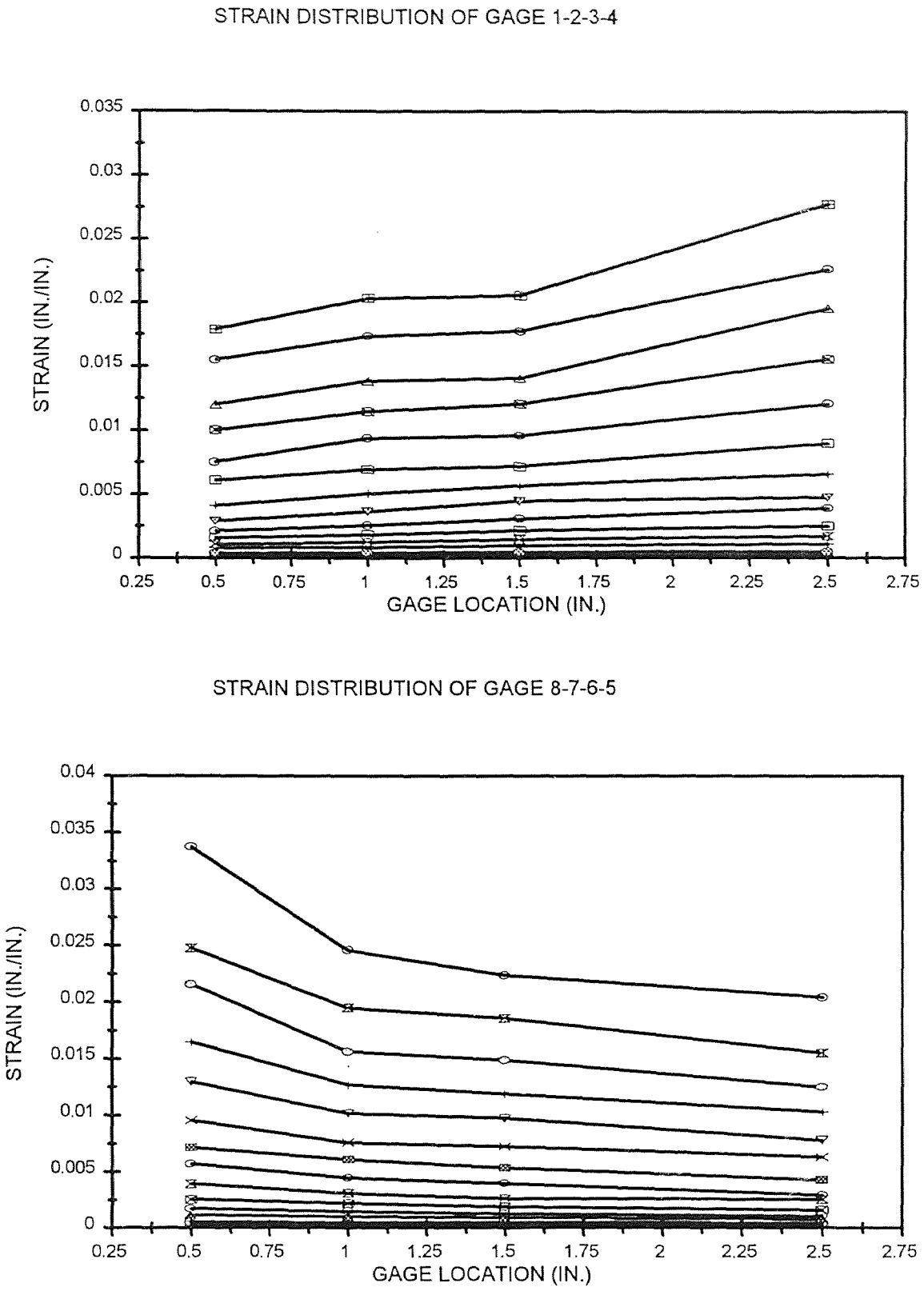

Figure 4.6 Typical Strain Distribution of Column on the Both Sides

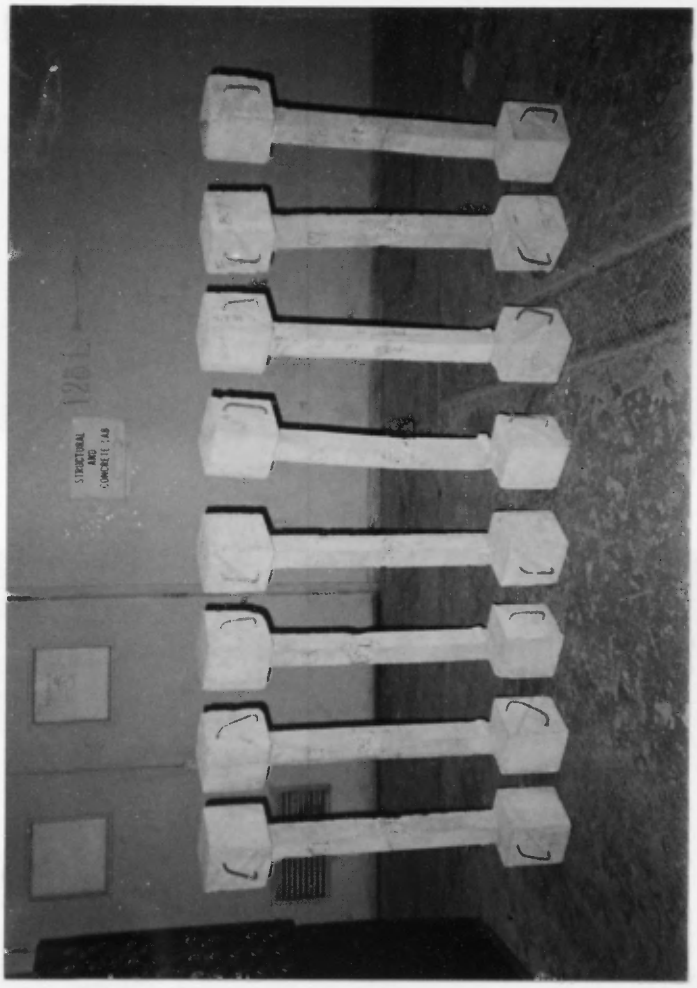

Figure 4.7 Deformed Column Specimens after Test

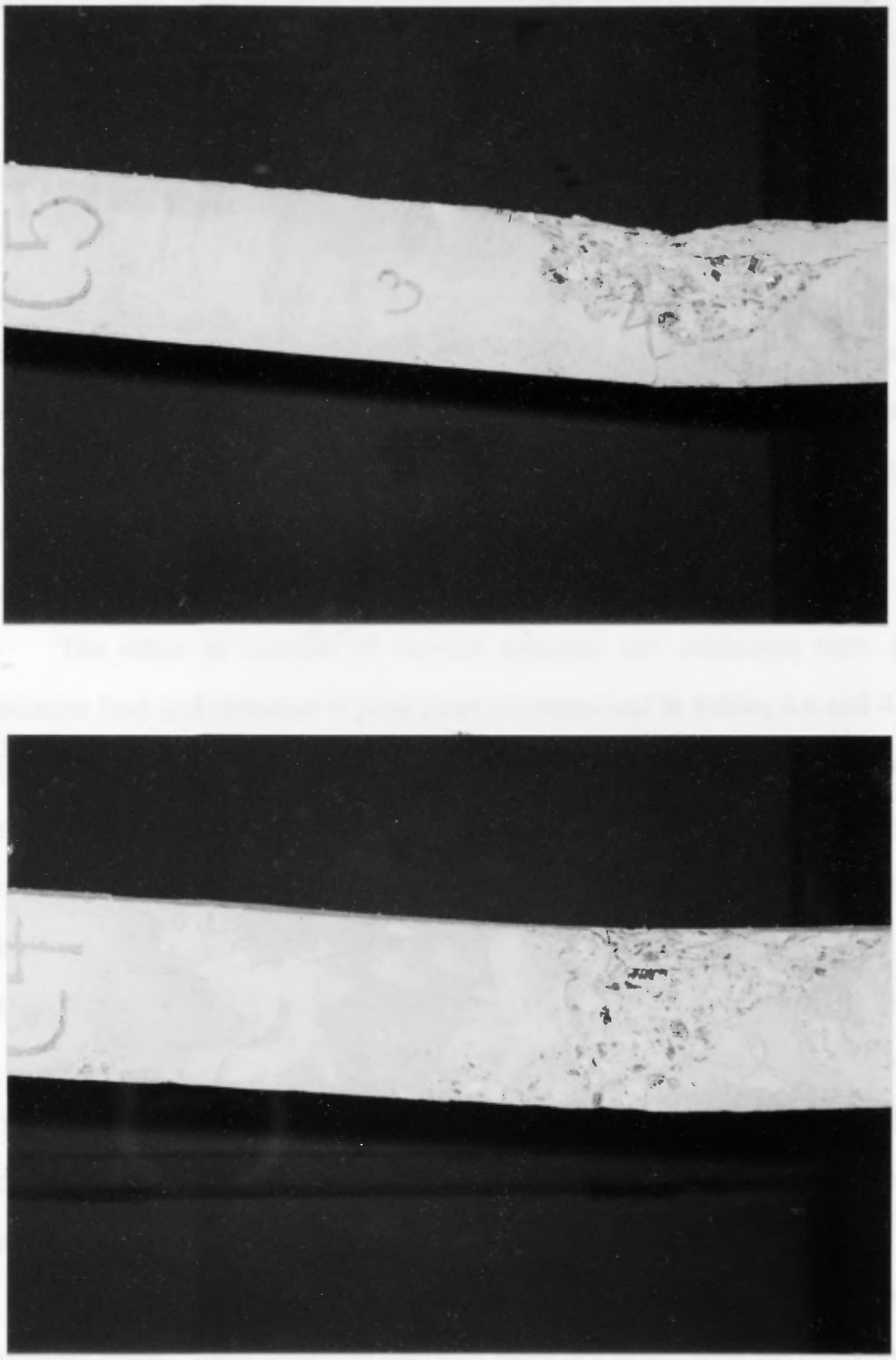

Figure 4.8 Close View of Crushed Concrete in Compression Zone

unloading produces a more uniformly loaded column. The test specimens under monotonic loads seem to fail at the weakest section of the column specimen.

4.2 Comparison of Test Results and Numerical Analysis

In this section, the validity of the computer model developed in chapter 3 is confirmed by the comparison with the experimental results of columns for the present study. A parametric study is made for various factors that may have an effect on the numerical solution. These parameters are the number of segments and number of discrete elements. The use of ten segments was considered to be small enough through the numerous preliminary analysis. The effect of the number of elements and additional term ϕEI of Equations 3.8 and 3.9 in chapter 3 are studied on the maximum load and moments at peak load.

The effect of number of discrete elements and additional term ϕEI on the maximum load and moments at peak point are examined in Tables 4.4 and 4.7. A closer solution to the experimental maximum load was obtained using comparatively less number of elements. Thus it can be concluded that if ϕEI terms are used in the extended formulation, the accuracy of computation can be achieved through the reduced number of elements used. Comparing the tabulated results of maximum load in Tables 4.4 and 4.5, the effect of additional term in 40 elements is greater than the effect of additional term in 64 elements. This implies that the effect of additional term is greater when the number of elements is decreased in the analysis. In the previous studies by Wang and Hsu [1990] and Tsao [1991], this term could not be considered because a finite difference approach was used to compute the deflection.

Table 4.6 shows the proposed analysis closely predicts the experimental maximum loads. Most predicted ultimate loads are lower than the experimental values and most experimental maximum load also shows a sharp increase at the peak. This phenomena could be due to somewhat stiffness relation between the column specimen

Table 4.4 Effect of ϕEI term on the Peak Load for 40 Elements

Specimen	Elment 40 w/o ϕEI	Element 40 w/ ϕEI	Ratio
	P_{max} (lbs)	P_{max} (lbs)	$\frac{P_{40}}{P_{40w}}$
C1	15438	16862	0.91
C2	9934	10762	0.92
C3	16970	18906	0.89
C4	10303	11342	0.91
C5	16701	18181	0.92
C6	18598	20544	0.90
C7	15918	17928	0.89
C8	9585	10905	0.88

Table 4.5 Effect of ϕEI term on the Peak Load for 64 Elements

Specimen	Elment 64 w/o ϕEI	Element 64 w/ ϕEI	Ratio
	P_{max} (lbs)	P_{max} (lbs)	$\frac{P_{64}}{P_{64w}}$
C1	17539	17886	0.97
C2	11129	11383	0.97
C3	20569	20993	0.98
C4	11994	12291	0.97
C5	18833	19212	0.98
C6	21999	22586	0.98
C7	18760	19152	0.96
C8	10972	11417	0.96

Table 4.6 Test Results and Predictions of Maximum Load and Deflection

Specimen	Experiment			Analysis			Ratio
	P_{max} (lbs)	V_x (in.)	V_y (in.)	P_{max} (lbs)	V_x (in.)	V_y (in.)	$\frac{P_{exp.}}{P_{ana.}}$
C1	18530	0.45	0.49	17886	0.41	0.41	1.04
C2	11610	0.37	0.59	11383	0.31	0.62	1.02
C3	21110	0.31	0.39	20993	0.26	0.51	1.03
C4	12730	0.40	0.41	12291	0.47	0.47	1.04
C5	20090	0.36	0.35	19212	0.39	0.39	1.05
C6	23110	0.32	0.31	22586	0.38	0.38	1.05
C7	19340	0.35	0.36	19152	0.39	0.39	1.02
C8	11670	0.47	0.48	11417	0.46	0.46	1.02

Table 4.7 Effect of ϕEI term on Moment at Peak Load for 40 Elements

Specimen	Element 40 w/o ϕEI		Element 40 w/ ϕEI		Ratio	
	$(M_x)_{max}$ (lb-in.)	$(M_y)_{max}$ (lb-in.)	$(M_x)_{max}$ (lb-in.)	$(M_y)_{max}$ (lb-in.)	$\frac{(M_x)_{40}}{(M_x)_{40w}}$	$\frac{(M_y)_{40}}{(M_y)_{40w}}$
C1	16284	16284	17921	17921	0.91	0.91
C2	22411	9899	25499	11153	0.88	0.89
C3	23495	10434	26462	12009	0.89	0.87
C4	18630	18630	20770	20770	0.90	0.90
C5	16932	16932	18636	18636	0.91	0.91
C6	19534	19534	21843	21843	0.89	0.89
C7	16210	16210	18396	18396	0.88	0.88
C8	16688	16688	18808	18808	0.89	0.89

and the test machine during testing and the strain rate may also play a role in this phenomena.

The predicted and experimental load-deflection curves are shown in Appendix B. The overall trend of experimental results is satisfactorily simulated. It should be noted that it is hard to control the points of envelope unloading deflection in numerical analysis based on the envelope unloading points of experimental results. Thus, the unloading points in column analysis do not necessarily coincide with the values of experimental unloading points.

The analysis results of moments at ultimate load are shown in Table 4.9 to examine the effect of the number of divided elements, and the comparison between the predicted and experimental results are tabulated in Tables 4.7 and 4.8, respectively. It should be mentioned that the theoretical values of maximum moments are not necessary to be the ultimate load because of the second order effect. Comparison of load-deflection and moment-curvature curves exhibit the desirable pattern between the experimental and predicted results as shown in Appendix B.

Observing the prediction of overall load-deformation curves in the descending branch, the results of present theoretical analysis show a slight overestimation than the experimental curves. This discrepancy may be due to the bond deterioration in column or the strength reduction of an envelope stress-strain curve for concrete under cyclic loading. These two factors, which may affect the results of the analysis, were not considered as described in the basic assumptions of the extended finite segment method. Above all, the strength degradation of an envelope curve due to cyclic loading may have to be left for future research because the strength degradation of concrete is rather complex. The size effect and the end condition of 3 by 6 inches cylinder tests may also play a role in this discrepancy.

Table 4.8 Effect of ϕEI term on Moment at Peak Load for 64 Elements

Specimen	Element 64 w/o ϕEI		Element 64 w/ ϕEI		Ratio	
	$(M_x)_{max}$ (lb-in.)	$(M_y)_{max}$ (lb-in.)	$(M_x)_{max}$ (lb-in.)	$(M_y)_{max}$ (lb-in.)	$\frac{(M_x)_{64}}{(M_x)_{64w}}$	$\frac{(M_y)_{64}}{(M_y)_{64w}}$
C1	19591	19591	19979	19979	0.98	0.98
C2	27355	11895	28095	12238	0.97	0.98
C3	29701	13424	30105	13570	0.98	0.99
C4	22597	22597	23156	23156	0.97	0.97
C5	20529	20529	21075	21075	0.97	0.97
C6	23693	23693	24551	24551	0.96	0.96
C7	20580	20580	21010	21010	0.98	0.98
C8	20451	20451	21395	21395	0.95	0.95

Table 4.9 Test Results and Predictions of Moment at Peak Load

Specimen	Experiment		Analysis		Ratio	
	$(M_x)_{max}$ (lb-in.)	$(M_y)_{max}$ (lb-in.)	$(M_x)_{max}$ (lb-in.)	$(M_y)_{max}$ (lb-in.)	$\frac{(M_x)_{exp}}{(M_x)_{ana}}$	$\frac{(M_y)_{exp.}}{(M_y)_{ana.}}$
C1	22180	21440	19979	19979	1.11	1.08
C2	28310	13180	28095	12238	1.01	1.07
C3	27740	14630	30105	13570	0.92	1.09
C4	23220	23090	23156	23156	1.01	0.99
C5	21240	21440	21075	21075	1.02	1.02
C6	23500	23730	24551	24551	0.94	0.96
C7	20640	20440	21010	21010	0.98	0.97
C8	22100	21990	21395	21395	1.03	1.02

* Moment at Peak Load is not necessary to be Maximum.

CHAPTER 5

SUMMARY AND CONCLUSIONS

5.1 Summary

Firstly, the purposes of present research work are to study the behavior of concrete subjected to cyclic uniaxial compressions and to develop an analytical model to predict the behavior of concrete cylinders under random cyclic loading. It is true that there is a gap between the theoretical model and real implementation in the stage of engineering analysis. Thus, the present research attempts to reduce the gap between the theoretical model of concrete under cyclic loading and the practical implementation of an idealized concrete model. Secondly, this research is to investigate into the behavior of slender reinforced concrete columns under cyclic axial compressive load with bidirectional eccentricities and to propose a suitable numerical analysis for the simulation of column test results.

To study the concrete behavior, experimental investigation and parametric study of the concrete under general cyclic loading were performed here. Through the parametric study, the applicability of previous concrete model was investigated and the physically motivated modeling for cyclic stress-strain relationships was proposed. It has been shown in this study that most previous cyclic models of the concrete can not be used together with other envelope curves. Due to this reason, the present modeling of concrete under general cyclic loading is initiated to propose the mathematical formulations with substantial applicability and flexibility in modeling.

The possible type of mathematical expressions has been obtained through a large amount of numerical and graphical simulations. For this purpose, a numerical and graphical simulator for the cyclic stress-strain relationships was constructed. The simulator developed is used to assist a modeling procedures and to present the model

prediction. Tests of concrete cylinder were conducted under four different loading regimes to determine the major experimental parameters for the proposed analytical expressions. Furthermore, the analytical model developed was calibrated by a trial and error to simulate the concrete behavior under random cyclic loadings.

Experimental column tests were carried out to examine the effect of various cyclic compressive load levels on the behavior of R/C slender columns with bidirectional eccentricities. All columns had a nominal cross-section of 3 by 3 inches and four feet long. The test parameters of column specimens were bidirectional eccentricities and its angle to the reference axis. For this study, the column tests of eight specimens were conducted by an closed loop servo controlled MTS under stroke control to achieve both ascending and descending branches of load-deformation curves in different loading paths. The ultimate strength of columns, load-deflection and moment-curvature curves in both X and Y directions were obtained in this experimental program.

Analysis of R/C column subjected to combined biaxial bending and axial load should be approached from the standpoint of a three dimensional problem. The numerical procedures adopted in the previous studies were not able to handle the unloading and reloading path of load-deflection curve due to the nature of incremental deflection. At the present study, a numerical analysis based on an extended finite segment method was proposed to predict the ultimate load, deflections and moment-curvature of experimental results.

5.2 Conclusions

Based on the present experimental investigations and theoretical study of concrete cylinders subjected to cyclic axial compressions and reinforced concrete slender columns under cyclic compressive load with bidirectional eccentricities, the following conclusions can be made.

1) For a more reliable concrete modeling, formulations of the cyclic stress-strain

relationships are desirable to be less dependent upon a mathematical expression of the envelope curve using certain monotonic stress-strain curves.

2) The common points limit depends on the adopted envelope curve. It is found that the location of common point has been shown to vary with the type of load applied. Thus, it is reasonable to assume that the stress-strain relationships may be derived without the terms of common point for random cyclic loading. However, in case of full unloading and reloading, the common point approach presents a more stable shape at each cycle with less sensitivity to the change in envelope reloading strain.

3) It is generally accepted in most previous study that the accumulation of reloading strain can be only defined at the maximum stress level of each cycle, i.e., on the envelope curve. However, the accumulation rate of reloading strain can be defined regardless of different stress level in the reloading path due to the history of partial unloading. This observation through the load pattern of random cycles enables to model the partial or full reloading curve which is a part of random cycle. Thus, it is possible to define the corresponding envelope reloading strain to the end point of arbitrary stress level in the partial unloading path. This observation can also back up the non-uniqueness concept of cycle and the proposed model is able to reflect this behavior. Otherwise, the above mentioned intermediate envelope reloading strain due to partial unloading can not exist between the envelope unloading strain and envelope reloading strain corresponding to full unloading path. In a similar manner, an imaginary envelope unloading strain with regardless of reloading stress level can be defined to obtain the unloading curve due to the history of partial reloading path.

4) An analytical model for the stress-strain relationships of concrete under general cyclic loading is proposed through the determination of a suitable equation type from the preliminary simulations of possible curve shape. The calibration of model parameters from the test results of four different loading regimes and the theoretical simulations are carried out to ensure the validity of the proposed analytical model. The proposed

mathematical expressions have a flexibility to deal with any possible future modifications for certain experimental data. The applicability of proposed model is confirmed through the simulation of cyclic stress-strain curve with different monotonic stress-strain relationships. The reloading curve is idealized to accomplish the random cycles and to incorporate into the procedures for analyzing R/C structures. The overall stress-strain behavior of the proposed model and test results show a favorable agreement with each other.

5) The change in stiffness of the stress-strain curves with increasing strains provides a relationship between the strain and the nature of stiffness degradation. Thus, the stiffness degradation of unloading and reloading paths is idealized and has been successfully implemented into the procedure of R/C column analysis.

6) It has been observed that there is a noticeable difference in the failure mode between current test series and pervious studies on biaxial bending columns under monotonic loading. The location of hinging region of previous research was not as predictable as would be desired. However, the hinging region of present column tests was formed near the expected location in all columns except one specimen. It can be hypothesized that the reason for this trend is an even distribution of cracking due to the stress relaxation of repeated unloading. This phenomena may produce a more uniformly stiff column in the predicted manner.

7) The comparisons between the predicted and experimental results of column tests show that the proposed numerical analysis can reasonably describe the behavior of reinforced concrete columns under cyclic axial compressive load with bidirectional eccentricities. Thus, the assumption of nonlinear variation of curvature in the column segments and the proposed modification procedure for the load factor are valid for the present column analysis.

8) Since the present column analysis has a capability to simulate the cyclic axial loading, the proposed numerical procedure may be incorporated in a suitable algorithm

for a nonlinear seismic analysis. Various phenomena such as stiffness degradation, material nonlinearity and loading-unloading-reloading can also be taken into account in the analysis.

APPENDIX A: COMPARISON OF TEST RESULT AND PREDICTION

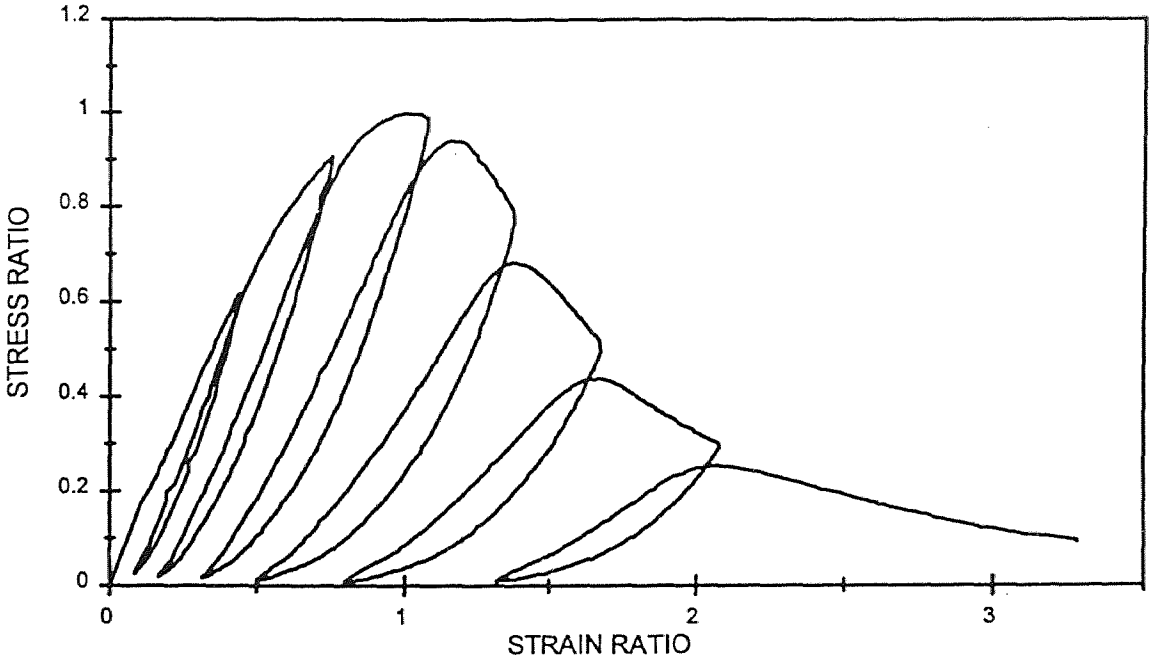

Figure A.1 Test Result for Cycles to Envelope

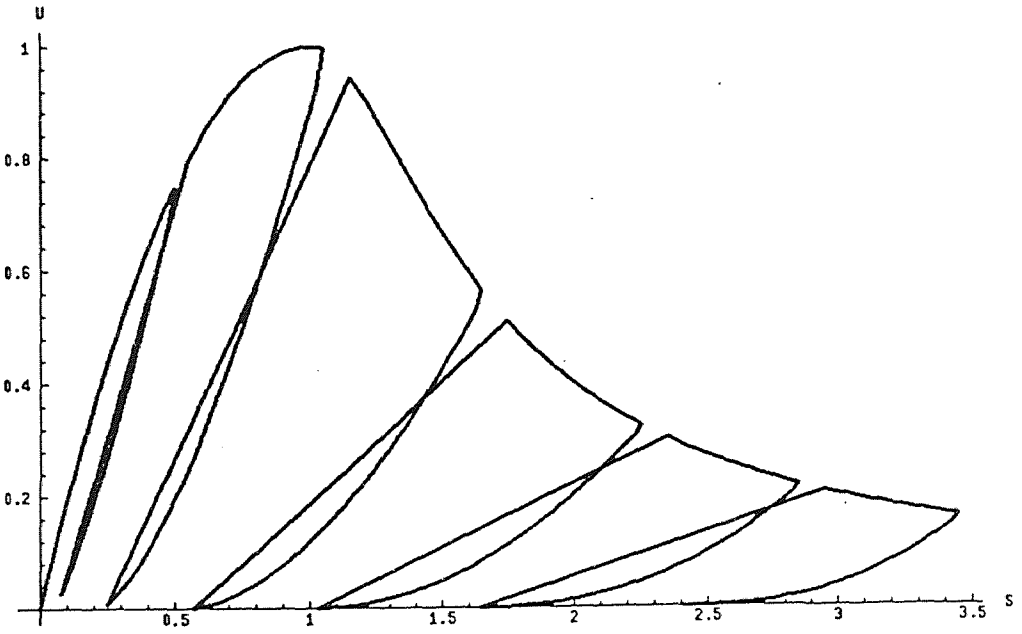

Figure A.2 Behavior of Proposed Model for Cycles to Envelope (with Tulin's Envelope)

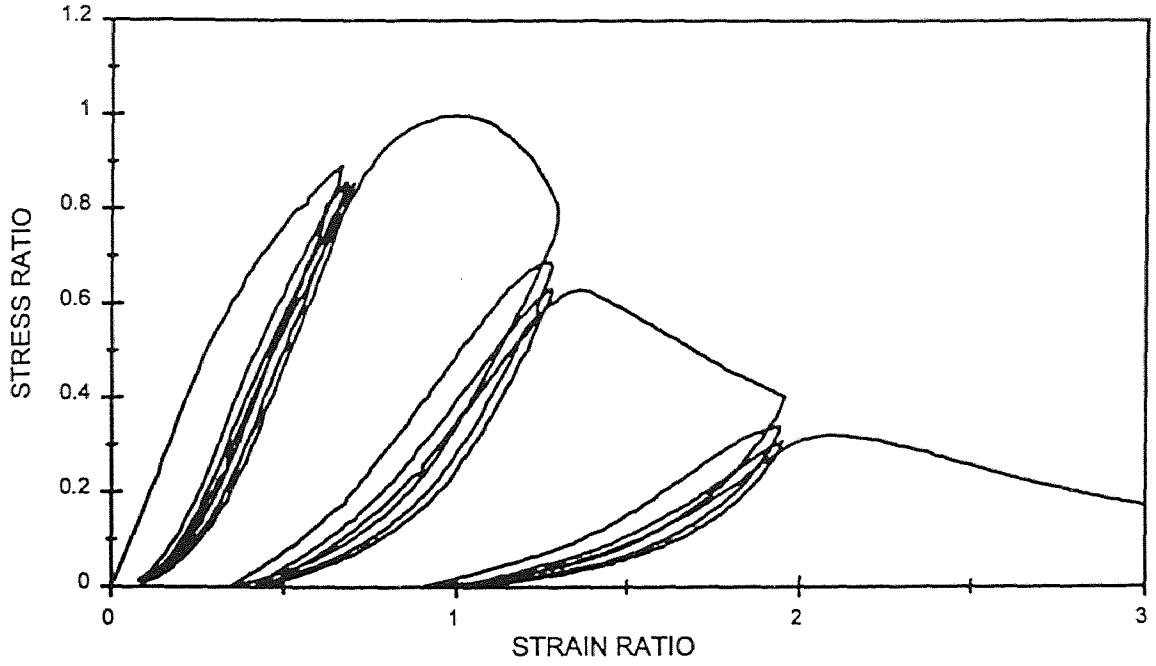

Figure A.3 Test Result for Cycles to Common Points

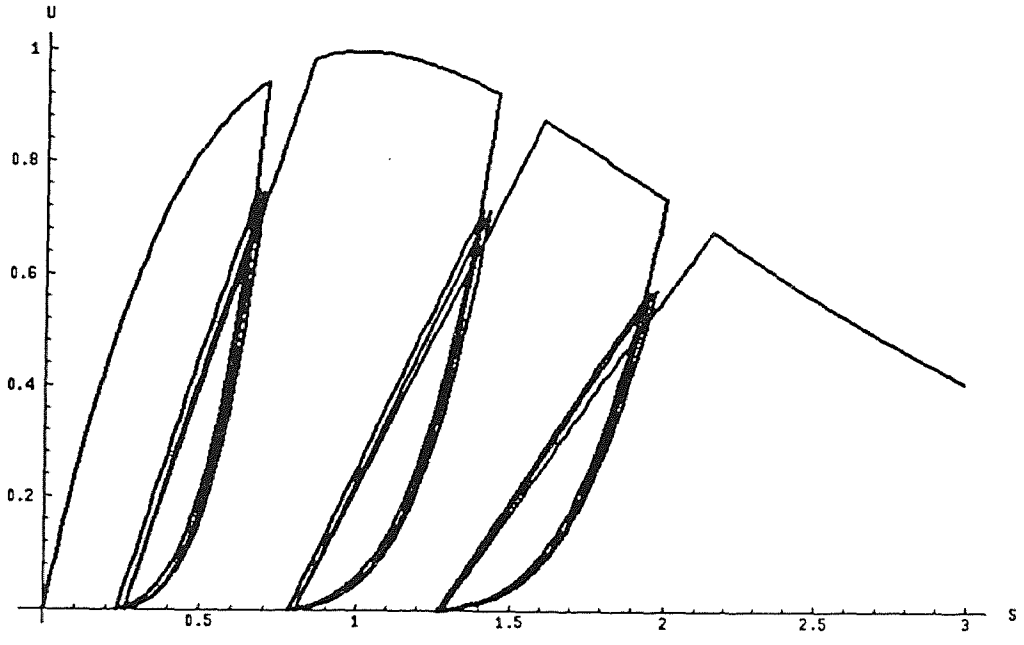

Figure A.4 Behavior of Proposed Model for Cycles to Common Points (with Smith's Envelope)

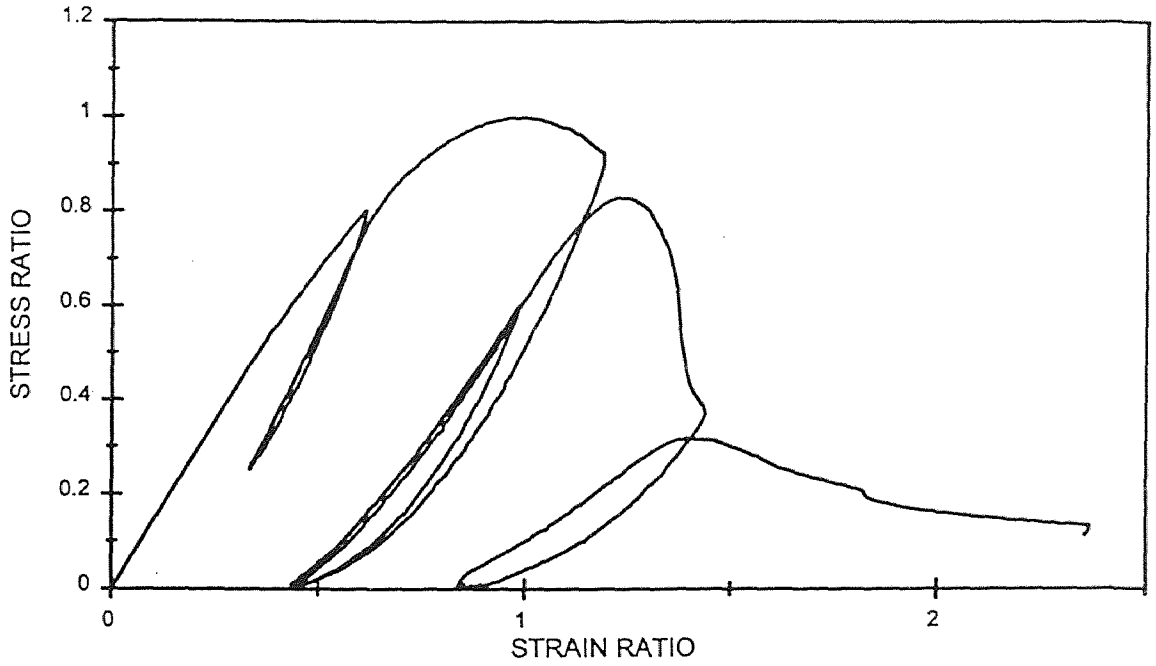

Figure A.5 Test Result for Random Cycles

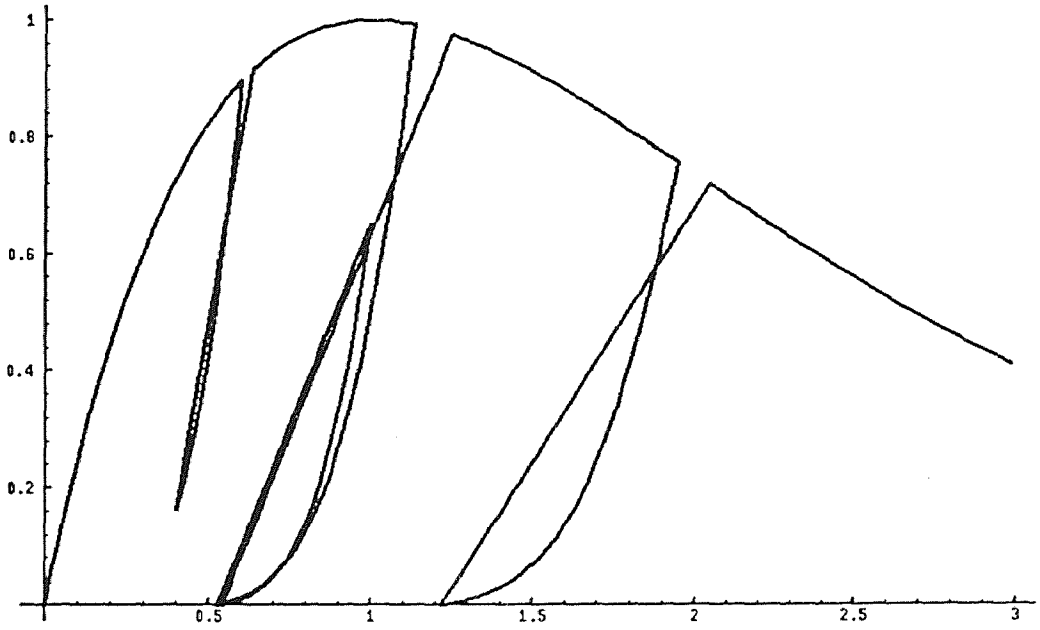

Figure A.6 Behavior of Proposed Model for Random Cycles
(with Smith's Envelope)

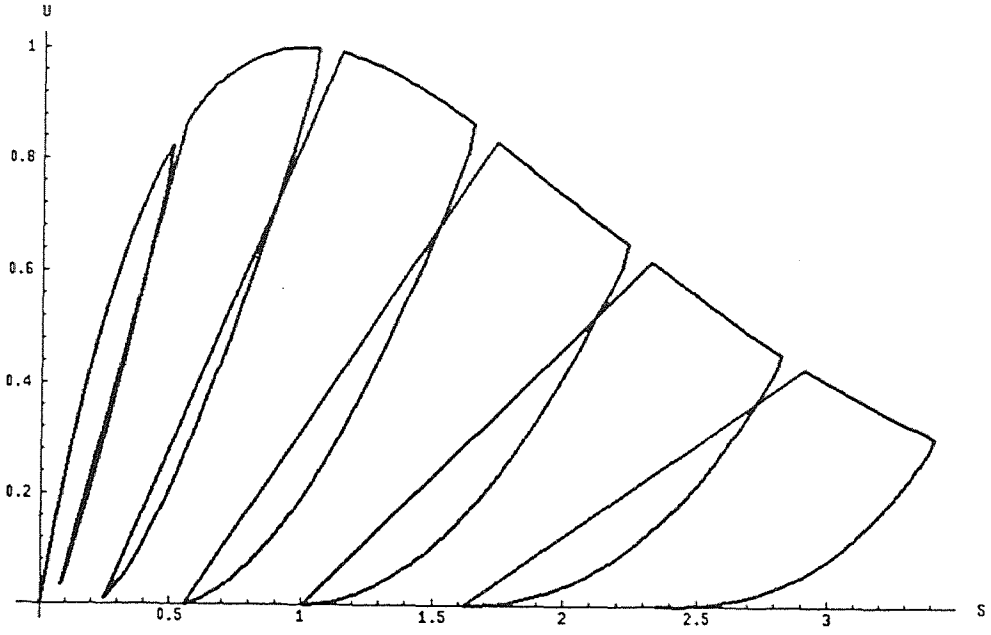

Figure A.7 Behavior of Proposed Model with Smith's Envelope

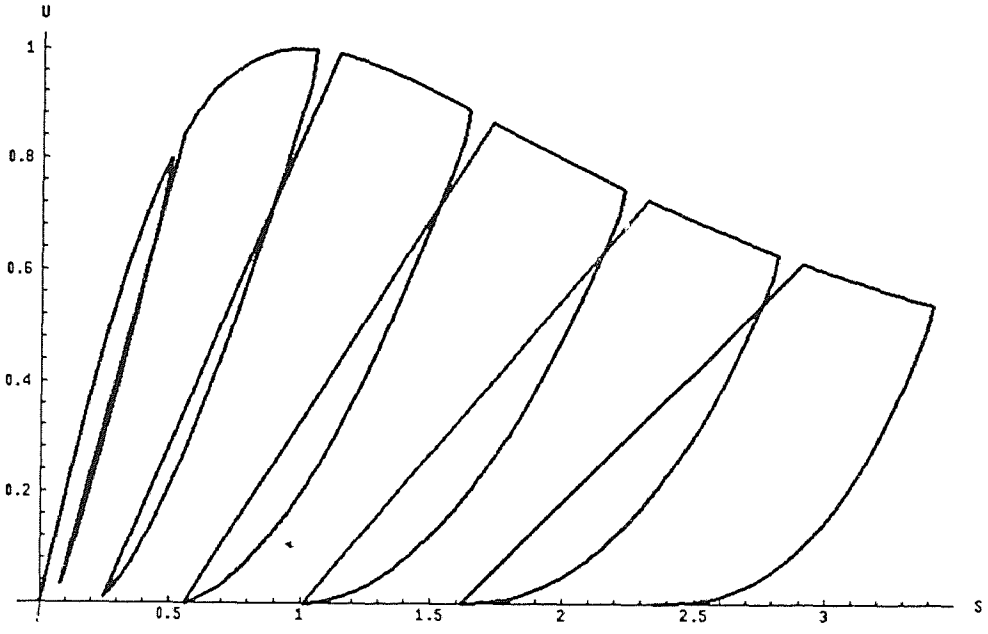

Figure A.8 Behavior of Proposed Model with Desayi's Envelope

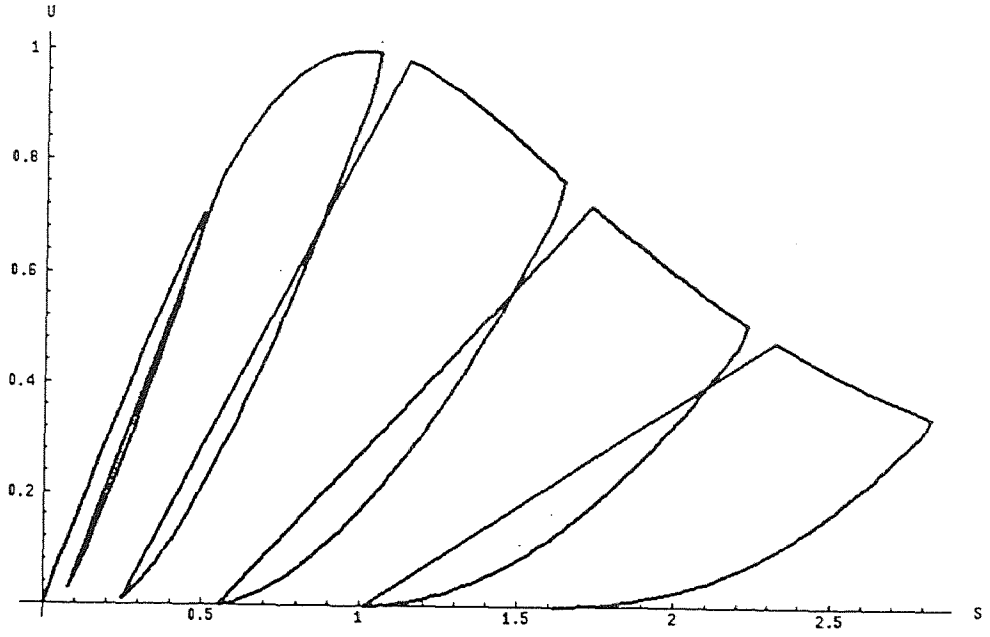

Figure A.9 Behavior of Proposed Model with Popovics's Envelope

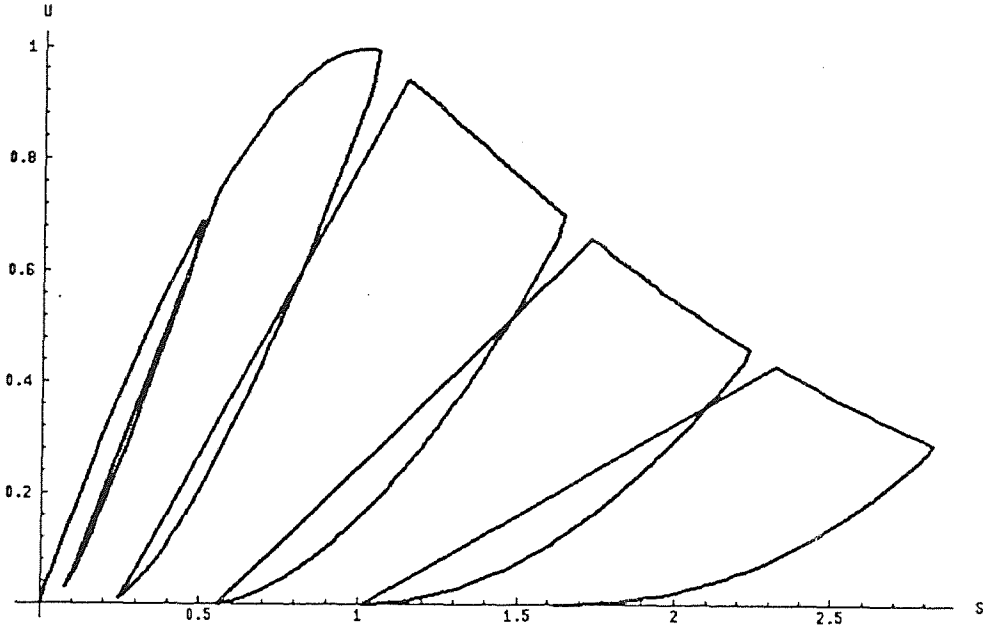

Figure A.10 Behavior of Proposed Model with Shah's Envelope

APPENDIX B: COMPARISON OF TEST RESULT AND ANALYSIS

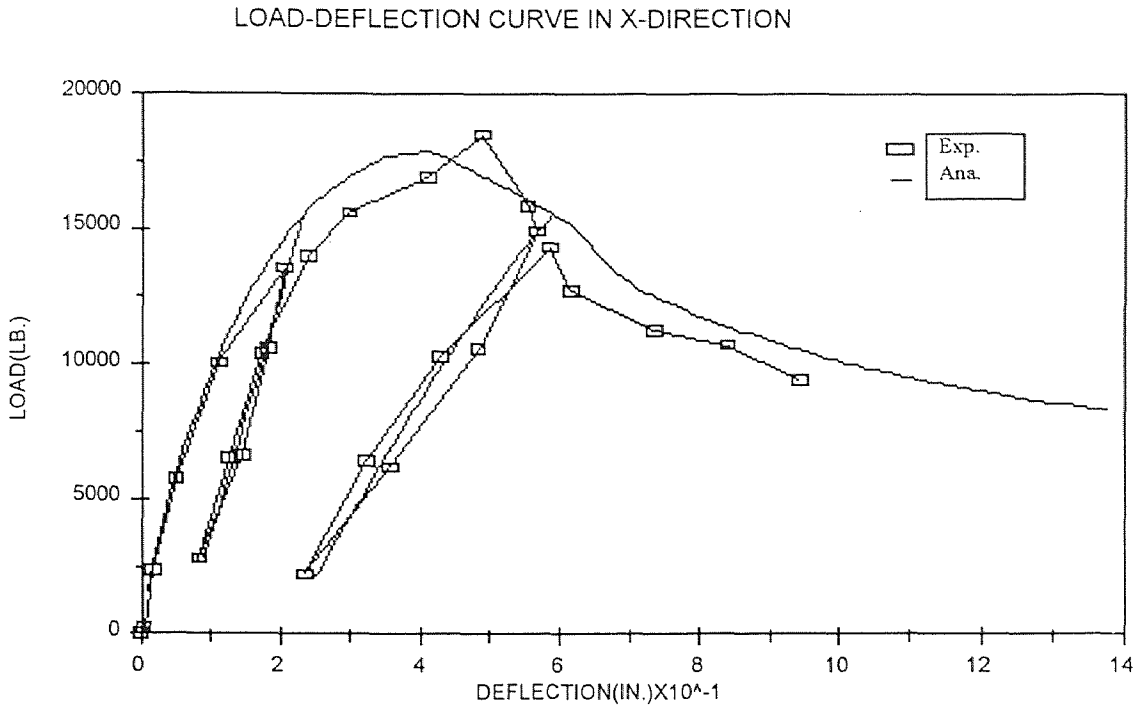

Figure B.1 Comparison of Load-Deflection Curve (X-DIR.) for Column C1

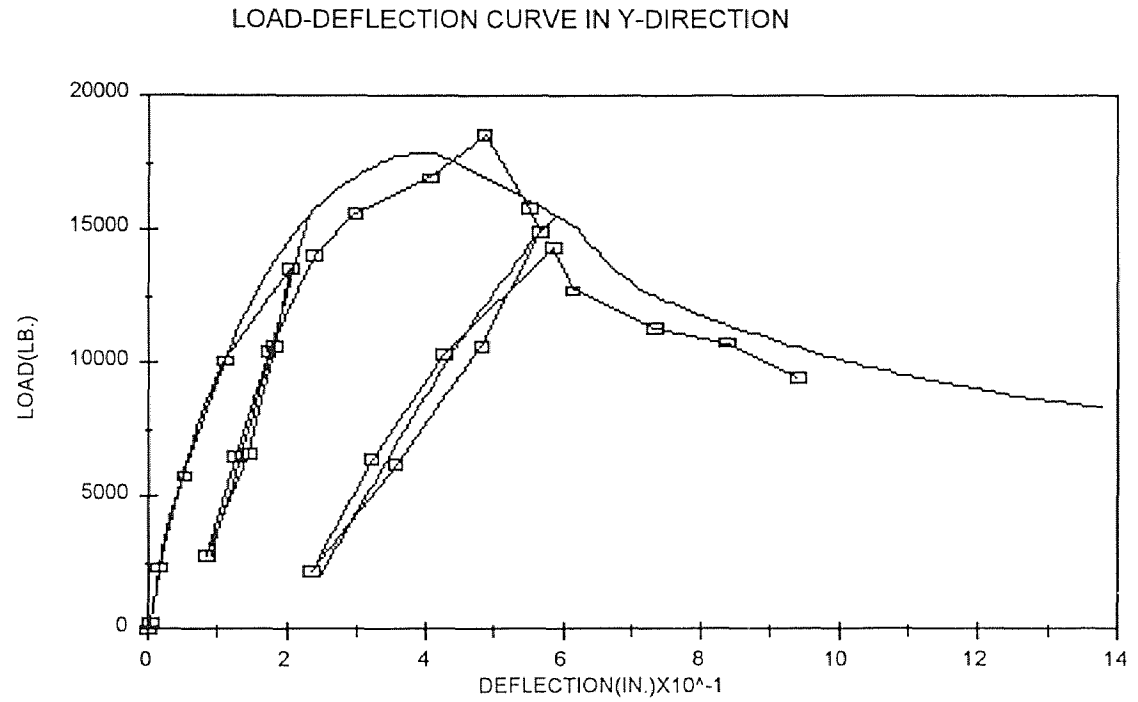

Figure B.2 Comparison of Load-Deflection Curve (Y-DIR.) for Column C1

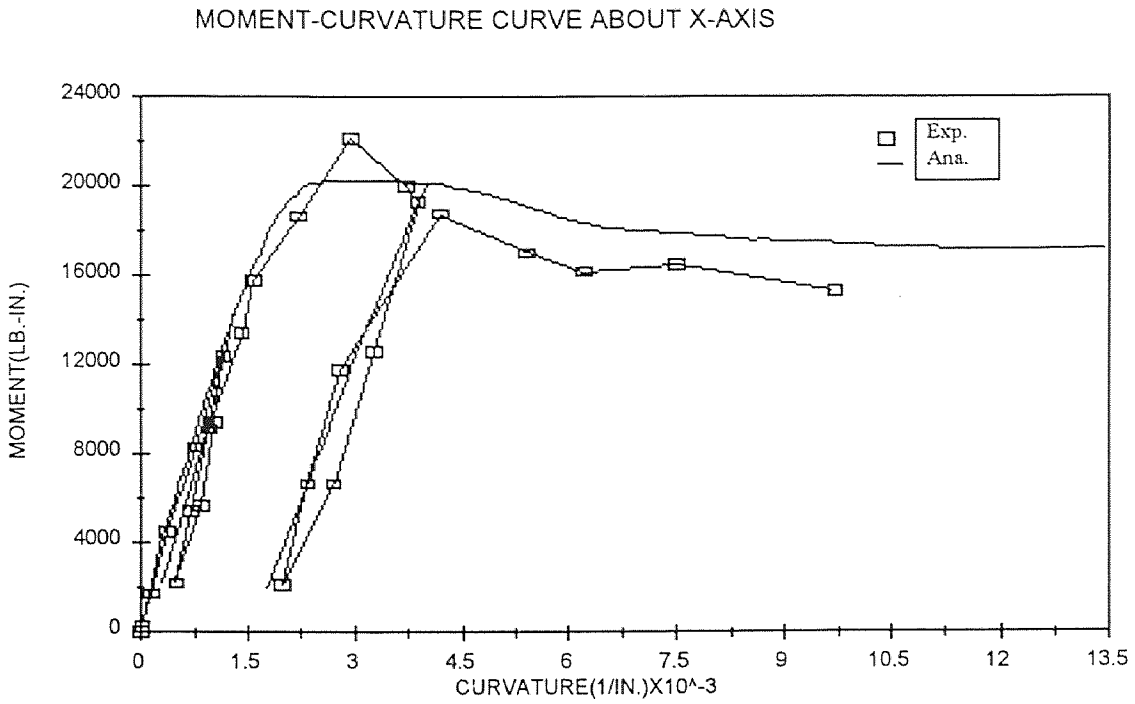

Figure B.3 Comparison of Moment-Curvature Curve (X-AXIS) for Column C1

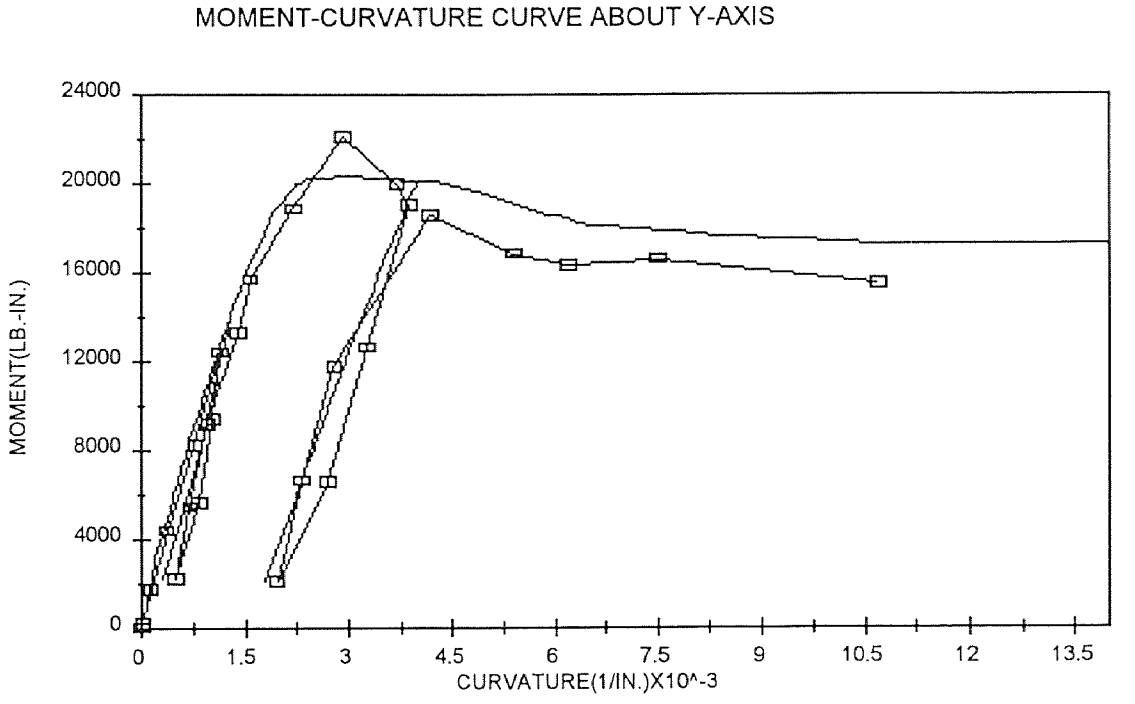

Figure B.4 Comparison of Moment-Curvature Curve (Y-AXIS) for Column C1

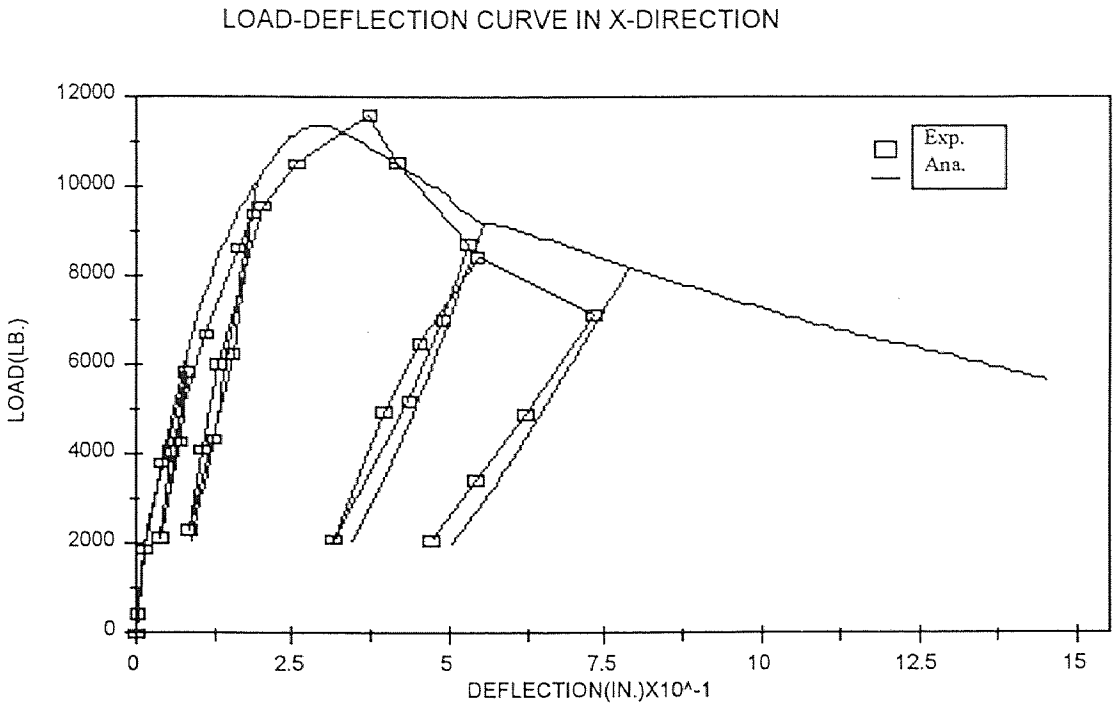

Figure B.5 Comparison of Load-Deflection Curve (X-DIR.) for Column C2

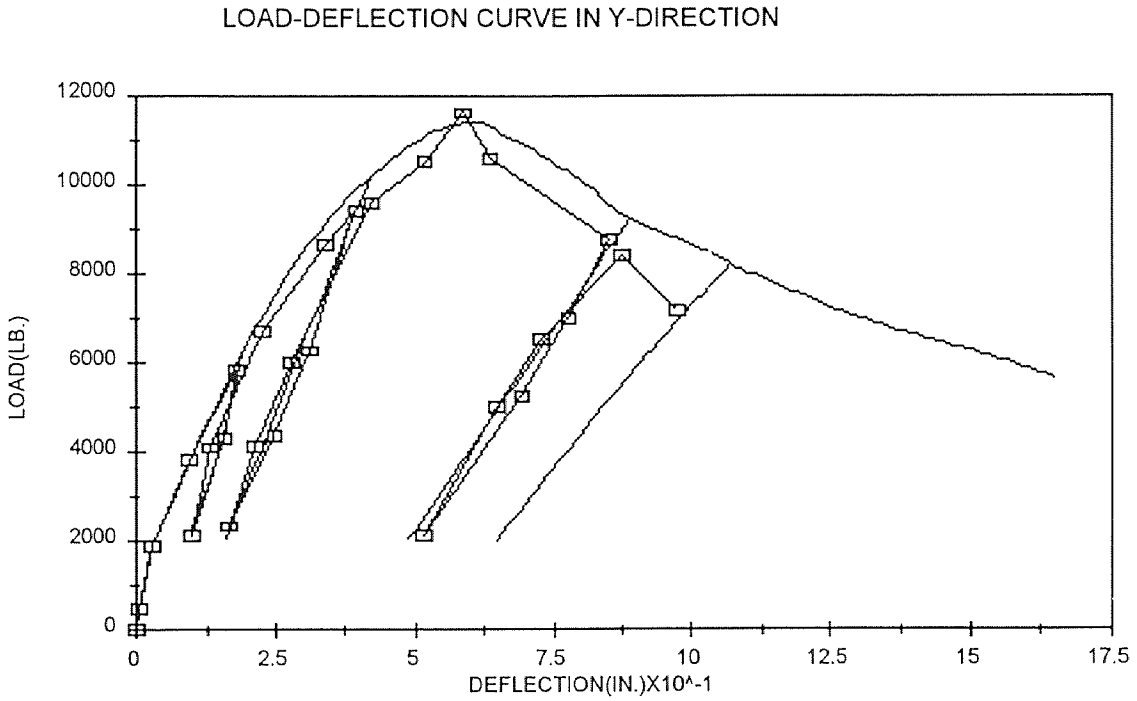

Figure B.6 Comparison of Load-Deflection Curve (Y-DIR.) for Column C2

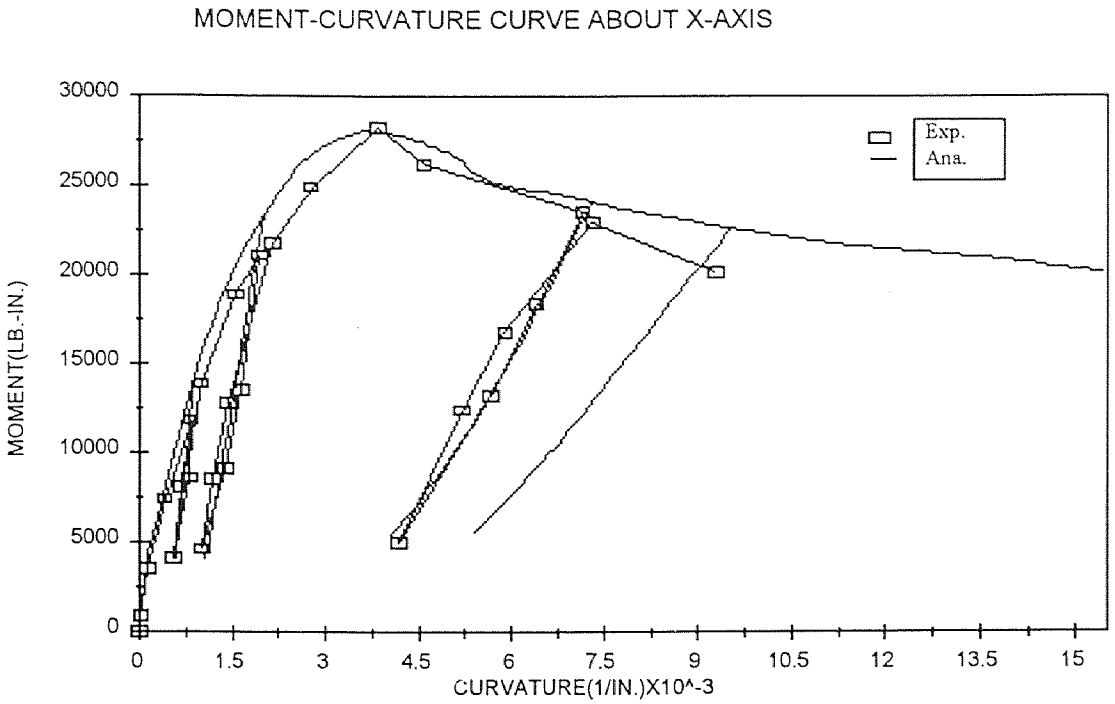

Figure B.7 Comparison of Moment-Curvature Curve (X-AXIS) for Column C2

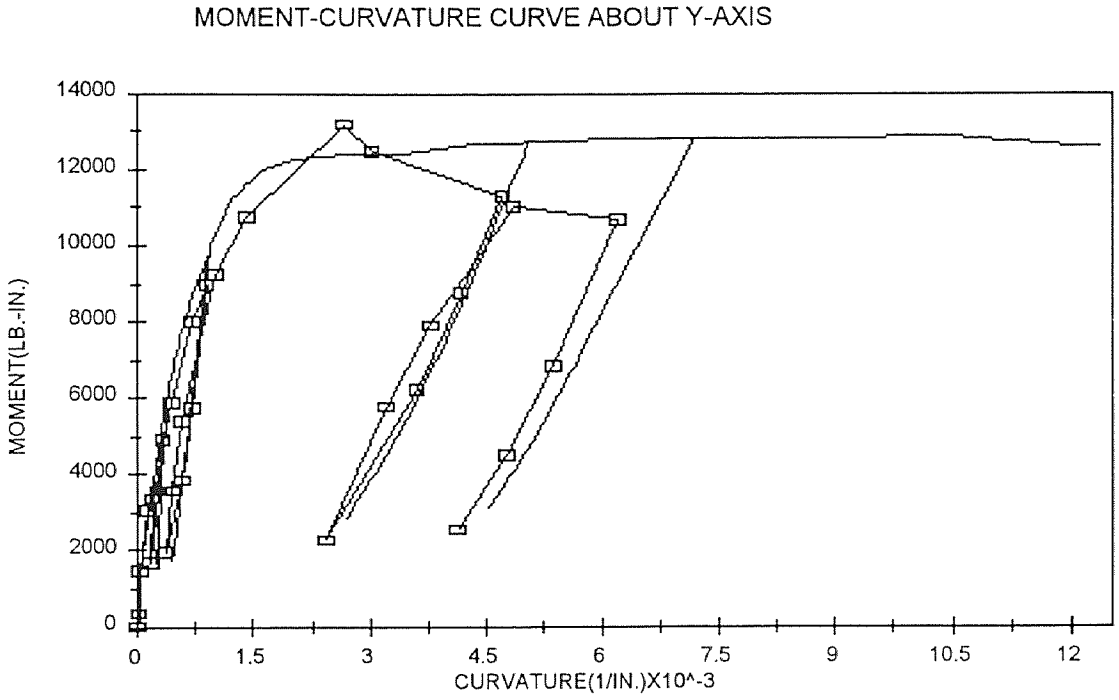

Figure B.8 Comparison of Moment-Curvature Curve (Y-AXIS) for Column C2

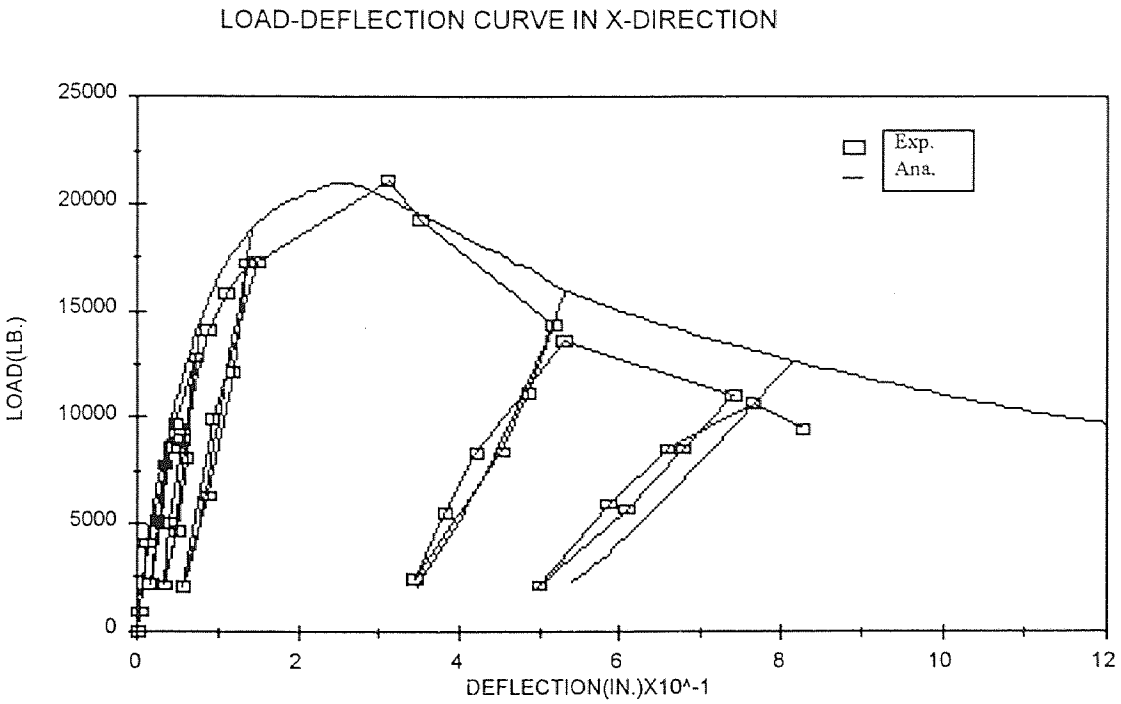

Figure B.9 Comparison of Load-Deflection Curve (X-DIR.) for Column C3

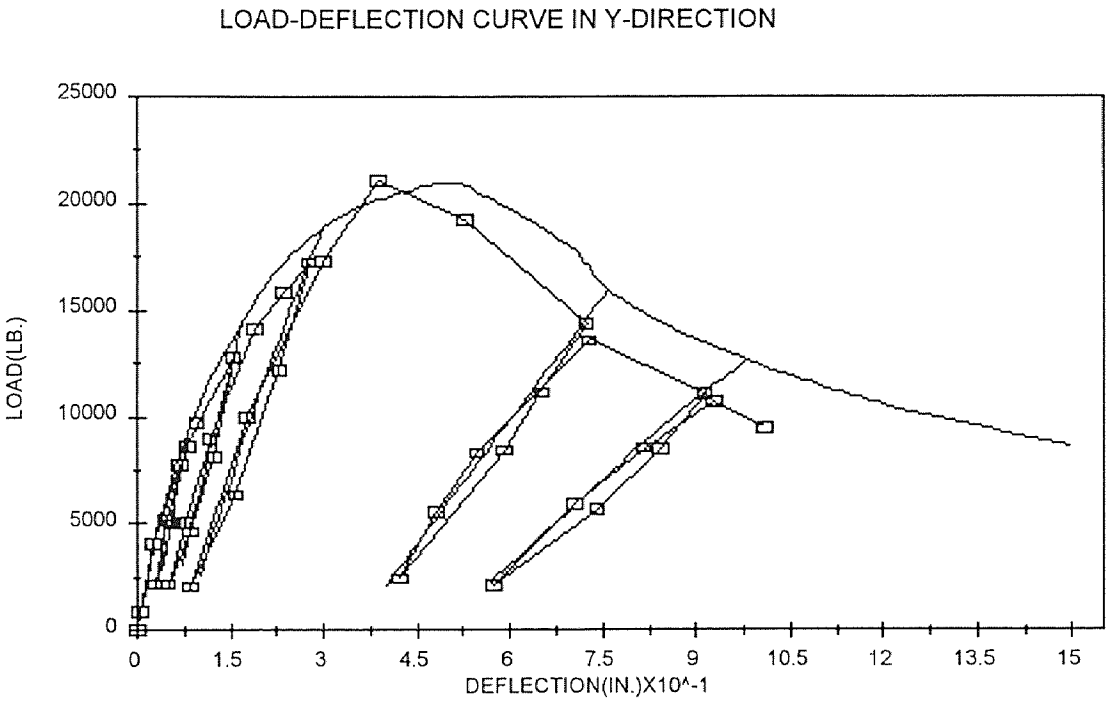

Figure B.10 Comparison of Load-Deflection Curve (Y-DIR.) for Column C3

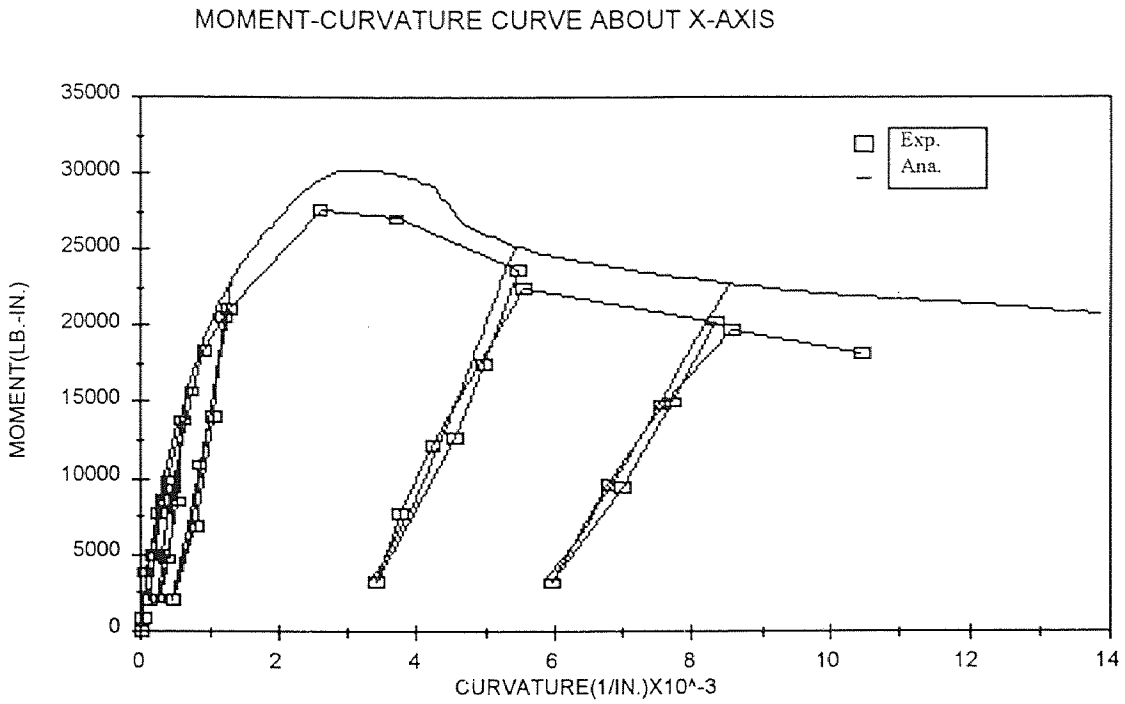

Figure B.11 Comparison of Moment-Curvature Curve (X-AXIS) for Column C3

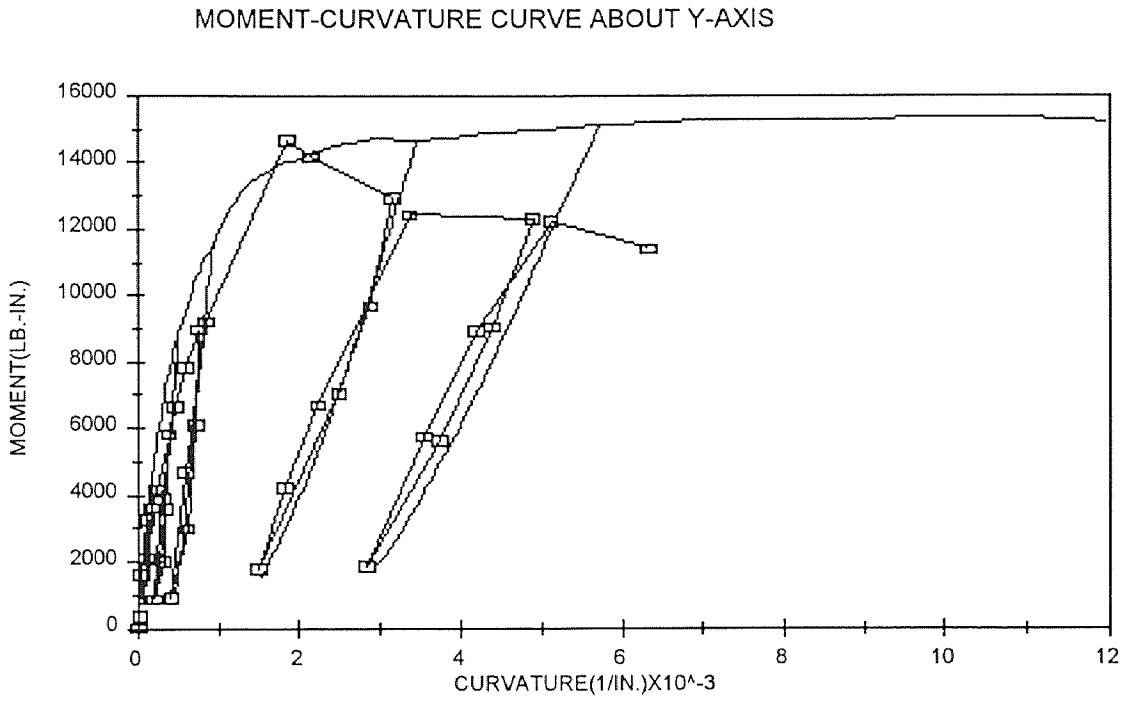

Figure B.12 Comparison of Moment-Curvature Curve (Y-AXIS) for Column C3

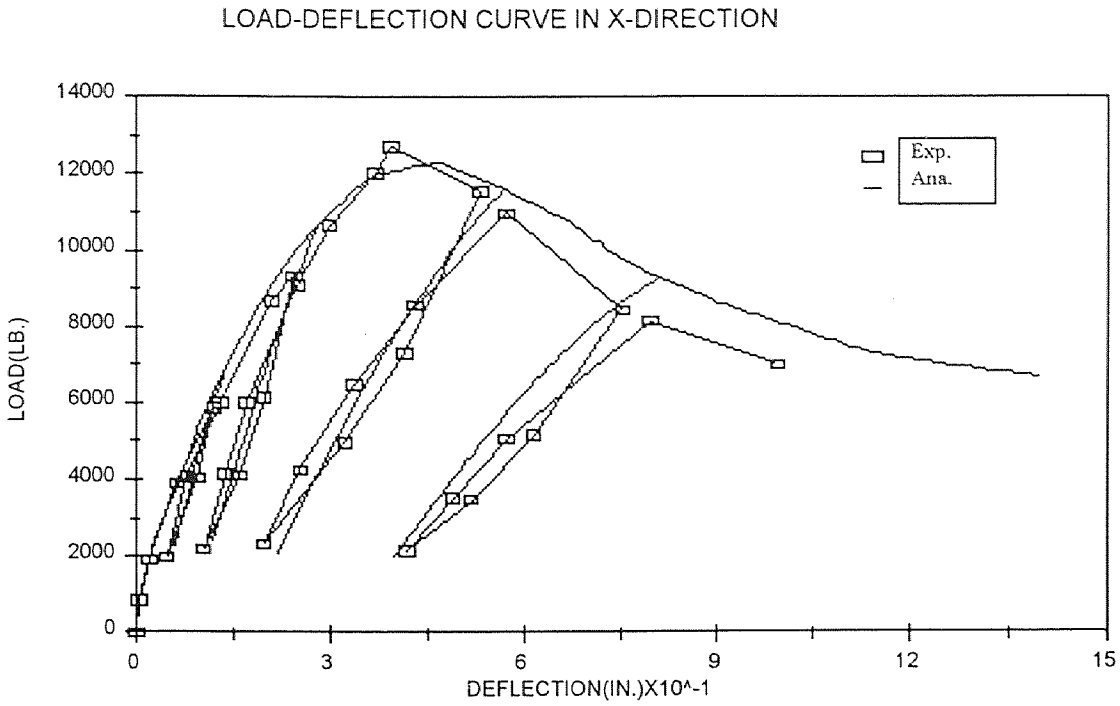

Figure B.13 Comparison of Load-Deflection Curve (X-DIR.) for Column C4

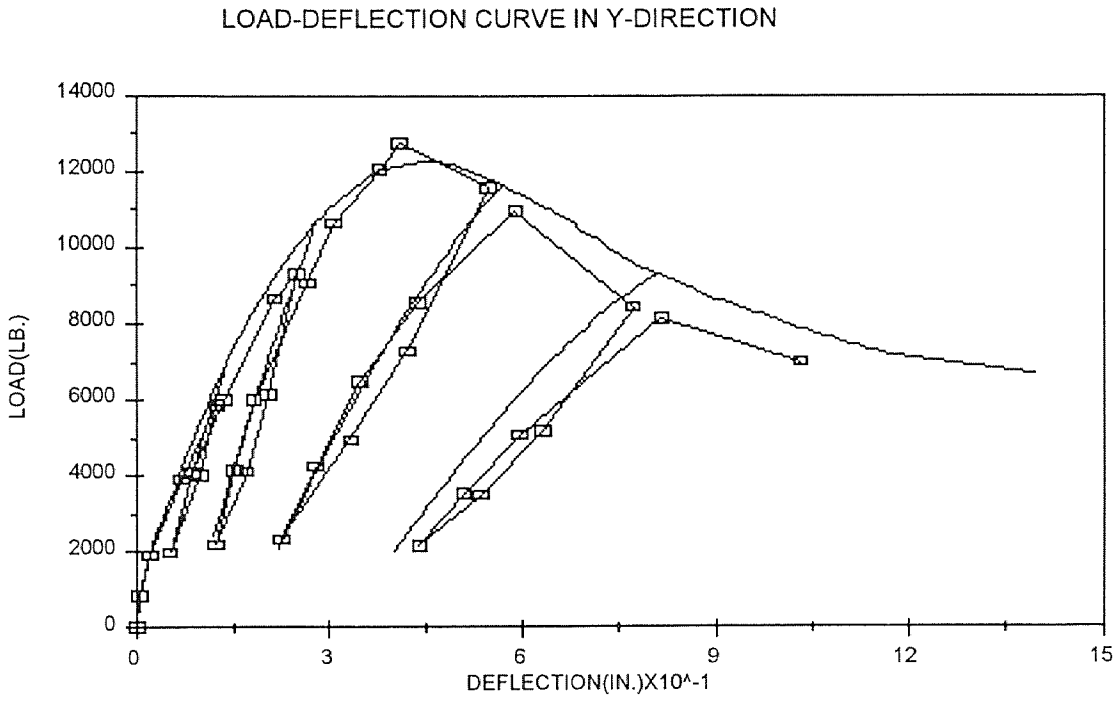

Figure B.14 Comparison of Load-Deflection Curve (Y-DIR.) for Column C4

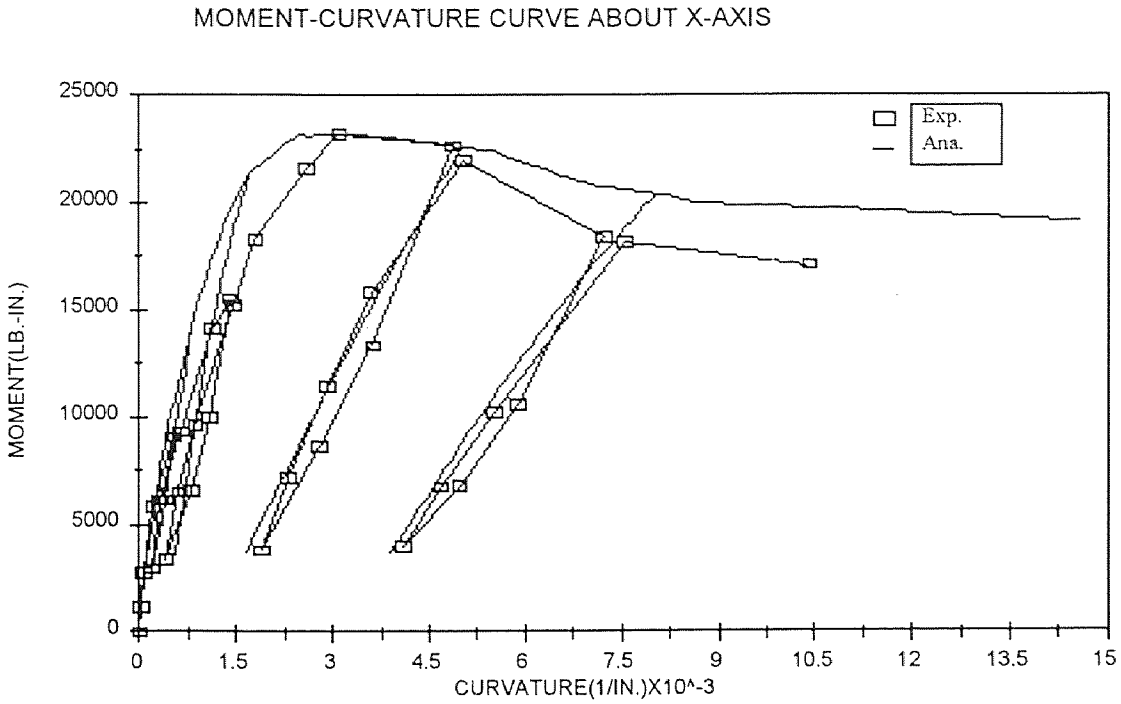

Figure B.15 Comparison of Moment-Curvature Curve (X-AXIS) for Column C4

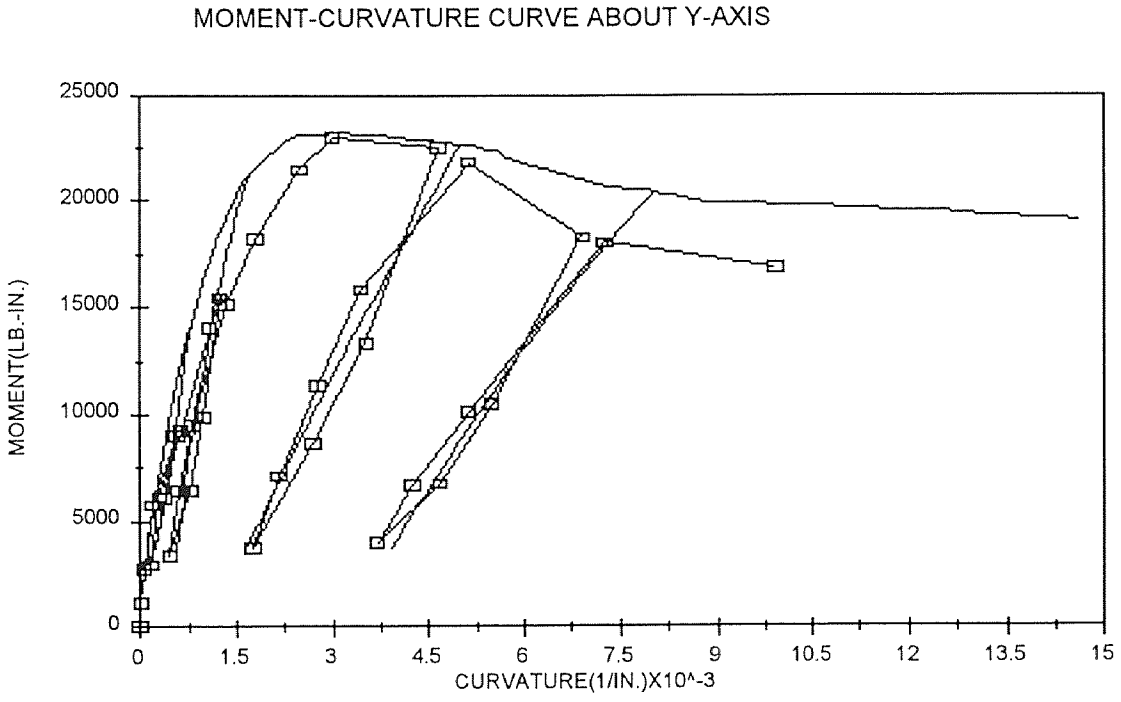

Figure B.16 Comparison of Moment-Curvature Curve (Y-AXIS) for Column C4

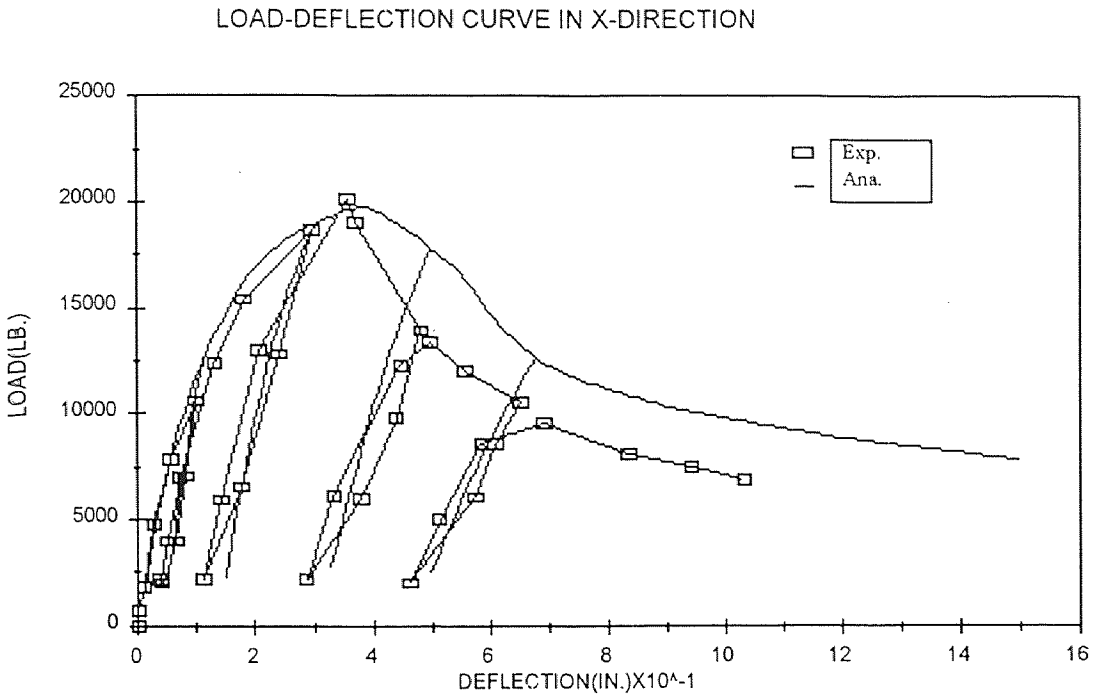

Figure B.17 Comparison of Load-Deflection Curve (X-DIR.) for Column C5

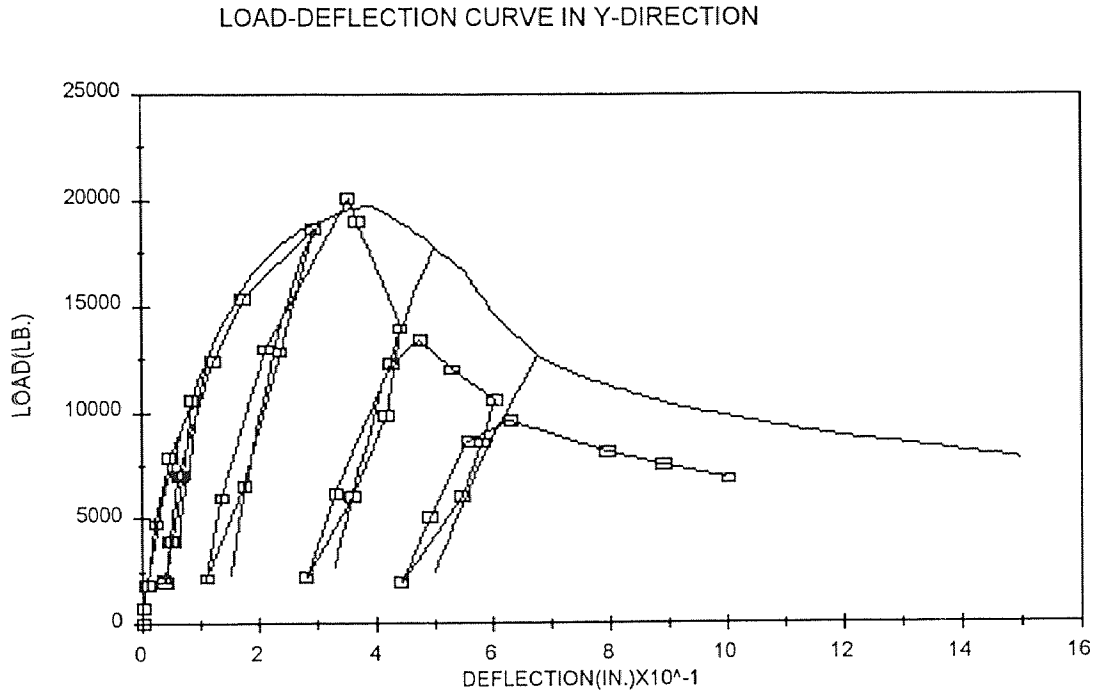

Figure B.18 Comparison of Load-Deflection Curve (Y-DIR.) for Column C5

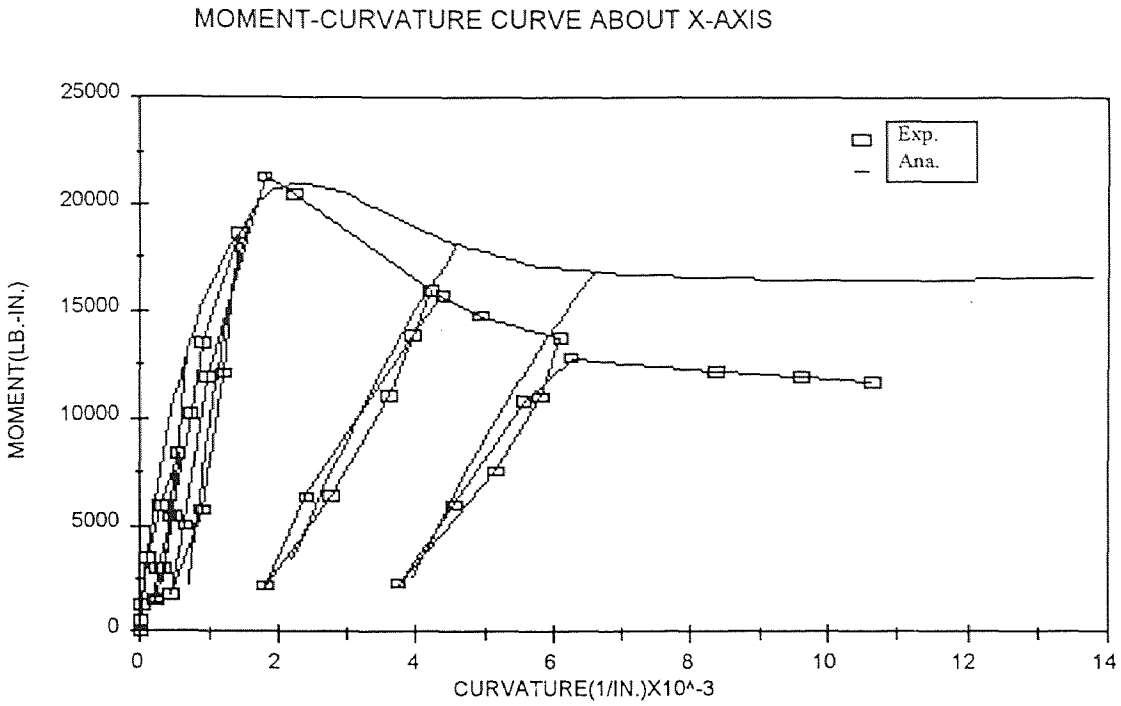

Figure B.19 Comparison of Moment-Curvature Curve (X-AXIS) for Column C5

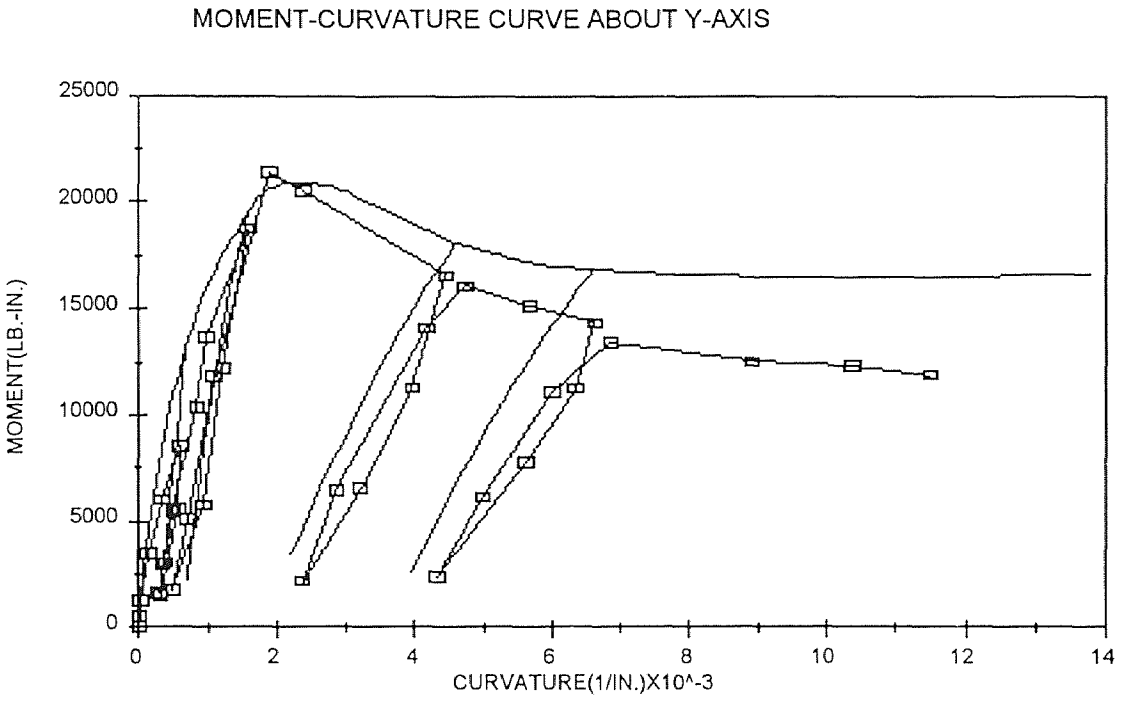

Figure B.20 Comparison of Moment-Curvature Curve (Y-AXIS) for Column C5

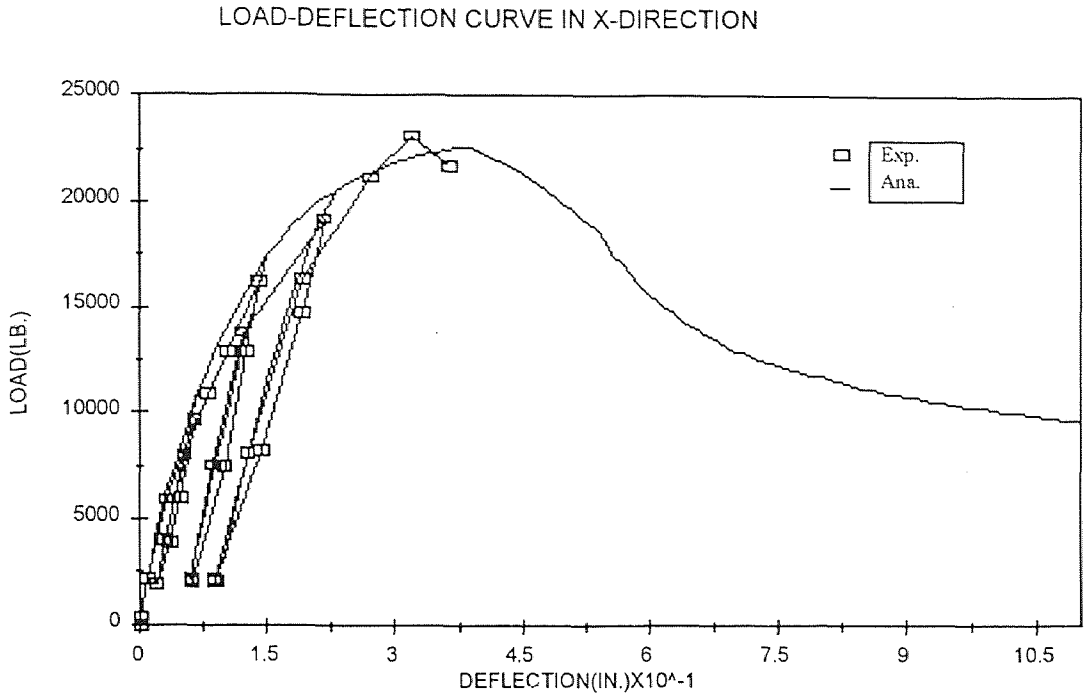

Figure B.21 Comparison of Load-Deflection Curve (X-DIR.) for Column C6

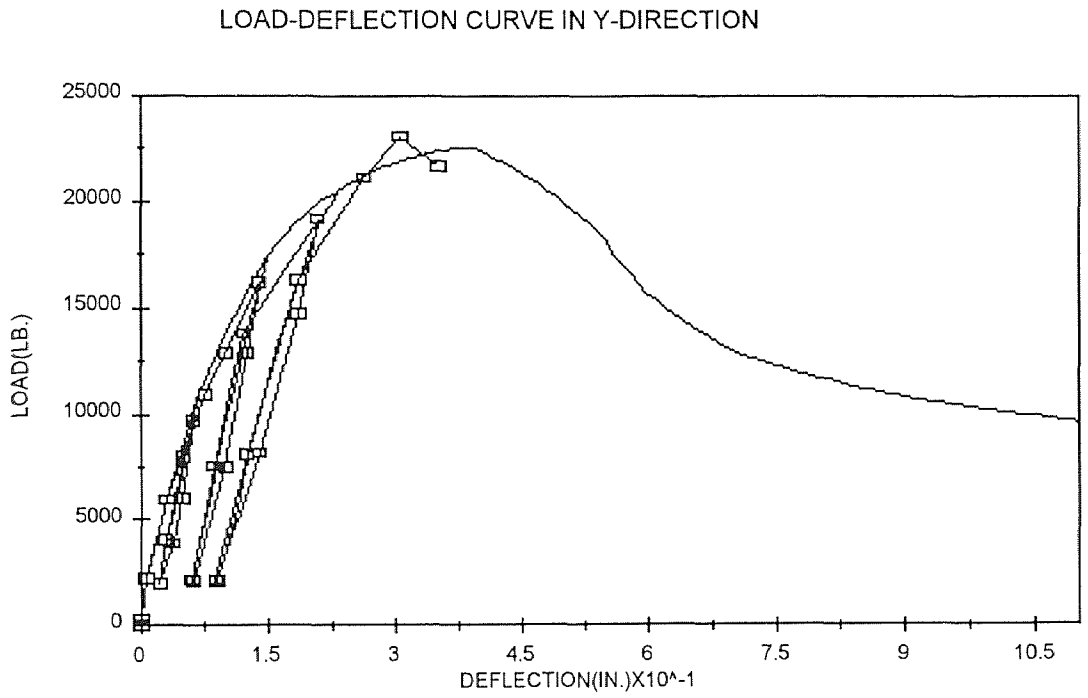

Figure B.22 Comparison of Load-Deflection Curve (Y-DIR.) for Column C6

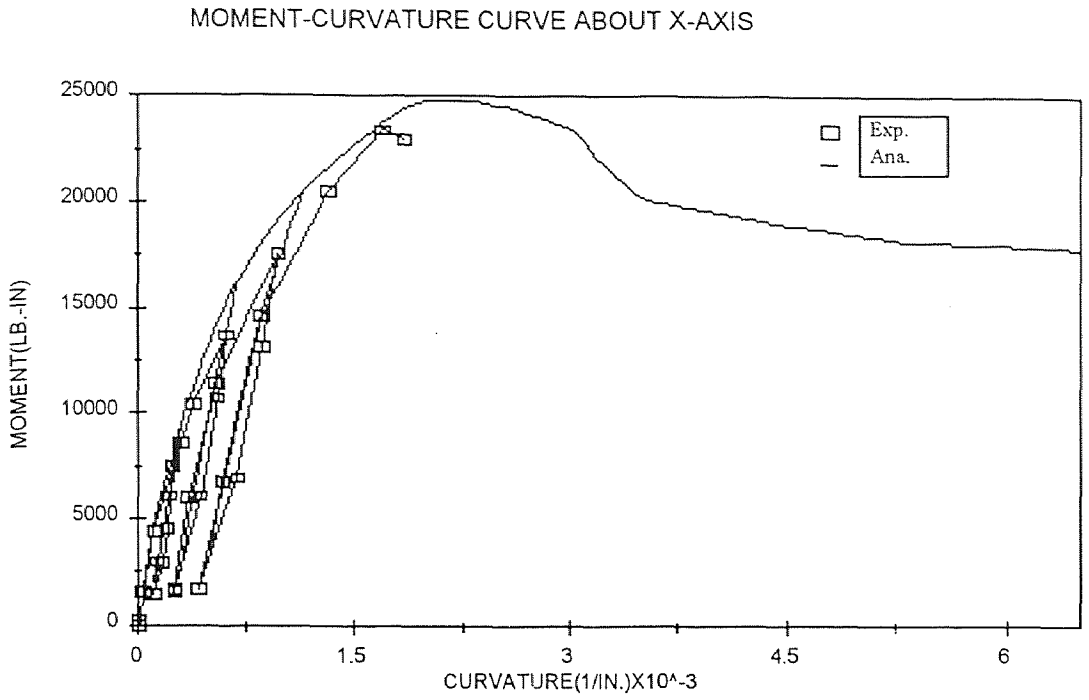

Figure B.23 Comparison of Moment-Curvature Curve (X-AXIS) for Column C6

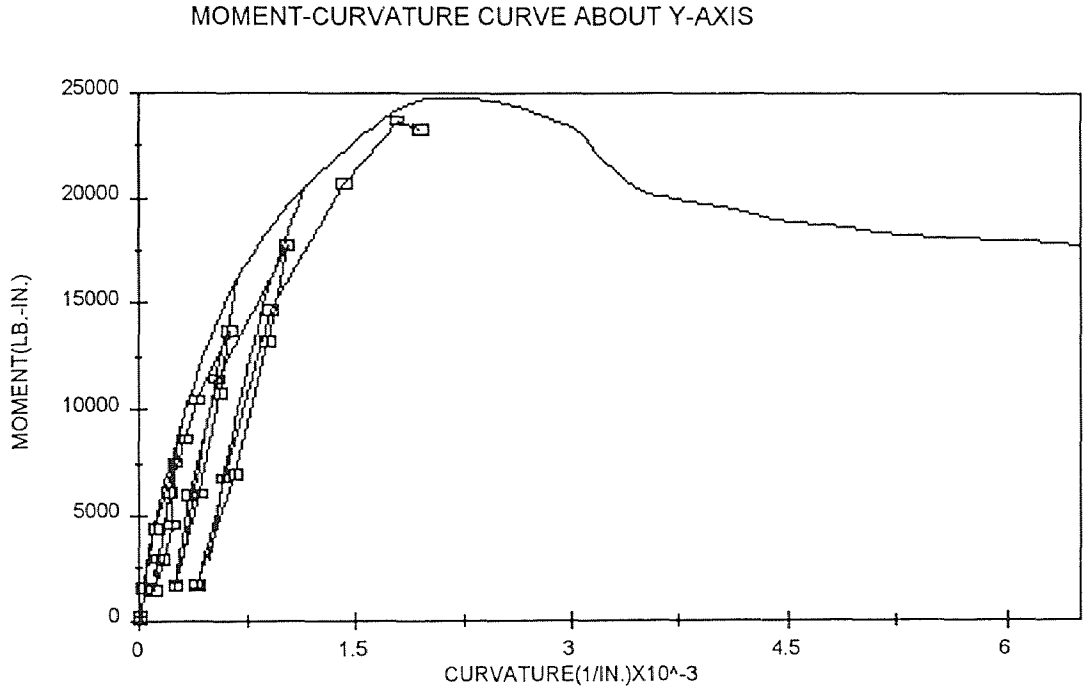

Figure B.24 Comparison of Moment-Curvature Curve (Y-AXIS) for Column C6

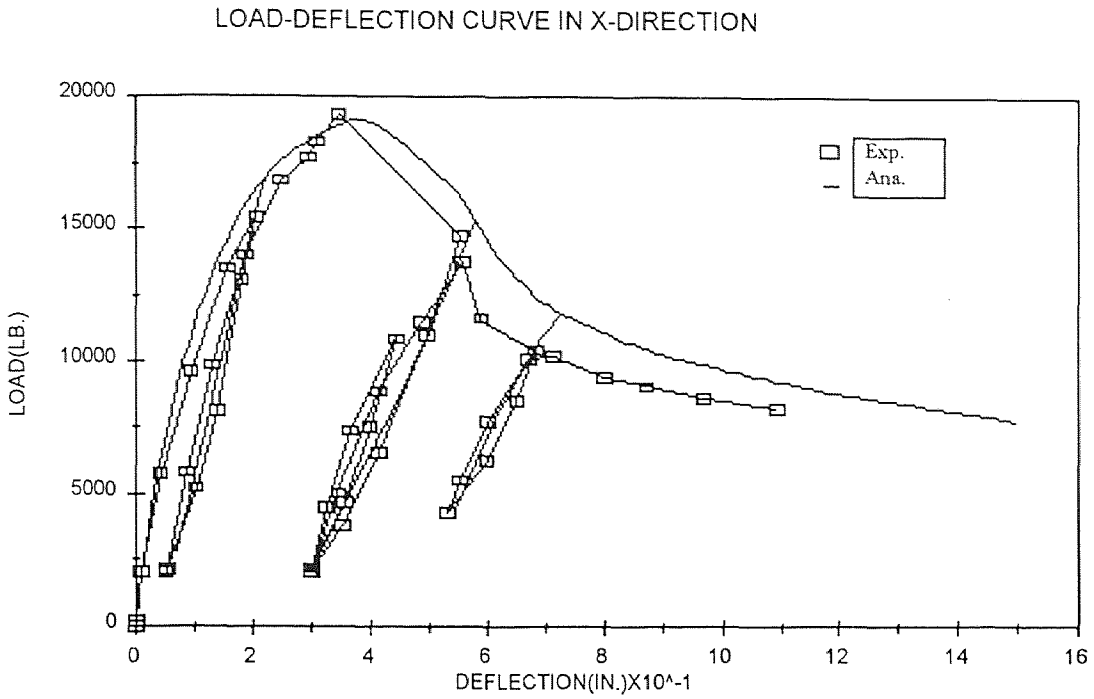

Figure B.25 Comparison of Load-Deflection Curve (X-DIR.) for Column C7

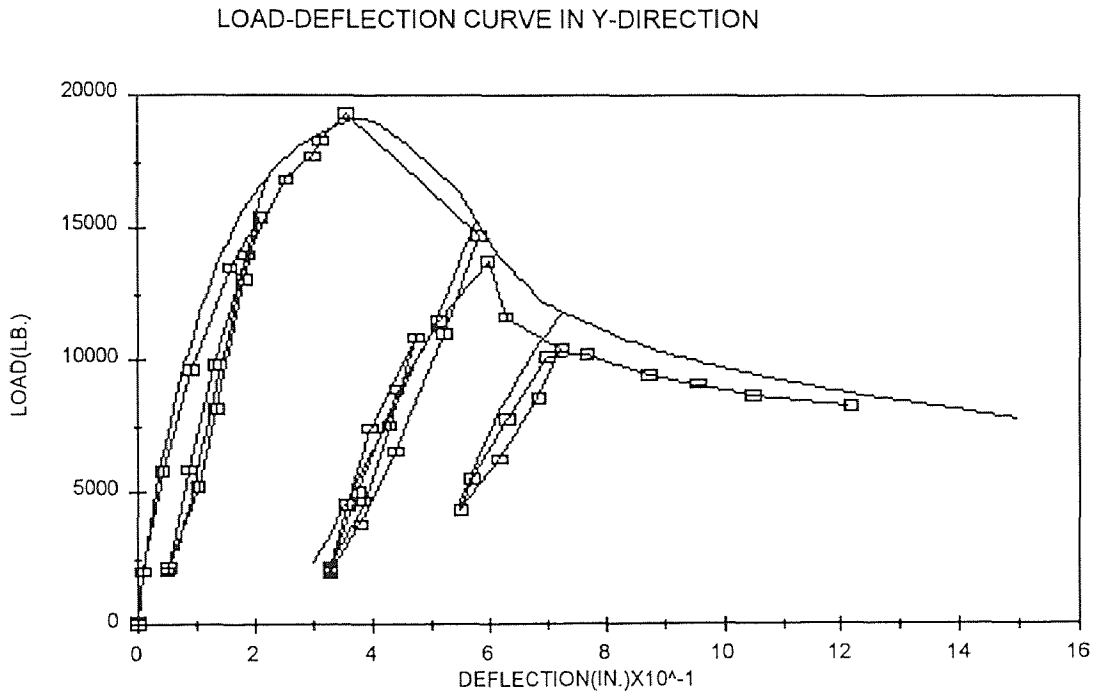

Figure B.26 Comparison of Load-Deflection Curve (Y-DIR.) for Column C7

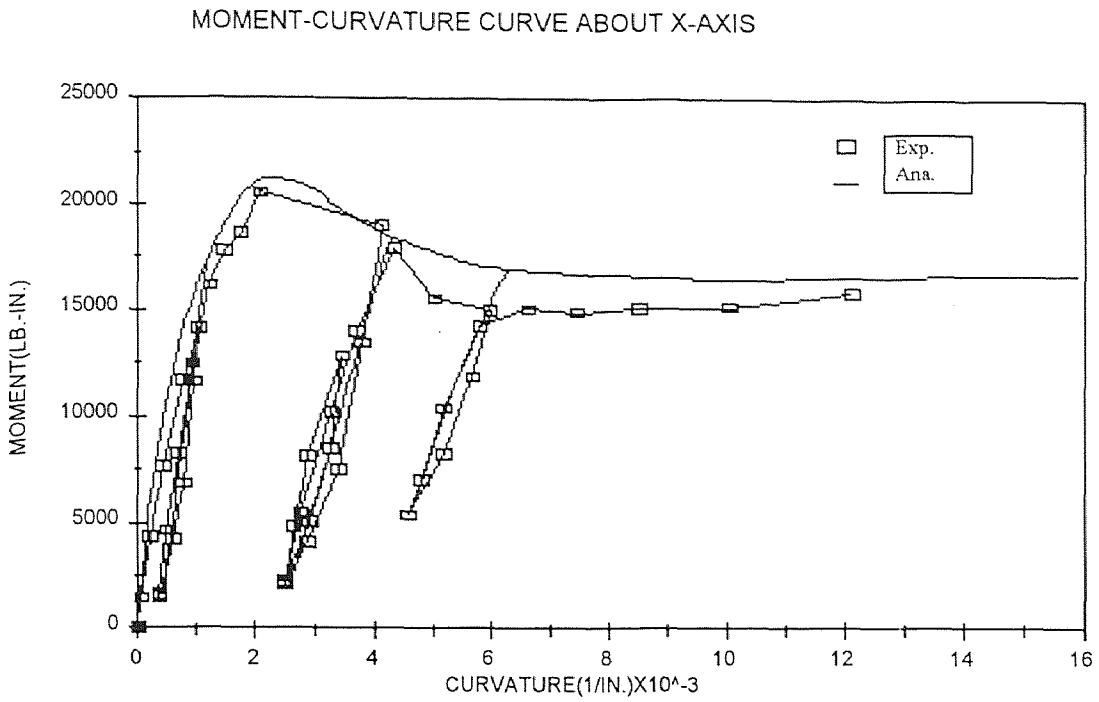

Figure B.27 Comparison of Moment-Curvature Curve (X-AXIS) for Column C7

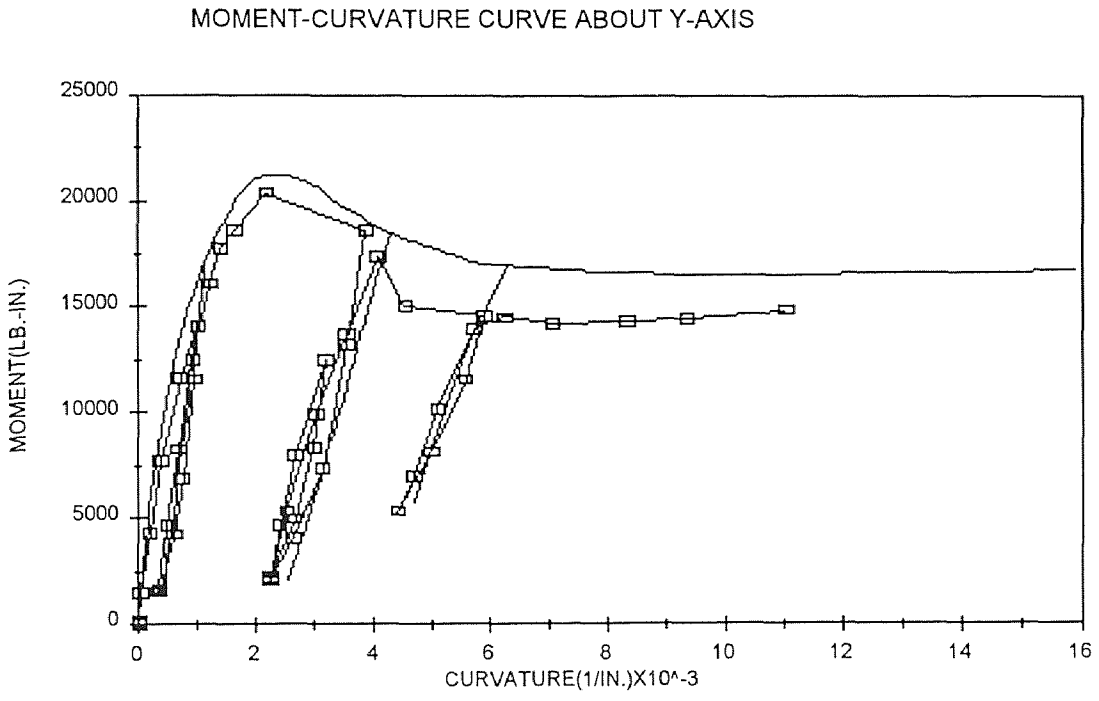

Figure B.28 Comparison of Moment-Curvature Curve (Y-AXIS) for Column C7

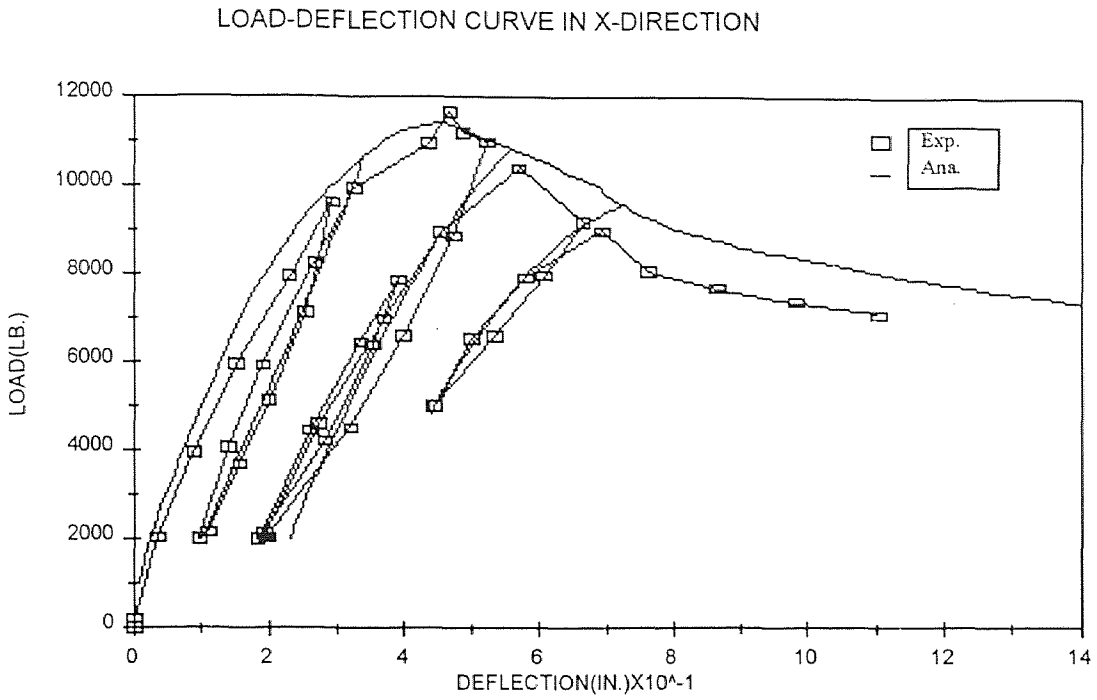

Figure B.29 Comparison of Load-Deflection Curve (X-DIR.) for Column C8

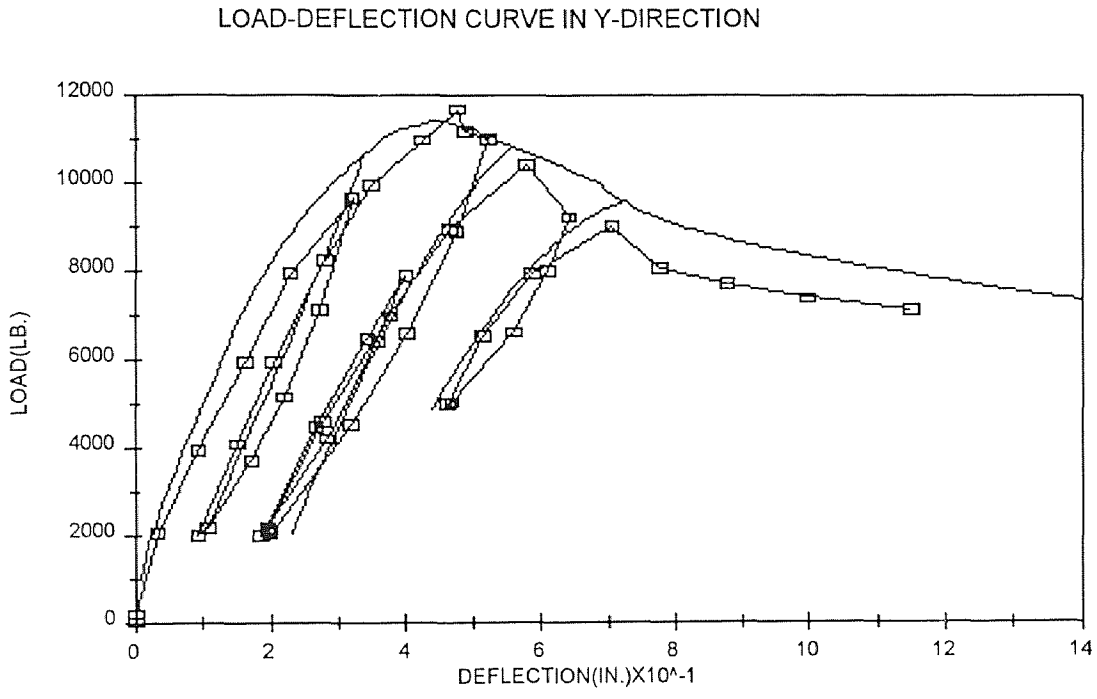

Figure B.30 Comparison of Load-Deflection Curve (Y-DIR.) for Column C8

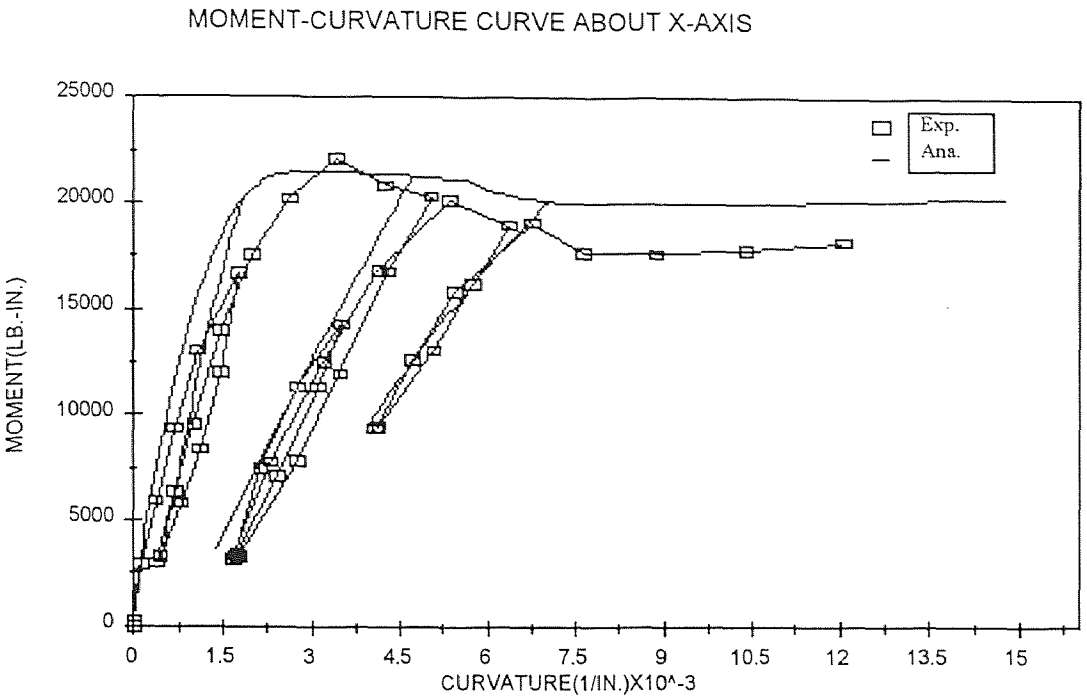

Figure B.31 Comparison of Moment-Curvature Curve (X-AXIS) for Column C8

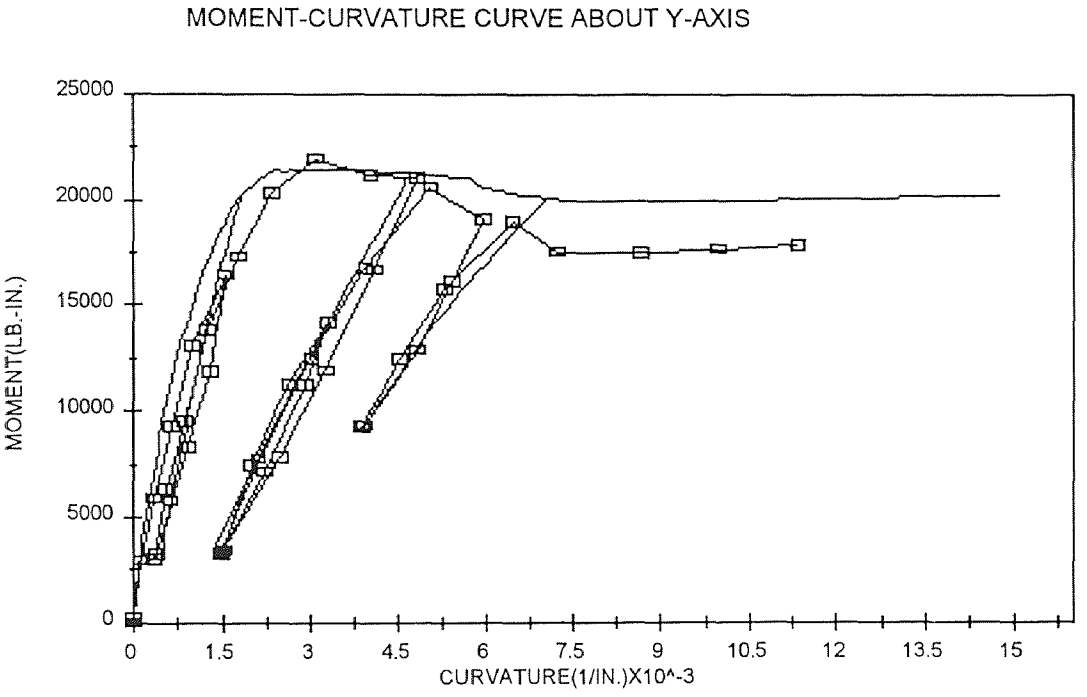

Figure B.32 Comparison of Moment-Curvature Curve (Y-AXIS) for Column C8

REFERENCES

Ahmad, S. H.,and S. P. Shah. 1985. "Behavior of Hoop Confined Concrete Under High Strain Rates." ACI Journal. Vol.82. Title No.82-55.634-647.

Ahmad, S. H., and S. P. Shah. 1982. "Stress-Strain Curves of Concrete Confined by Spiral Reinforcement." ACI Journal. Vol. 79 484-490

Al-Noury, S. I.; W. F. Chen. 1982. "Finite Segment Method for Biaxially Loaded RC Columns." ASCE ST4 Vol. 108 p780-799

Ang, C. C. L. 1961. "Square Column with Double Eccentricities Solved by Numerical Method." ACI Journal Vol. 57 p977-980

Bazant, Z. P.; L. Cedolin; M. R. Tabbara. 1991. "New Method of Analysis for Slender Columns." ACI Structure Journal p391-401

Bischoff, P.H., and S. H. Perry. 1990. "Compressive Behavior of Concrete at High Strain Rates." Material & Structure. Vol. 24. 5:425-450.

Blakeley, R. W., and R. Park. 1973. "Prestressed Concrete Sections with Cyclic Flexure." ASCE Journal. ST8, Vol. 99 , 1717-1742

Bresler, Boris. 1960. "Design Criteria for Reinforced Columns under Axial Load and Biaxial Bending." ACI Journal Vol. 57 p481-490

Brown, R. H., and J. O. Jirsa. 1971. "Reinforced Concrete Beams under Load Reversals." ACI Journal. Vol. 68, 380-390

Carreira, D. J.; Kuang-Han Chu. 1986. "The Moment-Curvature Relationship of Reinforced Concrete Members." ACI ST. Vol. 83 p191-198

Chang, W. F.; P. M. Ferguson. 1963. "Long Hinged Reinforced Concrete Columns." ACI Journal Vol. 60 p1-25

Chen, W. F; D. J. Han. 1988. "Plasticity for Structural Engineers." Springer-Verlag, New York, p11-23

Chen En-Sheng, and Buyukozturk Oral. 1985. "Constitutive Model for Concrete in Cyclic Compression." ASCE Journal of Engineering Mechanics. Vol. 111, 797-814

Choudhury, D.; A. R. Mari; A. C. Scordelis. 1988. "Design of Reinforced Concrete Bridge Columns Subjected to Imposed Deformations." ACI Structure Journal Vol. 115 p521-529

Cook, D. J., and P. Chindaprasirt. 1980. "Influence of Loading History upon the Compressive Properties of Concrete." Magzine of Concrete Research. Vol. 32, 111:89-100

REFERENCES
(Continued)

Crisfield, M. A. 1979. "A Faster Modified Newton-Raphson Iteration." Computer Method in Applied Mechanics & Engineering 20 p267-278

Darwin, D., and D. A. Pecknold. 1977. "Analysis of Cyclic Loading of Plane R/C Structures." Computers & Structures Vol. 7, 1:137-147

Desayi, P., K. T. Iyengar, and T. S. Reddy. 1979. "Stress- Strain Characteristics of Concrete Confined in Steel Spirals under Repeated Loading." Materials & Structures Vol. 12, 71:375-383

Dundar, C. 1990. "Concrete Box Sections under Biaxial Bending and Axial Load." ASCE Journal of Structure Engineering Vol. 116 p860-865

El-Metwally, S. E.; W. F. Chen. 1989. "Load-Deformation Relations for Reinforced Concrete Sections." ACI Structure Journal Vol. 86 p163-167

Espion, E.; Pierre Halleux. 1988. "Moment Curvature Relationship of Reinforced Concrete Sections Under Combined Bending and Normal Force." Materials & Structures 21 p341-351

Fafitis, A., and S. P. Shah. 1984. "Rheological Model for Cyclic Loading of Concrete." ASCE Journal of Structure Engineering. Vol. 110, 2085-2102

Farah, A.; M. W. Huggins. 1969. "Analysis of Reinforced Concrete Columns Subjected to Longitudinal Load and Biaxial Bending." ACI Journal Vol. 66 p569-575

Fardis, M. N., B. Alibe, and J. L. Tassoulas. 1983. "Monotonic and Cyclic Constitutive Law for Concrete." ASCE Journal of Engineering Mechanics. Vol. 109, 516-536

Furlong, W. F. 1979. "Concrete Columns Under Biaxially Eccentric Thrust." ACI Journal Vol. 76 p1093-1118

Ghaboussi, J., J. H. Garrett Jr., and X. Wu. 1991. "Knowledge-Based Modeling of Material Behavior with Neural Networks." ASCE Journal of Engineering Mechanics. Vol. 117 ,p132-153

Goyal, B. B.; N. Kackson. 1971. "Slender Concrete Columns under Sustained Load." ASCE ST11 Vol. 97 p2729-2750

Gurfinkel, G.; A. Robinson. 1967. "Determination of Strain Distribution and Curvature in a Reinforced Concrete Section Subjected to Bending Moment and Longitudinal Load." ACI Journal Vol. 64 p398-403

Hsu, C. T. Thomas. 1988. "Analysis and Design of Square and Rectangurlar Columns by Equation of Failure Surface." ACI Structure Journal p167-179

REFERENCES
(Continued)

Hsu, C. T. Thomas. 1974. "Behavior of Structural Concrete Subjected to Biaxial Flexure and Axial Compression." Ph.D. Thesis McGill Univ., CANADA, p182-204

Hsu, Cheng-Tzu; M. S. Mirza. 1973. "Sructural Concrete Biaxial Bending and Compression." ASCE ST2 Vol. 99 p285-290

Hughes, V. P. and R. Gregory. 1972. "Concrete Subjected to High Rates of Loading in Compression" Magzine of Concrete Research. Vol.24, 78:25-36

Iyengar, K. T., P. Desayi and K. N. Reddy. 1970. "Stress-Strain Characteristics of Concrete Confined in Steel Binders" Magazine of Concrete Research. Vol.22, 72:173-184

Karsan, I. D., and J. O. Jirsa. 1969. "Behaviour of Concrete under Compressive Loadings." ASCE Journal of ST12 Vol. 95, 2543-2563

Kent, D. C. and R. Park. 1971. "Flexural Members with Confined Concrete" ASCE ST7. Vol.97:1969-1990

Liu, X. L.; W. F. Chen. 1984. "Reinforced Concrete Pipe Columns: Behavior and Design." ASCE Journal of Structure Engineering Vol. 110 p1356-1373

Maher, A., and D. Darwin. 1982. "Mortar Constituent of Concrete in Compression." ACI Journal. Vol. 79, 100-109

Mander, J. B., M. J. N. Priestley, and R. Park. 1988. "Theoretical Stress-Strain Model for Confined Concrete." ASCE Journal of Structure Engineering. Vol. 114, 1804-1826

Mattock, A. H.; L. B. Kriz; E. Hognestad. 1961. "Rectangular Concrete Stress Ditribution in Ultimate Strength Desigh." ACI Journal Vol. 57 p875-928

Mau, S. T. 1990. "Numerical Simulation of the Behavior of Axilly Loaded Reinforced Concrete Columns." Computers & Structures Vol. 35 p361-368

Mekonnen, B. 1984. "Reinforced Concrete Column Design Equations." ACI Journal Vol. 61 p242-250

Menegotto, M.; P. E. Pinto. 1977. "Slender RC Compressed Members in Biaxial Bending." ASCE ST3 Vol. 103 p587-605

Mirza, S. A. 1990. "Flexural Stiffness of Rectangular Reinforced Concrete Columns." ACI Journal Vol. 46 p425-435

Mirza, S. A.; J. G. Macgregor. 1989. "Slenderness and Strength Reliability of Reinforced Concrete Columns." ACI Structure Journal Vol. 86 p428-438

REFERENCES
(Continued)

Otter D. E., and A. E. Naaman. 1989. "Model for Response of Concrete to Random Compressive Loads." ASCE Journal of Structure Engineering. Vol. 115, 2794-809

Otter, D. E., and A. E. Naaman. 1988. "Properties of Steel Fiber Reinforced Concrete under Cyclic Loading." ACI Material Journal. Vol. 85, 254-261

Park, R., D. C. Kent, and R. A. Sampson. 1972. "Reinforced Concrete Members with Cyclic Loading." ASCE Journal of Structure Engineering. Vol. 98, 1341-1359

Popovics, S. 1973. "A Numerical Approach to the Complete Stress-Strain Curve of Concrete" Cement & Concrete Research. Vol.3, 583-597

Pfrang, E. O.; C. P. Siess. 1964. "Behavior of Restrained Reinfroced Concrete Columns." ASCE ST5 Vol. 90 p113-136

Pfrang, E. O.; C. P. Siess; M.A. Sozen. 1964. "Load-Moment-Curvature Characteristics of Reinforced Concrete Cross Sections." ACI Journal Vol. 61 p763-777

Poppvics, S. 1970. "A Review of Stress-Strain Relationships for Concrete" ACI Journal. Vol.67, 243-248

Prakhya, G. K. V.; C. T. Morley. 1990. "Tension-Stiffening and Moment-Curvature Relations of Reinforced Concrete Elements." ACI Structure Journal p597-605

Priestley, J. N.; R. Park; R. T. Potangaroa. 1981. "Ductility of Spirally-Confined Concrete Columns." ASCE Journal of Structure Vol. 107 p181-202

Rao, P. S.; B. V. Subrahmanyam. 1973. "Trisegmental Moment-Curvature Relations for Reinforced Concrete Members." ACI Journal Vol. 117 p346-351

Rotter, J. M. 1985. "Rapid Exact Inelastic Biaxial Bending Analysis." ASCE Journal of Structure Engineering Vol. 111 p2659-2674

Sakai, K.; S. A. Sheikh. 1989. "What Do We Know about Confinement in Reinforced Concrete Columns?(A Critical Review of Previous Work and Code Provisions)." ACI Structure Journal Vol. 86 p192-207

Sargin, M., S. K. Ghosh, and V. K. Handa. 1971. "Effects of Lateral Reinforcement upon the Strength and Deformation Properties of Concrete" Magzine of Concrete Research. Vol.23, 75:99-110

Scott, B. D., R. Park, and M. J. N. Priestley. 1982. "Stress-Strain Behavior of Concrete Confined by Overlapping Hoops at Low and High Strain Rates." ACI Journal. Vol. 79, 13-27

REFERENCES
(Continued)

Shah, S. P., A. Fafitis, and R. Arnold. 1983. "Cyclic Loading of Spirally Reinforced Concrete." ASCE Journal of Structure Engineering. Vol. 109, 1695-1710

Sheikh, S. A.; C. C. Yeh. 1992. "Analytical Moment-Curvature Relations for Tied Concrete Columns." ASCE Journal of Structure Engineering Vol. 118 p529-544

Sheikh, S. A.; C. C. Yeh; S. Khoury. 1990. "Concrete Strength in Tied Columns." ACI Journal Vol. 103 p379-385

Sinha, B. P., K. H. Gerstle, and L. G. Tulin. 1964. "Stress-Strain Relations for Concrete Under Cyclic Loading." ACI Journal. Vol. 61, 195-210

Smith, G. M., and L. E. Young. 1956. "Ultimate Flexural Analysis Based on Stress-Strain Curves of Cylinders." ACI Journal. Vol. 53, 597-609

Somes, N. F. 1970. "Compression Test on Hoop-Reinforced Concrete." ASCE ST7 Vol. 96, 1495-1509

Spooner, D. C., and J. W. Dougill. 1975. "A Quantitative Asseeement of Damage Sustained in Concrete during Compressive Loading." Magzine of Concrete Research. Vol. 27, 92:151-160

Timoshenko S. P. and G. M. Gere. 1963. "Theory of Elastic Stability." McGraw-Hill, New York, p116-123

Tsao, Wen Hu. 1991. "Square and L-Shaped Slender Reinforced Concrete Columns Under Combined Biaxial and Axial Compression." Ph.D Thesis, New Jersey Institute of Technology, p28-36

Venkateswarlu, S. T.; V. J. Rao. 1977. "Strain Matrix Method of Analysis for Reinforced Concrete Members under Combined Bending and Direct Load." Materials & Structures Vol. 10, 55:33-37

Wang, G., C. T. Thomas Hsu. 1990. "Complete Load-Deformation Behavior of Biaxially Loaded Reinforced Concrete Columns." Technical Report Structural Series No. 90-2, Department of Civil and Environmental Eng., New Jersey Institute of Technology, p4-10

Wang, P. T., S. P. Shah and A. E. Naaman. 1978. "Sress-Strain Curves of Normal and Lightweight Concrete in Compression." ACI Journal Vol. 75:603-611

Warner, R. F. 1969. "Biaxial Moment Thrust Curvature Relations." ASCE ST5 Vol. 95 p923-940

Watstein, D. 1953. "Effect of Straining Rate on the Compressive Strength and Elastic Properties of Concrete" ACI Journal. Vol.49, 729-744

Whaley, C. P., and A. M. Neville. 1973. "Non-elastic Deformation of Concrete under Cyclic Compression." Magzine of Concrete Research. Vol. 25, 84:145-154

Wolfram, S., D. Grayson, R. Marder, H. Cejtin, T. Gray, S. Omohundro, D. Ballman and J. Keiper. 1988. "Mathematica: A System for Doing Mathematics by Computer." Addison Wesley

Yankelevsky, D. Z., and H. W. Reinhardt. 1987. "Model for Cyclic Compressive Behavior of Concrete." ASCE Journal of Structure Engineering. Vol. 113, 228-240